INL/EXT-21-62939
Revision 2

Light Water Reactor Sustainability Program

Energy Arbitrage: Comparison of Options for use with LWR Nuclear Power Plants

September 2021
U.S. Department of Energy
Office of Nuclear Energy

DISCLAIMER

This information was prepared as an account of work sponsored by an agency of the U.S. Government. Neither the U.S. Government nor any agency thereof, nor any of their employees, makes any warranty, expressed or implied, or assumes any legal liability or responsibility for the accuracy, completeness, or usefulness, of any information, apparatus, product, or process disclosed, or represents that its use would not infringe privately owned rights. References herein to any specific commercial product, process, or service by trade name, trade mark, manufacturer, or otherwise, does not necessarily constitute or imply its endorsement, recommendation, or favoring by the U.S. Government or any agency thereof. The views and opinions of authors expressed herein do not necessarily state or reflect those of the U.S. Government or any agency thereof.

INL/EXT-21-62939
Revision 2

Energy Arbitrage: Comparison of Options for use with LWR Nuclear Power Plants

L. Todd Knighton, Amey Shigrekar, Daniel S. Wendt, Konor L. Frick and Richard D. Boardman
(Idaho National Laboratory)

Amgad A. Elgowainy, Adarsh Bafana, Hla Tun, and Krishna R. Reddi
(Argonne National Labortory)

September 2021

Prepared for the
U.S. Department of Energy
Office of Nuclear Energy

Page intentionally left blank

EXECUTIVE SUMMARY

Arbitrage is the opportunistic buying and selling of a commodity during local pricing valleys and peaks respectively to maximize economic value. This report evaluates options for energy arbitrage integrated with existing light water reactor (LWR) nuclear power plants (NPPs) where nuclear energy could be stored in a variety of forms and later recovered to generate electrical power during periods when grid electricity demand and pricing are high. The forms of energy storage examined in this report include the potential value of batteries, hydrogen, and thermal energy storage for coupling with nuclear power. Various large demand response options are also analyzed, including the production of liquid nitrogen via air separation and liquefaction, liquefaction of hydrogen, compressed hydrogen, and the cryogenic capture of CO_2. Demand response refers to dispatchable loads that can cycle up or down depending on-grid electricity demand to aid in balancing the grid. Large demand response options could dispatch to aid nuclear power stations in avoiding power turndowns by providing an alternate disposition for electrical energy by producing marketable products (e.g., liquid nitrogen, hydrogen, or captured CO_2).

Static conditions were chosen and analyzed in this report for each option. Dynamic operation or optimization of energy arbitrage or demand response are out of scope for this report. The analysis is based on storage systems with discharge capacities of 500 MW for which various durations of storage and costs of charging (electricity cost) are examined.

While the value of thermal energy to an industrial user for flexible plant operations has been previously proven as a business case, this report evaluates costs of hydrogen energy storage and leading thermal energy storage options, and large demand response loads that could be integrated with LWRs in comparison to utility-scale battery storage for use of off-peak nuclear energy. Compilation of this information will be used by the Idaho National Laboratory (INL) RAVEN/HERON systems integration and economics tool to evaluate thermal energy dispatch to industrial users.

Relative ranking of energy storage options was done using a levelized cost of storage (LCOS) metric which calculates a rough breakeven cost for the system, taking into account the capital and operating costs as well as the revenue from arbitrage. Table ES1 below shows the LCOS for each of the energy storage options considered. First, in the table, lithium iron (Fe) phosphate batteries are listed as the base case for comparison against the other options. Next is hydrogen storage where most of the hydrogen analyses assumed the hydrogen to be produced using solid oxide electrolytic cell (SOEC) high-temperature steam electrolysis (HTSE). The others used existing models of polymer electrolyte membrane (PEM) low temperature electrolysis to produce hydrogen. HTSE performance parameters and costs were taken from existing INL models. Various means were assumed to convert the hydrogen to electricity, including PEM fuel cells (FCs) and a gas turbine mixed in a 30 vol% mixture with natural gas. Physical storage (pressure vessels) and geological storage (natural underground features) were used to store the hydrogen as noted. Geological storage is more economical, but the locations are limited because of the requirement for pre-existing geological formations that will support storage. Thermal energy storage (TES) options were also analyzed including electro-thermal energy storage (ETES) and four different liquid sensible heat TES storage media as noted (Hitec, Hitec XL, Therminol-66, and Dowtherm A). The ETES process considered was modified using existing public documentation on an Echogen process and uses a separate supercritical CO_2 charge and discharge cycle with sand as the heat storage media.

Table ES1. Comparison of energy storage options for power arbitrage discharge capacity of 500MWe and charging the cost of $30/MWh.

Technology		Charging Cost ($/MWhe)						
		0	15	20	25	30	35	40
Li-ion LFP Battery	LCOS ($/MWhe)	322 (6h & 12h)	339 (6h & 12h)	345 (6h & 12h)	351 (6h & 12h)	357 (6h & 12h)	363 (6h & 12h)	369 (6h & 12h)
H_2 Geological Storage, SOEC / PEM FC		194 (6h) 98 (12h)	212 (6h) 115 (12h)	218 (6h) 121 (12h)	224 (6h) 127 (12h)	230 (6h) 133 (12h)	236 (6h) 139 (12h)	241 (6h) 145 (12h)
H_2 Physical Storage, SOEC / PEM FC		213 (6h) 115 (6h)	231 (6h) 133 (12h)	237 (6h) 139 (12h)	242 (6h) 145 (6h)	248 (6h) 151 (12h)	254 (6h) 156 (12h)	260 (6h) 162 (12h)
H_2 Physical Storage, PEM EC / Gas Turbine		86 (6h) 71 (12h)	110 (6h) 95 (12h)	119 (6h) 103 (12h)	127 (6h) 112 (12h)	135 (6h) 120 (12h)	143 (6h) 128 (12h)	151 (6h) 136 (6h)
Thermal (ETES)		129 (6h) 77 (12h)	-	172 (6h) 120 (12h)	-	194 (6h) 141 (12h)	-	215 (6h) 163 (12h)
Thermal (sensible / Hitec)		58 (6h) 50 (12 h)	80 (6h) 72 (12h)	87 (6h) 79 (12h)	94 (6h) 86 (12h)	101 (6h) 93 (12h)	108 (6h) 101 (12h)	116 (6h) 108 (12h)
Thermal (sensible / Hitec XL)		62 (6h) 53 (12h)	84 (6h) 75 (12h)	91 (6h) 82 (12h)	98 (6h) 89 (12h)	105 (6h) 96 (12h)	112 (6h) 104 (12h)	120 (6h) 111 (12h)
Thermal (sensible / Therminol-66)		159 (6h) 151 (12)	181 (6h) 172 (12h)	188 (6h) 180 (12h)	195 (6h) 187 (12h)	202 (6h) 194 (12h)	210 (6h) 201(12h)	217 (6h) 209 (12h)
Thermal (sensible / Dowtherm A)		116 (6h) 108 (12h)	138 (6h) 130 (12h)	145 (6h) 137 (12h)	152 (6h) 144 (12h)	159 (6h) 151 (12h)	167 (6h) 159 (12h)	174 (6h) 166 (12h)

Figure ES1 below shows the data from the table above plotted in graphical form for a subset of the energy storage options.

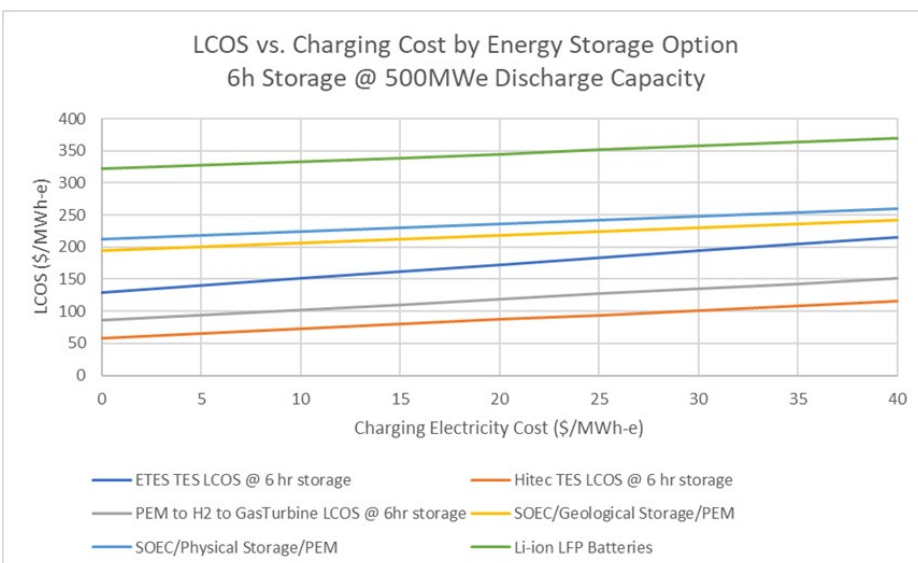

Figure ES1. LCOS versus charging cost for various energy storage options.

From this analysis the relative economic ranking of the energy storage options analyzed by LCOS for 6h of storage of 500MWe discharge capacity can be deduced from most economic to least as:

1. Liquid sensible heat thermal energy storage using Hitec fluid as the thermal media,
2. Power to H_2 via PEM/H_2 to electricity via mixing up to 30 vol% H_2 with natural gas in a gas turbine, physical H_2 storage (producing the H_2 via HTSE instead of PEM may prove more economical but was not analyzed in this specific case),
3. Electro thermal energy storage (ETES) with a supercritical CO_2 cycle and sand thermal storage media,
4. Power to H_2 via SOEC/Geological H_2 Storage/H_2 to electricity via PEM fuel cell,
5. Power to H_2 via SOEC/Physical H_2 Storage/H_2 to electricity via PEM fuel cell, and
6. Lithium -on Batteries.

Other permutations of hydrogen production, storage, and H_2 to electricity not analyzed include reversible SOEC/FC which can operate either as an electrolytic cell to produce hydrogen using electricity or as a fuel cell to produce electricity using hydrogen. Reversible SOEC/FCs should be fully analyzed with the most up-to-date modeling in future work and compared to these results.

Steam accumulators were analyzed using numbers from Khi Solar one and found that 19 steam accumulators can provide 50 MWe, which is about 15% of a 1 GW NPP assuming a conversion efficiency of 33%. Although the amount of energy stored and recovered from the steam accumulators is significant, the number of storage tanks required to provide 500 MWe for 6-12 hours is very large. Based on another recent analysis, the pressure vessel's cost accounts for about 60-70% of the total TES cost. Nevertheless, steam accumulators can be discharged rapidly and have a round-trip efficiency ranging between 60 and 80%. The discharged steam can either be superheated using electrical topping heat before its delivery to the power block, or it can be introduced into a low-pressure turbine in a Rankine power cycle. Due to this flexible nature and ease of use of steam accumulators, they are an attractive TES option for coupling with existing LWRs where the energy stored is at small scale.

In addition, this study has applied the greenhouse gas (GHG), regulated emissions, and energy use in technologies (GREET) model to analyze the low CO_{2e} emissions of the various arbitrage energy storage options when integrated with nuclear power. This information is valuable for organizations that have set goals relating to staged decarbonization to help them understand the approximate ranking and cost/benefit comparisons of various carbon reduction strategies. This information will also be used to enhance the GREET model for the assessment of energy systems that include LWR energy inputs.

Figure ES2 shows the GHG emissions per kWh kilowatt-hour for storing LWR energy using batteries, hydrogen, and thermal options compared with electricity from natural gas generators with simple cycle (SC), combined cycle (CC), and CC with carbon capture and storage. The electricity from LWR energy storage scenarios has emissions of 8–20 gCO2e/kWh whereas electricity from natural gas generators is between 112–727 gCO2e/kWh.

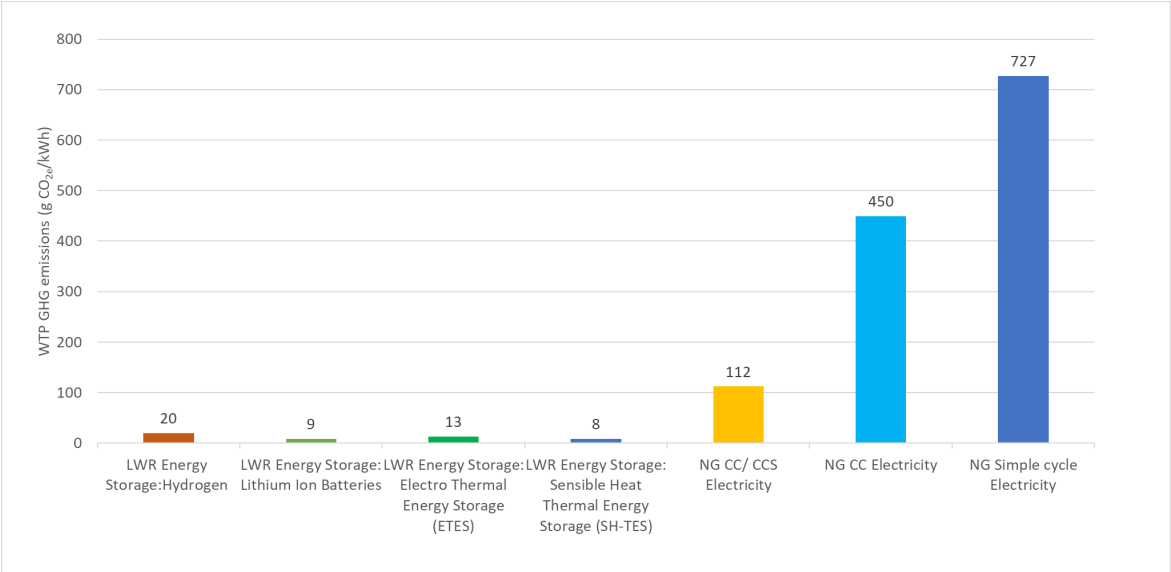

Figure ES2. Life cycle GHG emissions for electricity from energy storage compared to electricity generated from natural gas.

Finally, large demand response options were analyzed and a summary of these options considered is shown in Table ES2 below. Separation and liquefaction of nitrogen is one of the lower-cost options for demand response followed by new and innovative cryogenic carbon capture via the sustainable energy solutions (SES) process. The analysis for these processes did not take into account at this time the sales revenue from each product and market analysis and pricing which could be done in future work.

Table ES2. Summary of demand response options considered. $30/MWh nuclear electricity cost is assumed in these calculations.

Technology		Energy Required (kWh/kg)	Cost	Efficiency
Hydrogen Compression (to 350bar)	Hydrogen	2	$60/MT [a]	
Liquefaction	Hydrogen	11	$330/MT [a]	
	Nitrogen	0.528	$16/MT [a]	
CO_2 capture	Cryogenic capture (A3C)	0.332 (for 12vol% CO_2) 0.831 (for 3 vol% CO_2)	$49/MT (for 12vol% CO_2) $112/MT (for 3 vol% CO_2)	90%
	Cryogenic Carbon Capture (SES)	0.242 (for 16 vol% CO_2)	$45/MT (for 16 vol% CO_2)	90%
	Amine (MEA)	0.372 (for 12vol% CO_2) 0.476 (for 3 vol% CO_2) 0.291 (for 16 vol% CO_2)	$56/MT (for 12vol% CO_2) $108/MT (for 3 vol% CO_2) $69/MT (for 16 vol% CO_2)	90%
Cryogenic Air separation	Nitrogen	0.162	$5/MT [a]	

CONTENTS

EXECUTIVE SUMMARY iii
LIST OF ACRONYMS xiii
1. INTRODUCTION 16
1.1 Energy Arbitrage 17
1.2 Scope of this Report 19
2. NUCLEAR POWER-STORAGE-POWER 20
2.1 Energy Storage Using Lithium-Ion Batteries 20
2.2 Hydrogen Production, Storage, and Power Generation 21
2.2.1 HTSE CAPEX (Current and Future) 21
2.2.2 Hydrogen Storage (Geological and Physical) 22
2.2.3 Hydrogen Transportation 23
2.2.4 Hydrogen to Power – Fuel Cells 23
2.2.5 Hydrogen to Power – Gas Turbines 24
2.2.6 Hydrogen to Power versus Li-ion LFP Batteries to Power 24
2.3 Thermal Energy Storage 29
2.3.1 Echogen Electro Thermal Energy Storage 30
2.3.2 Liquid-Based Sensible Heat Thermal Energy Storage 51
2.3.3 Steam Accumulators 66
2.4 Lifecycle Analysis of Energy Storage Options 67
2.5 Summary of Nuclear Power Energy Storage Options 68
3. DEMAND RESPONSE OPTIONS FOR INTEGRATION WITH NUCLEAR POWER 72
3.1 Liquid Nitrogen 72
3.1.1 Liquid Nitrogen Market 72
3.1.2 Liquid Nitrogen Production Cost 73
3.2 Liquid Hydrogen 74
3.3 Hydrogen Compression 74
3.4 Liquid Nitrogen and Liquid Hydrogen Offsite Transportation 75
3.5 Cryogenic Carbon Capture 76
3.5.1 Cryogenic Carbon Capture 76
3.5.2 A3C Carbon Capture Process 78
3.6 Lifecycle Analysis of Demand Response Options 81
3.7 Summary of Demand Response Options 84
4. CONCLUSION 84
APPENDIX A STATE-OF-THE ART OF TES 90
APPENDIX B COST BREAKDOWN FOR THE SH-TES SYSTEM FLUIDS 104
APPENDIX C TES TECHNOLOGY CONSIDERATIONS 118

5. REFERENCES 123

FIGURES

Figure ES1. LCOS versus charging cost for various energy storage options. iv

Figure ES2. Life cycle GHG emissions for electricity from energy storage compared to electricity generated from natural gas vi

Figure 3. Illustrative consequences of excess solar energy power generation. 16

Figure 4. Flexible Plant Operation and Generation concept for nuclear power plant. 18

Figure 5. U.S. Salt Deposits for Geological Storage with overlayed locations of U.S. NPPs 23

Figure 6. Hydrogen production, storage, and co-firing through natural gas turbines. 24

Figure 7. Energy storage cost comparison for lithium-ion (LFP) batteries and H_2 (using HTSE-SOEC for H_2 production and PEM FC for H_2 to power). Physical hydrogen storage at 1500–2000 psi. $30/MWh system charging cost used. 500 MW charging capacity. 25

Figure 8. Energy-storage cost for lithium-ion (LFP) battery and H_2 (using SOEC for H_2 production and PEM for H_2 to power). Geologic hydrogen storage at 1500–2000 psi. $30/MWh system charging cost used. 500 MW charging capacity 26

Figure 9. LCOS for Lithium-ion LFP batteries 27

Figure 10. LCOS for Power-Hydrogen-Power (geological and physical storage). SOEC assumed for H_2 production and PEM for H_2 to power. 27

Figure 11. LCOS of hydrogen to power (geological and physical storage) as a function of the charge mode power cost (electricity cost). SOEC is assumed for H_2 production and PEM for H_2 to power. 28

Figure 12. LCOS comparison for hydrogen to power (geological and physical storage) systems operating with selected discharge intervals/durations and charging costs. SOEC assumed for H_2 production and PEM for H_2 to power 28

Figure 13. Tornado chart illustrating sensitivity of hydrogen to power (geological and physical storage) LCOS to selected parameters. SOEC assumed for H_2 production and PEM for H_2 to power. 29

Figure 14. Process flow diagrams of the Echogen ETES charging and discharging cycles. Figure adapted from diagrams presented in Echogen technical documents [33,34]. 30

Figure 15. ETES charging cycle (heat pump mode) process flow diagram 33

Figure 16. ETES discharge cycle (power generation mode) process flow diagram. 34

Figure 17. RTE as a function of process waste heat rejection temperature; standalone ETES process configuration (electrical power input only). 36

Figure 18. Estimated ETES capital costs (per unit of electrical energy storage capacity) as a function of storage capacity. 41

Figure 19. Comparison of estimated ETES and Li-ion battery capital costs. Lithium-ion battery energy storage costs (orange) and CO_2 ETES costs (blue) are reproduced from available Echogen technical information [34]. ETES costs (green) estimated in this report are included for comparative purposes 41

Figure 20. LCOS as a function of discharge cycle duration with the interval between initiation of discharge cycles as a parameter (standalone ETES process configuration with heat pump mode waste heat rejection). 43

Figure 21. Tornado chart illustrating sensitivity of ETES LCOS to selected parameters. 44

Figure 22. ETES LCOS as a function of the charge mode power cost (electricity cost) for a non LWR integrated ETES system configuration. 45

Figure 23. LCOS comparison for ETES systems operating with selected discharge intervals/durations and charging costs. 45

Figure 24. ETES heat pump cycle with nuclear process heat input (CO_2 working fluid heating). 46

Figure 25. ETES heat pump cycle with nuclear process heat input (HTR media heating). 46

Figure 26. LWR-integrated ETES process configuration and operating conditions. Heat pump mode (charging cycle) shown in top diagram and power generation mode (discharge cycle) is shown in bottom diagram. 47

Figure 27. Effect of nuclear heat addition to ETES process working fluid for configurations with and without heat pump mode waste heat rejection. Data labels indicate LWRX heat exchanger cold side (CO_2 ETES working fluid) outlet temperature. 48

Figure 28. ETES process configuration with heat pump mode LWR thermal integration and waste heat rejection (denoted as "secondary cooling" in the diagram). 48

Figure 29. LWR integrated ETES process QoP (heat pump mode with waste heat rejection), $\eta_{thermal}$ (power generation mode), and RTQE (inclusive of charge and discharge mode system operations). 49

Figure 30. Solar power tower and parabolic trough concentrated solar power systems (CPSs) with integrated thermal storage systems. 52

Figure 31. Schematic and PFD of SH-TES charge cycle. 54

Figure 32. Schematic and PFD of SH-TES discharging cycle. 55

Figure 33. PFD of the charging cycle of SH-TES with Hitec as the storage medium. 56

Figure 34. PFD of the discharging cycle of SH-TES with Hitec as the storage medium. 57

Figure 35. PFD of a standalone heat exchanger model for the condenser of Rankine power cycle. 57

Figure 36. Estimated SH-TES capital costs (per unit of electrical energy storage capacity) as a function of storage capacity. 60

Figure 37. LCOS as a function of discharge cycle duration with an interval between initiation of discharge cycles as a parameter for Hitec-based SH-TES. 62

Figure 38. Tornado chart illustrating the sensitivity of Hitec-based SH-TES LCOS to selected parameters. 62

Figure 39. LCOS as a function of the charging electricity for an SH-TES with Hitec. 63

Figure 40. LCOS comparison for Hitec-based SH-TES systems operating with selected discharge intervals/durations and charging costs. 64

Figure 41 Life cycle GHG emissions for electricity from energy storage compared to electricity generated from natural gas. 68

Figure 42. LCOS vs. Charging Cost by Energy Storage Option. 71

Figure 43. Sensitivity study on the effects of various factors on the cost of nitrogen production via air separation. 74

Figure 44. Cost of energy for H_2 compression to 350 bars and liquefaction at different electricity prices. 75

Figure 45. Cost of transporting liquid H_2 and liquid N_2 in liquid tankers. 76

Figure 46 Outline of the simplified CCC process with EL . 77

Figure 47. Cost and energy penalty of CCC process with plant size for coal power plant with 16 vol% CO_2 in the flue gas 78

Figure 48. Cost and energy penalty of SES CCC process with CO_2 composition in the flue gas[72] 78

Figure 49. Outline of the two stages of A3C process[65] 79

Figure 50. LCCC with the concentration of CO_2 in the flue gas for A3C and amine-based processes. 81

Figure 51. GHG emissions for utilizing LWR nuclear electricity for liquefaction and cryogenic seperation and compared to U.S. mix Grid. 82

Figure 52 GHG emissions for CO_2 capture. 83

Figure 53 WTP GHG emissions for NGCC electricity generators. 83

Figure 54. LCOS versus charging cost for various energy storage options. 86

Figure 55. Life cycle GHG emissions for electricity from energy storage compared to electricity generated from natural gas. 87

TABLES

Table ES1. Comparison of energy storage options for power arbitrage discharge capacity of 500MWe and charging the cost of $30/MWh. iv

Table ES2. Summary of demand response options considered. $30/MWh nuclear electricity cost is assumed in these calculations. vi

Table 3. General hypothetical conditions are used for comparison of uses of nuclear energy in this report. 20

Table 4. Financial parameters are used in the LCOS calculations for the various energy storage options. 20

Table 5. Lithium-ion LFP 2020 and 2030 total installed cost and performance estimates. 21

Table 6. Total installed capital investment cost for HTSE. 22

Table 7. Total Installed cost for PEM fuel cells. 23

Table 8. Energy storage installation costs and performance assumptions for a 500 MW power capacity option for 6 h of storage for lithium-ion (LFP) and H_2 power-storage-power. 25

Table 9. Particle/sCO_2 heat exchanger sizing calculation input/output for the high temperature exchanger. 37

Table 10. Estimated equipment costs for an ETES system with 500 MWe net power generation capacity. 38

Table 11. Energy storage media estimated costs. 39
Table 12. Particle containment CAPEX.[ ] 40
Table 13. Estimated costs for liquid/solid slurry tank with varying cold storage capacity. 40
Table 14. Summary of ETES system LCOS analysis input parameters and key results. 42
Table 15. ETES Process Performance Summary (LWR-integrated process configuration with heat input to CO_2 working fluid; standalone and LWR-integrated processes based on charging cycle with waste heat rejection). 50
Table 16. SH-TES storage media properties. 52
Table 17. Operating conditions of a typical nuclear power plant steam generators. 54
Table 18. Estimated equipment costs for an SH-TES system with 500 MWe net power generation capacity with Hitec as a storage medium. 58
Table 19. Estimated storage capacity dependent costs for Hitec at 6 and 12 hours of storage. 59
Table 20. Estimated total capital investment costs for SH-TES system with 500 MWe net power generation for 6 and 12 hours. 59
Table 21. Summary of LCOS analysis for SH-TES with Hitec as the storage medium. 61
Table 22. Summary of Liquid-Based SH-TES 65
Table 23. Steam accumulator sizing analysis results 67
Table 24. Comparison of energy storage options for power arbitrage discharge capacity of 500MWe and charging cost of $30/MWh. 69
Table 25. Summary of sensitivity of LCOS to charging cost for the various energy storage technologies. 500MWe discharge capacity 70
Table 26. Cryogenic ASU Design 73
Table 27. ASU base case design conditions. 73
Table 28. Comparison of LCCC for MEA and A3C for the different applications at baseline energy cost (Willson, Lychnos et al. 2019). 79
Table 29. CO_2 capture cost from different process effluent sources with amine and cryogenic processes. 80
Table 30. Summary of compression and cryogenic options. Cost of nuclear electricity assumed at $30/MWh. 84
Table 31. Comparison of energy storage options for power arbitrage discharge capacity of 500MWe and charging cost of $30/MWh. 85
Table 32. Summary of demand response options for compression and cryogenics. $30/MWh nuclear electricity cost is assumed in these calculations. 88

Page intentionally left blank

LIST OF ACRONYMS

ANL	Argonne National Laboratory
APEA	Aspen Plus Process Economic Analyzer
ASU	air separation unit
ATC	around-the-clock (price)
CC	combined cycle
CCC	cryogenic carbon capture
CCGT	combined cycle gas turbine
CCS	carbon capture and storage
CFD	computational fluid dynamics
CoP	coefficient of performance
CSP	concentrated solar power
CT	combustion turbines
CTES	concrete thermal energy storage
DoD	depth of discharge
DOE	Department of Energy
DSG	direct steam generation
ECL	external cooling loop
EL	external cooling loop
ETES	electro thermal energy storage
FC	fuel cell
FCEV	fuel cell electric vehicles
FE	Fossil Energy
FIRES	firebrick resistance heat energy storage
FPOG	Flexible Plant Operations and Generation
GH2	gaseous H_2
GHG	greenhouse gas
GREET	Greenhouse gases, Regulated Emissions, and Energy use in Transportation model
HDSAM	Hydrogen Delivery Scenario Analysis Model
HFTO	Hydrogen Fuel Cell Technology Office
HTR	high temperature reservoir
HTSE	high temperature steam electrolysis
HTX	high temperature exchanger
IES	Integrated Energy Systems

IHX	intermediate heat exchanger
INL	Idaho National Laboratory
IPA	Intermountain Power Agency
IPP	Intermountain Power Project
ITC	investment tax credits
L.N	liquid nitrogen
LCCC	levelized cost of carbon capture
LCOS	levelized cost of storage
LFP	lithium iron (Fe) phosphate
LH-TES	latent heat thermal energy storage
LMP	local marginal price
LMTD	log mean temperature difference
LTR	low temperature reservoir
LTX	low temperature exchanger
LWR	light water reactor
LWRS	Light Water Reactor Sustainability Program
MEA	methanol amine
MITA	minimum internal temperature approach
NG	natural gas
NGCC	natural gas combined cycle
NMC	nickel-manganese-cobalt
NPP	nuclear power plants
NPV	net present value
NREL	National Renewable Energy Laboratory
O&M	operations and maintenance
PCM	phase change materials
PEM	polymer electrolyte membrane
PG	polyethylene glycol
PNNL	Pacific Northwest National Laboratory
PTC	production tax credits
PWR	pressurized water reactor
RFC	reversible-fuel-cell
RHX	recuperator heat exchanger
RTE	round-trip efficiency
RTQE	round trip thermal-equivalent efficiency

RWGS	reverse water-gas-shift
SC	simple cycle
SES	Sustainable Energy Solutions
SETO	Solar Technologies Energy Office (SETO)
SHS	sensible heat storage
SOEC	solid-oxide electrolysis cell
SOFC	solid-oxide fuel cell
TCI	total capital investment
TEMA	Tubular Exchanger Manufacturers Association
TES	thermal energy storage
TPE	thermal power extraction
TRL	technology readiness level
UTES	underground thermal energy storage
WTP	well-to-plug

Energy Arbitrage: Comparison of Options for use with LWR Nuclear Power Plants

1. INTRODUCTION

Nuclear energy is increasingly being recognized as a valuable low-carbon, a low-emissions energy source that can help achieve clean energy targets being set by states, commissions, and utilities in the United States. Currently, nuclear power provides about one-fifth of the country's electricity. Nuclear power plants (NPPs) further provide the grid with all-weather season-long baseload capacity that is important to grid reliability and resiliency. Light water reactor (LWR) NPPs in the United States, like other sources of electricity generation, are facing increasing economic pressure due to electricity grid competition from historically low-priced natural gas prices and the rapid expansion of solar and wind energy supported by government subsidies.

Electricity markets are undergoing rapid transition given the advent of low-cost wind and solar energy that is driven as much by policy incentives in the form of investment tax credits (ITCs) and production tax credits (PTCs) for clean energy as it is for least-cost power generation sources. Regardless of public policy and preferences, solar and wind energy is projected to increase in the South/Southwest and Midwest where there is already a high capacity of solar and wind energy. The variable nature of wind and solar energy requires that other dispatchable generation sources respond to load-demand in an increasingly dynamically responsive manner. Figure 3 illustrates the consequences of the buildout of roof-top and utility-scale solar photovoltaic energy. Unable to compete with the marginal cost of electricity production from those sources, NPPs and other baseload generators must either be curtailed or pay solar and wind generators to curtail.

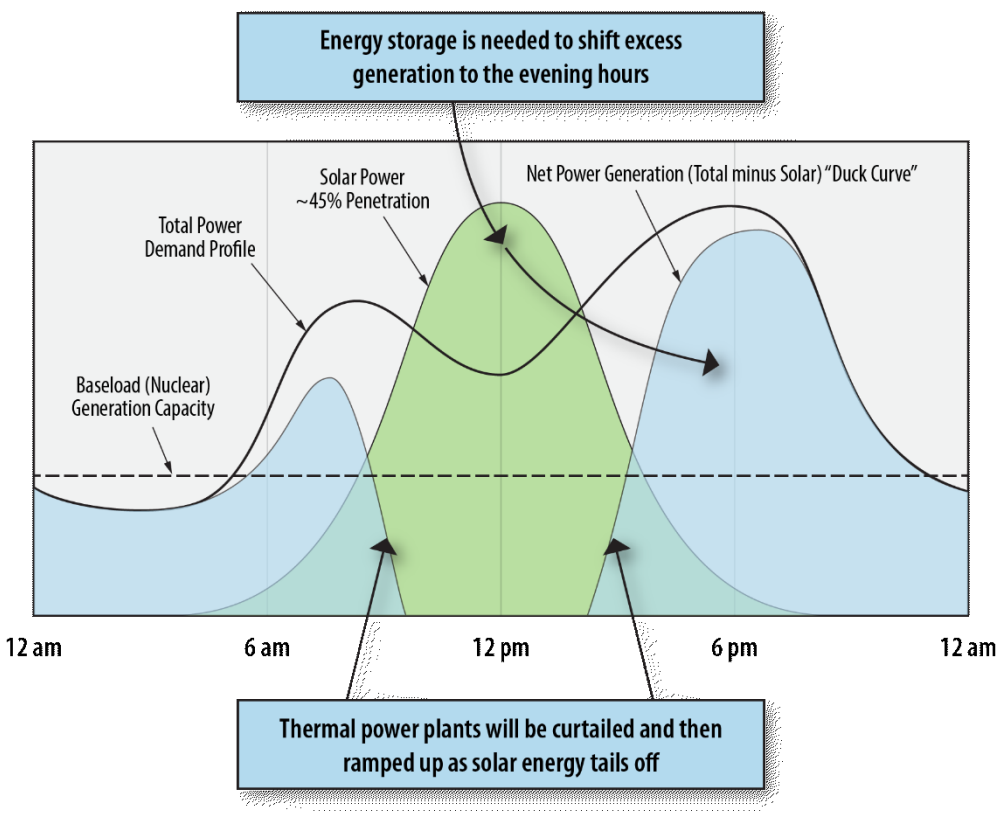

Figure 3. Illustrative consequences of excess solar energy power generation.

Excess generation capacity is having a profound impact, causing minute-by-minute electricity pricing drops during daytime hours. Instances of negative pricing have been experienced and this trend will likely continue. This phenomenon is understood and utilities are seeking options to address this situation. It is the impetus for energy storage solutions that can reserve excess power for late-afternoon and evening power demand as solar energy tails off. It has motivated utility-wide demand response studies and the implementation of smart appliances.

Wind energy has a similar impact on the grid, load-matching generation demand—except greater uncertainty in wind output increases uncertainty in net load makeup that must be met with conventional generators. Variation in wind-generation output also requires steeper ramp rates and range.[1]

In most regions of the country, but especially in the Northeast, Midwest, and Southeast, low-cost natural gas is leading to the retirement of coal-fired power plants. The load is shifting to natural gas turbines. This, too, is having a profound impact on the prices of electricity wholesale markets which ultimately impacts NPP revenue.

1.1 Energy Arbitrage

Considering grid-market fluctuations, the notion of energy arbitrage is becoming increasingly important to NPPs. Arbitrage is the opportunistic buying and selling of a commodity during local pricing valleys and peaks respectively in order to maximize economic value. The concept is to simply generate and sell the most energy possible to the highest price taker. For the electricity market, the highest prices occur during the periods when demand is higher than the set of least-cost generation sources. NPPs can also look to non-electricity markets to sell energy, although the possibility of doing this may be tied to grid regulations and utility market structures, and local or state policy. However, in theory, the current fleet of LWR NPPs has five potential operating options:

- *Traditional Baseload*. The NPP operates as a baseload power station, at near full capacity except during regular outages to refuel and perform maintenance or plant upgrades. This mode of operation is declining in the United States as baseload capacity demand shrinks with increasing variable generation in both deregulated and regulated markets, and as the selling price of electricity—locational marginal price (LMP), or the around-the-clock (ATC) price—falls below the total electricity production cost of nuclear stations.
- *Flexible Plant Operation*. A nuclear power station dispatches power by ramping down and up to meet the electricity-market demands meaning "net power for load minus variable generation." Besides selling less electricity throughout the year, this mode of operation could impact revenues due to lower usage, higher maintenance costs, and impacts on the fuel cycle.
- *Dedicated Energy Park*. A traditional nuclear power-generation station is dedicated to selling power and thermal energy (steam or a secondary heat-delivery loop) to one or more energy users according to the energy demands of the user or users under a direct energy purchase agreement. This paradigm will require a coordinated buildup of energy users near the power plant where a dedicated, off-the-grid, power-line, and heat-delivery system supplies energy to industrial users. An earlier market study by Idaho National Laboratory (INL) and the National Renewable Energy Laboratory (NREL) showed a wide variety of industrial users could take advantage of low-cost steam produced by an LWR.[2] A follow-on effort by the LWRS Program was completed in June 2020, considered markets located within a reasonable reach of NPPs.[3]
- *Hybrid Operations*. The nuclear plant participates in the electricity grid market while apportioning electricity or thermal energy to one or more energy users and/or energy storage according to market signals. The purpose of this mode of operations is to maximize revenue for the nuclear plant. The business case for hybrid options depends on the efficient use of both the energy and the capital of the overall system. Hybrid operations will usually require energy storage to ensure a constant supply of energy is sent to the industrial manufacturing plant. Hybrid operations could open the potential for the

nuclear plant to be used as either spinning or non-spinning reserves when the industrial customer rapidly ramps down energy use and gives up the electricity to the grid. Once the grid load generation is stabilized by reduced demand or other capacity reserves, the industrial user will ramp back up to normal operations. If the industrial energy user involves large resistive loads, then it may also be possible to provide voltage or frequency regulation by taking up or giving up power to the grid in a matter of a few seconds or less. The industrial loads tied to the nuclear plant can also be curtailed or increased to adjust the power factor of the grid.

- *Power Revenue Optimization*. The nuclear plant produces and stores energy during periods of oversupply to dispatch additional electricity to the grid during periods of scarcity. This mode of Flexible Plant Operations and Generation (FPOG) can also be considered a special case of hybrid operation. It is unique in the sense that power revenue may be optimized with energy storage (in thermal, electrical, or chemical forms) with the pure motive of regenerating electrical power to send to the grid. In this case, new concepts for energy diversion will be required that are similar to hybrid operations.

All but the first option constitute a form of FPOG and subscribe to the goal of optimizing the revenue of each of the participating partners. FPOG operations are naturally becoming necessary in regions of the country where wind or solar energy is increasing and in regions where the low-cost and high availability of natural gas has driven down the price of electricity. Many nuclear plants have responded to increasing volatility in net demand by operating flexibly. Although this practice preserves the contribution of nuclear energy to grid stability, it does not reduce plant operating costs; instead, it increases the cost of nuclear-sourced electric power ($/MWh) as the fixed costs of operations are allocated to a lower production base. Nor does it represent full asset usage from a capital investment standpoint.

Figure 4 illustrates the concept of FPOG hybrid plant operations. The NPP dispatches power to the grid or sends steam and electricity to an industrial user. In this manner, the nuclear reactor can produce nonelectric products during periods of excess power-generation capacity when these plants are not able to clear the day-ahead electricity market. This practice preserves the contribution of nuclear energy to grid stability and reduces economic losses associated with negatively priced electricity sales. It provides an offtake for energy produced by a nuclear power generating station when the price offered for committing electricity to the grid is lower than the cost of producing this electricity. A secondary user benefits by purchasing electrical power, steam, or thermal energy directly from the NPP at a cost that is presumably lower than can be purchased from the grid at either the electricity transmission-customer level or the electricity distribution-customer level.

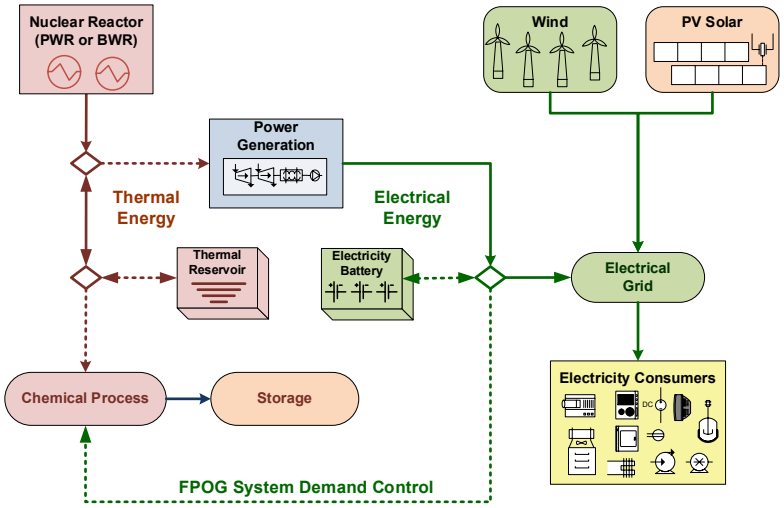

Figure 4. Flexible Plant Operation and Generation concept for nuclear power plant.

Utility companies are beginning to add utility-scale battery storage to help smooth the spikes and overgeneration exacerbated by non-dispatchable variable resources, but the size of battery storage needed and the expense of it will mean that there will be a continued opportunity for baseload generators, such as NPPs, to provide electricity to the grid when solar- and wind-energy installations are producing little output. Therefore, the U.S. Department of Energy (DOE) Light Water Reactor Sustainability (LWRS) Program is addressing flexible plant operations that can diversify the use of energy and the revenue of NPPs. Parallel with the LWRS Program, the Department of Energy, Office of Nuclear Energy (DOE-NE), Integrated Energy Systems (IES) Program, led by INL, researches how to best integrate thermal-energy storage technologies with industrial heat producers (e.g., nuclear plants, coal plants, natural gas peakers) to ensure stability and economic viability.

Previous reports have evaluated opportunities to couple LWRs with hydrogen production and other industrial processes to use LWR energy during off-peak times.[4,5,6,7,8,9,10] The preponderance of these reports indicates NPPs that providing electrical and thermal power to water-splitting electrolysis plants can competitively produce hydrogen for industrial use when either marginal clean-energy credits similar to those currently extended to wind and solar energy are realized or when by-product oxygen sales or electricity market-capacity payments are taken.

1.2 Scope of this Report

The goal of this report is to analyze energy-storage technologies that can be integrated with existing LWRs. Energy storage as well as demand response options, are here discussed. The energy-storage options are those which store electrical or other forms of energy so that, at a later time, the energy may be released to generate electricity during peak grid demand. Demand response refers to loads that are dispatchable and can use energy during off-peak times but go on stand-by during peak grid demand in order to free up energy for the grid. The demand-response options considered are large-scale loads that can provide a disposition for large amounts of off-peak nuclear energy when needed while also providing a value-added product or service. These demand-response options are not meant to be an exhaustive list; instead, they provide a subset of options for consideration.

This report first analyzes three main options for LWR energy storage during off-peak times for the purpose of generating electricity at peak electricity pricing: hydrogen, batteries, and thermal energy. First, the storage of energy in the form of hydrogen is discussed. For the purposes of this report, the hydrogen is assumed to be produced via coupling of a high-temperature steam electrolysis (HTSE) solid-oxide electrolysis (SOEC) production facility with an existing LWR NPP. This topic has been studied and reported extensively elsewhere in the previous reports mentioned; therefore, the current analysis will focus on storage costs and round-trip power-to-storage/storage-to-power (or to be short, power-storage-power). Hydrogen storage and conversion to electricity, as well as reversible systems, are compared to the storage of energy in a conventional state-of-the-art battery system and conversion to electricity in terms of duration of storage, capacity of storage, energy efficiency, and cost of storage. Various analyses on specific thermal-energy storage for power-storage-power options are provided. For background, a short review on the state-of-the art in thermal-energy storage is found in the appendix, which mainly recapitulates prior works of the authors that embody the larger effort by DOE under the Solar Technologies Energy Office (SETO) and Office of Fossil Energy (FE). The various forms of thermal-energy storage are highlighted to provide a relevant understanding of the value of future work that may be supported by LWRS research and development.

Next a cursory evaluation of some large demand response options are analyzed. Options discussed include production of liquid nitrogen via air separation and liquefaction, liquefaction of hydrogen, compressed hydrogen, and cryogenic capture of CO_2. Unlike the energy storage options, these options do not entail conventional energy storage in the sense of being able to regenerate electricity to support grid needs. The end result would instead be demand dispatch to aid nuclear power stations in avoiding power

turndowns by having an alternative disposition for the electrical energy in order to produce marketable products (liquid nitrogen and hydrogen, captured CO_2).

2. NUCLEAR POWER-STORAGE-POWER

One energy-storage technology that is beginning to be widely deployed at the utility-scale is battery storage. Any energy-storage technology will need to be contrasted with battery storage and be competitive in terms of capital expense, duration of storage, cycle time, round-trip efficiency, and overall quality of investment. This section begins by citing the current state of the art of battery storage—namely, Li-ion batteries—for comparison to other energy-storage technologies to be discussed. Hydrogen production via HTSE is one technology that may pair well with an LWR, as analyzed in studies already cited. The production of hydrogen to be stored and later converted to electricity is then compared with utility-battery energy storage. Next, a sample thermal-energy storage concept (electro-thermal energy storage [ETES]) and various permutations thereof are evaluated to gain an appreciation for the comparative potential of this option for nuclear energy arbitrage.

For comparison, the following conditions in Table 3 represent a general hypothetical region in the U.S. which will be used throughout this report.

Table 3. General hypothetical conditions are used for comparison of uses of nuclear energy in this report.

Capacity / Duration of Storage	3000 MWh (500 MWe for 6h) 6000 MWh (500 MWe for 12h) 9000 MWh (500 MWe for 18h)
Cost of charging (electricity cost assumed)	$30/MWh

Levelized cost of storage (LCOS) for the various options discussed will be calculated using the methodology described in Lazard LCOS v6.0 [11]. The financial parameters used in these LCOS calculations are listed in Table 4.

Table 4. Financial parameters are used in the LCOS calculations for the various energy storage options.

Financial Parameters for LCOS Calculations	
Debt Fraction	60%
Discount rate for debt	5%
Equity Fraction	40%
Discount rate for equity	10%
Combined Tax Rate	26%
Contract Term / Project Life	20

2.1 Energy Storage Using Lithium-Ion Batteries

"Lithium-ion" is a general term for a class of batteries that can refer to a wide array of chemistries; however, it ultimately consists of a battery based on charge and discharge reactions from a lithiated metal oxide cathode and a graphite anode. One of the more commonly used lithium-ion chemistries is lithium iron phosphate (LFP) and nickel-manganese-cobalt (NMC). These batteries are used in a variety of ways, especially for grid-scale applications.[12] A recent report[12] on energy storage cost and performance published by Pacific Northwest National Laboratory (PNNL) estimated the installed cost for different energy storage options like lithium-ion LFP and NMC batteries. The report has estimated the cost and performance of lithium-ion LFP batteries for the year 2020 and 2030. These cost estimates are for 1–100 MW batteries and for the time duration of 2–10 hrs. These cost estimates were used to calculate the

cost of a 500-MW-capacity storage system. For lithium-ion batteries, the rate of discharge is twice that of the rate of charge. This was factored into the sizing and installed cost calculation, assuming that the discharge load will not change and is continuous.

The performance metrics for these batteries are 10-year calendar life, round-trip efficiency of about 86–88%, and 5% downtime. Table 5 shows these cost estimates tabulated for lithium-ion LFP batteries for 2020 and 2030.

Table 5. Lithium-ion LFP 2020 and 2030 total installed cost and performance estimates.

	Capacity	Total Installed Cost ($/kWh)					Round Trip Efficiency %
		2hr	4hr	6hr	8hr	10hr	
2020	1 MW	519	448	424	410	402	86%
	10 MW	461	411	393	383	377	
	100 MW	427	385	370	362	356	
2030	1 MW	378	317	297	286	280	88%
	10 MW	330	289	274	266	261	
	100 MW	305	270	258	251	247	

The total installed cost includes the costs for the energy-storage system (storage system and power equipment), project development, construction, grid integration, etc. For this analysis, we have considered the cost for a 100 MW power system with an energy duration of 10 h (the longest considered in the PNNL report) and extrapolated the cost linearly for energy-storage generating capacity of 500 MW with 6, 12, and 18 h duration. The total installed cost for the 100 MW systems for the year 2020 and 2030 were estimated to be $356/kWh and $247/kWh,[13] respectively. The round-trip efficiency of 86% and depth-of-discharge (DOD) for this battery system were assumed to be 86 and 80% in 2020. In the following sections, this battery system's total installed cost is compared to costs for hydrogen energy storage for a range of 0–10,000 MWh or 0–5 days of storage.

2.2 Hydrogen Production, Storage, and Power Generation

2.2.1 HTSE CAPEX (Current and Future)

Hydrogen-production costs from HTSE were reported separately by the DOE Hydrogen and Fuel Cell Technology Office (HFTO) record of 2020[14] and also by an internal INL integrated LWR-HTSE analysis which will soon be released as a separate report. The installed capital cost for a high-temperature electrolyzer producing 50 MT/day of H_2 was estimated using reported cost estimations on costs for the electrolyzer stack, installation, and balance of plant. It should be noted that generally, the cost of all centralized process plants decreases with scale-up, which applies to the balance of plant, but the electrolyzer system is modular, so the decreases are less pronounced with these components and increasing scale. The average NPP is capable of producing more than 600 MT/day of hydrogen. Therefore, the analysis that follows is considered conservative with respect to hydrogen production, but the trends that are observed are considered accurate for the purposes of comparing batteries to hydrogen production and storage.

Current and future technology, based on assumed improvements and a learning curve, were evaluated. The total installed capital cost for the HTSE system per kilowatt is shown in Table 6.

For this analysis, it is assumed that the electrolyzer will produce hydrogen that will be stored and converted back to electricity using a polymer electrolyte membrane (PEM). For a 500-MW-capacity HTSE producing H_2 for several hours, the HTSE size remains constant, and the PEM fuel-cell size will change with the hours available for discharge. H_2 production efficiency for HTSE is assumed to be 89% (HHV).

Table 6. Total installed capital investment cost for HTSE.

	INL Internal Report 2020 ($/kW)	INL Internal Report ~2030 ($/kW)	HFTO DOE 2035 ($/kW)
Total installed capital cost	742	446	576
H_2 production efficiency	88%	89%	89%

2.2.2 Hydrogen Storage (Geological and Physical)

Both geological and physical storage options were considered for this analysis of energy storage using hydrogen, given the diverse geographical location of NPPs. Hydrogen can be compressed and stored in physical tanks or stored underground in geological formations such as salt caverns or domes. Figure 5 shows two different maps of the availability of geologic storage across the U.S. that roughly agree. The majority of existing LWRs in the U.S. would require physical hydrogen storage if paired with an HTSE hydrogen plant. About ten existing NPPs may have the option to store hydrogen in a geological formation.

An example is the Intermountain Power Project (IPP), owned by the Intermountain Power Agency (IPA), which will install a gas turbine capable of burning a mix of natural gas and hydrogen on the site of an existing coal power plant and build an energy-storage and arbitrage system based on hydrogen at a facility in Delta, Utah, near the Sevier River Basin bedded salt formation (see Figure 5). The produced hydrogen will be stored in the salt dome. The stored hydrogen will be used to generate electricity during peak periods. The gas turbine system that will be built will first burn up to 30 vol% H_2 with natural gas and, later, up to 100% H_2 [15,16,17,18].

For geologic storage, H_2 can be stored at low-cost and in large quantities. Geologic storage needs a cushion gas (minimum amount of gas that must be left in storage) which, for natural gas, is about 15% of the storage capacity. For hydrogen, it is near 30% of the total storage capacity. The estimated cost for geological storage varies by scale and location between $36 and $38/kg H_2. For the base case analysis, it was assumed to be $38/kg for large salt caverns, including the cost of the cushion gas and the compressor [19]. Geological storage of H_2 is not viable for small quantities (10–30 MT), and physical storage should be considered. Geological underground storage in salt caverns should be considered beyond 30 MT because it would be economically viable.

For physical storage, hydrogen can be stored in banks of pressure vessels. This option requires a large space for storage due to the low volumetric density of gaseous hydrogen, and so it increases the amount of land area required. It is desirable to store hydrogen at high-pressure to increase its volumetric energy density, but due to the disproportionate increase in the cost of storage with pressure, a trade-off must be made between the real estate value and the pressure-vessel costs. [20] The uninstalled cost of physical storage is approximately $450/kg H_2, [21] and the installation cost is assumed to be 30% of this uninstalled cost.

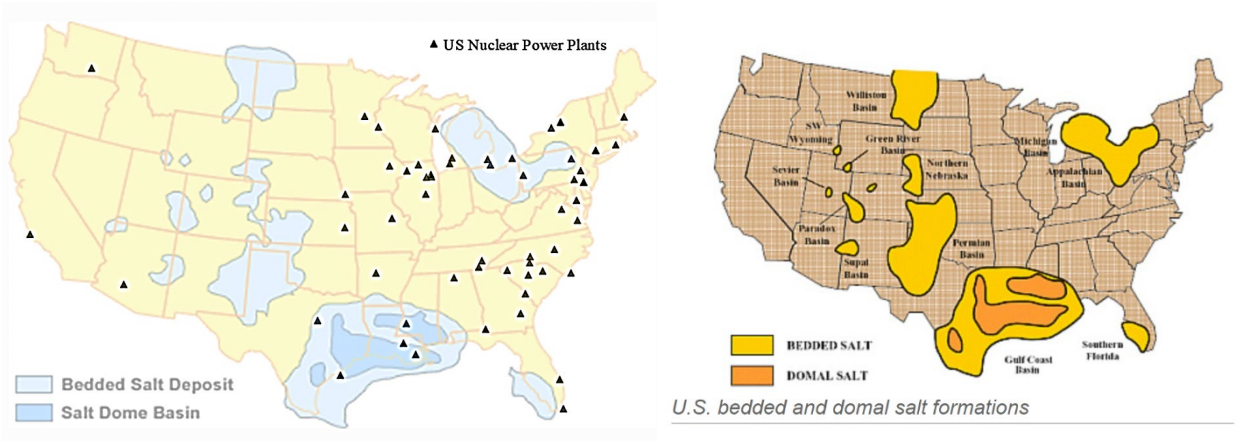

Figure 5. U.S. Salt Deposits for Geological Storage with overlayed locations of U.S. NPPs[22,23,24].

2.2.3 Hydrogen Transportation

In the present study, it is assumed that hydrogen production and storage are closely coupled and performed in the same location. Hence, the costs of hydrogen transportation will not be considered in this analysis.

2.2.4 Hydrogen to Power[25] – Fuel Cells

The few options for conversion of hydrogen back to electricity include fuel-cell technologies, reversible solid-oxide fuel cells/solid-oxide electrolysis cell (SOFC/SOEC), blending hydrogen with natural gas in gas turbines, and advanced hybrid power cycles SOFC/gas turbines. Separate efforts are underway to understand the best approach to produce hydrogen and convert it back to electricity. Presently, PEM fuel cells deliver high power density and are used in stationary applications.[26] Briefly, PEM fuel cells use a solid polymer as an electrolyte and porous carbon electrodes containing a platinum or platinum alloy catalyst. They are typically fueled with pure hydrogen supplied from storage tanks. PEM fuel cells operate at relatively low temperatures, around 80°C, and require that a noble-metal catalyst (typically platinum) be used to separate the hydrogen's electrons and protons, adding to system cost.

PEM fuel-cell stack cost estimates reported by the energy-storage and performance database at PNNL were used and are tabulated in Table 7. The total fuel-cell cost includes the fuel-cell stack cost, inverter, controls and communication, and grid-integration cost. The base case considers a total PEM fuel-cell cost of $1011/kW. These costs have been combined with the total installed cost for electrolyzer and H_2 storage and have been plotted alongside the estimates for battery energy storage in Figure 7 and Figure 8

Reversible-fuel-cell (RFC) technology was also considered which could improve the outlook for hydrogen storage and power-to-storage/storage-to-power options. The projected costs for these PEM RFC were reported at the DOE HFTO 2020 AMR[27] and are noted in Table 7.

Table 7. Total Installed cost for PEM fuel cells.

	PEM Fuel Cells			PEM Reversible Fuel cell (2030)	
	Base	High	Low	High	Low
Fuel Cell Capital Cost ($/kW)	$1,011	$1,550	$911	$1,750	$1,250
System Efficiency (HHV) (%)	50%			40%	50%

2.2.5 Hydrogen to Power – Gas Turbines

INL has separately performed an analysis of the economics of hydrogen generation, storage, and usage in gas turbines in up to a 30vol% mix of hydrogen with natural gas for energy storage.[28] This analysis was done in the Arizona region where large expansions of solar energy are continuing. The analysis uses forecasts of electricity grid pricing for 2025 and 2030 with 2030 showing a larger spread between the average highs and lows, with more frequent hours of negative electricity prices.

Figure 6 displays the hydrogen system, which involves purchasing electricity from the grid during low-priced hours, performing low-temperature electrolysis of water using PEM units, storing the hydrogen in trailers, and co-firing it at a natural gas turbine at 30% hydrogen by volume for selling electricity back to the grid during high-priced hours.

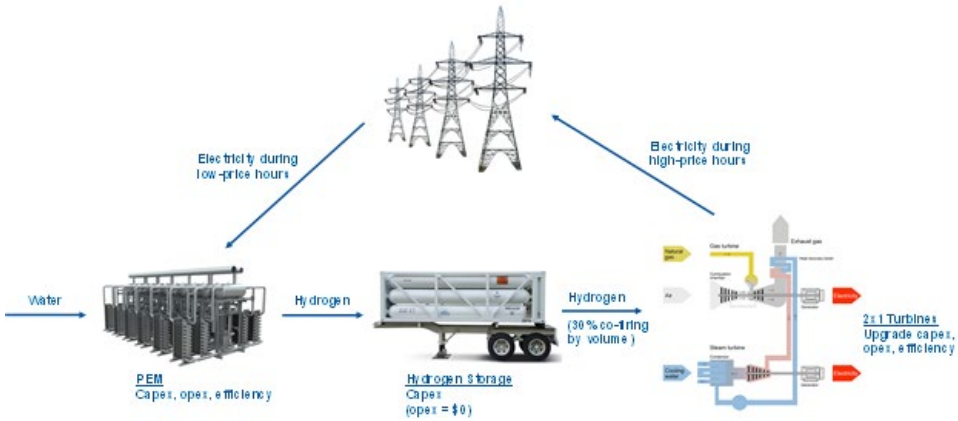

Figure 6. Hydrogen production, storage, and co-firing through natural gas turbines.

The system is assumed to follow a repeating diurnal pattern of hydrogen production (buying electricity during low-priced hours) and usage (selling electricity during high-priced hours). The analysis ordered hourly electricity price forecasts to determine the prices at which electricity would be bought and sold across a range of discharge duration per day. The necessary number of electrolyzers and hydrogen storage capacity were also calculated for each discharge duration. Total costs for the hydrogen co-firing system account for CAPEX, fixed and variable O&M expenditures, and net arbitrage profits from daily electricity purchases and sales. Additional details on the analysis are discussed in the forthcoming report cited above. LCOS calculations were performed with the parallel methodology used for all other energy storage options in this report for 6 and 12 hours of storage and the results are included in Table 24 and Table 25.

2.2.6 Hydrogen to Power versus Li-ion LFP Batteries to Power

Figure 7 and Figure 8 compare battery energy storage to hydrogen energy storage. Li-ion LFP batteries are compared to hydrogen production storage and usage via SOEC for hydrogen production and PEM for hydrogen to power as well as PEM RFC (Power-Hydrogen-Power) for hydrogen stored physically and geologically. The energy storage systems were sized by assuming that they are discharging for 6 hr (3000 MWh), 12 hr (6000 MWh), and 18 hr (9000 MWh). The electrolyzer and fuel-cell costs for these cases are tabulated in Table 8.

For energy storage using hydrogen, the electrolyzer, hydrogen-storage, and fuel-cell costs are included for a 500-MW-capacity system. Using hydrogen as energy storage for less than 3 hr (1500 MWh) has a higher installed cost due to the capital cost of the electrolyzer, hydrogen-storage system, and fuel cells. This is a generally accepted conclusion, that at lower energy-storage amounts and

for shorter durations, batteries are very competitive. But at higher amounts of energy storage, hydrogen energy storage becomes more advantageous than batteries. The cost of storing energy in lithium-ion batteries (2020 and 2030) over 4–5 hr (500 MW capacity) or over 2000–2500 MWh is more expensive than hydrogen energy storage.

Table 8. Energy storage installation costs and performance assumptions for a 500 MW power capacity option for 6 h of storage for lithium-ion (LFP) and H_2 power-storage-power.

Energy Storage Technology (500 MW)	Discharge in 6 hrs. (MWh)	Total capital cost ($MM)		Roundtrip Efficiency (RTE)	Storage Usability factor
		Geological H_2 Storage	Physical H_2 Storage		
HTSE -H_2 -PEM FC (Base)	3,000	1500	1644	33-50%[a]	G-70%[b] P-80%[b]
HTSE -H_2 -PEM FC (High)		1769	1913		
HTSE -H_2 -PEM FC (Low)		1184	1594		
PEM RFC H_2 (High) (2030)		882	1026		
PEM RFC H_2 (Low)		507	651		
Battery (2020)		2484		86%	80%
Battery (2030)		1684		88%	

38% Round Trip Efficiency (RTE) with SOEC HTSE and PEM Fuel Cell; 40-50% for PEM-RFC.
Geological storage (G) requires higher cushion gas over Physical storage (P)

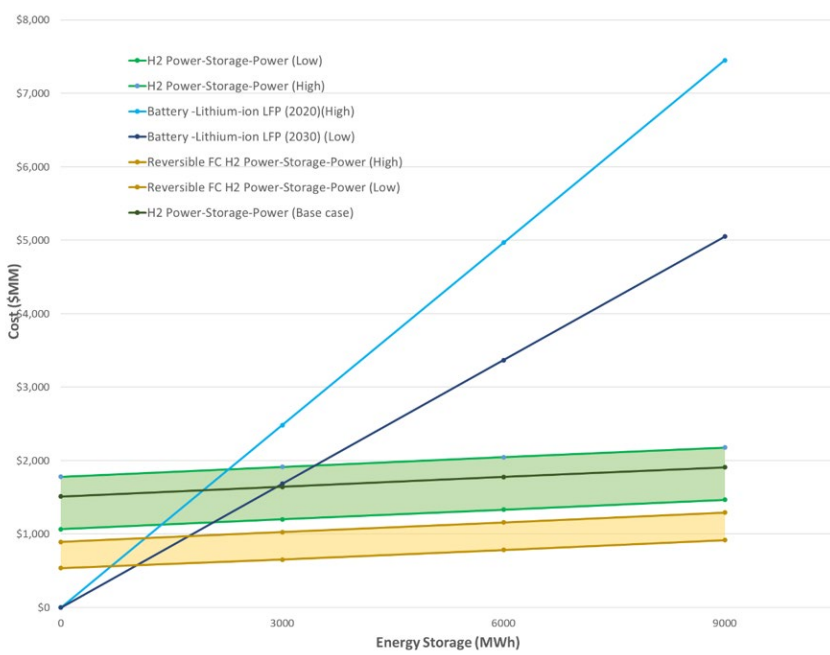

Figure 7. Energy storage cost comparison for lithium-ion (LFP) batteries and H_2 (using HTSE-SOEC for H_2 production and PEM FC for H_2 to power). Physical hydrogen storage at 1500–2000 psi. $30/MWh system charging cost used. 500 MW charging capacity.

The base case cost for HTSE hydrogen production is assumed to be $742/kW and for H_2 to power PEM fuel cell is $1011/kW and PEM RFC. Hours of storage are 6, 12, and 18 h for 3000, 6000, and 9000 MWh, respectively.

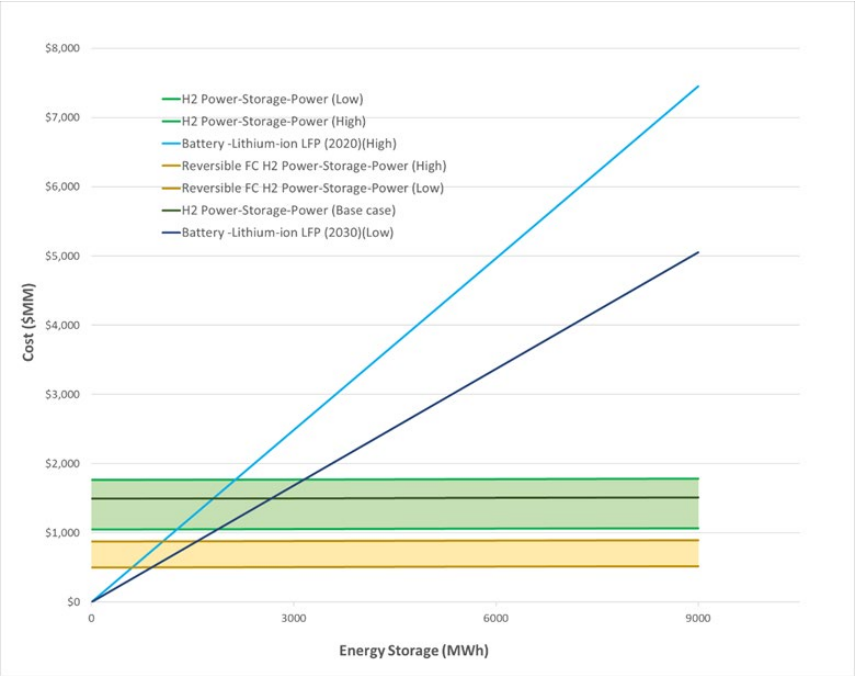

Figure 8. Energy-storage cost for lithium-ion (LFP) battery and H_2 (using SOEC for H_2 production and PEM for H_2 to power). Geologic hydrogen storage at 1500–2000 psi. $30/MWh system charging cost used. 500 MW charging capacity.

The LCOS was calculated in terms of energy for lithium-ion LFP batteries and geological storage of hydrogen at different time intervals for discharging and for a cost of charging of $30/MWh. To calculate the levelized cost system performance, CAPEX and OPEX were considered. The financial parameters listed in Table 4 were used. Figure 9 shows levelized cost for energy storage using lithium-ion batteries for 2020 and 2030 with discharge duration. Figure 10 shows the LCOS for Power-Hydrogen-Power case with geological and physical storage for discharge duration and discharge intervals.

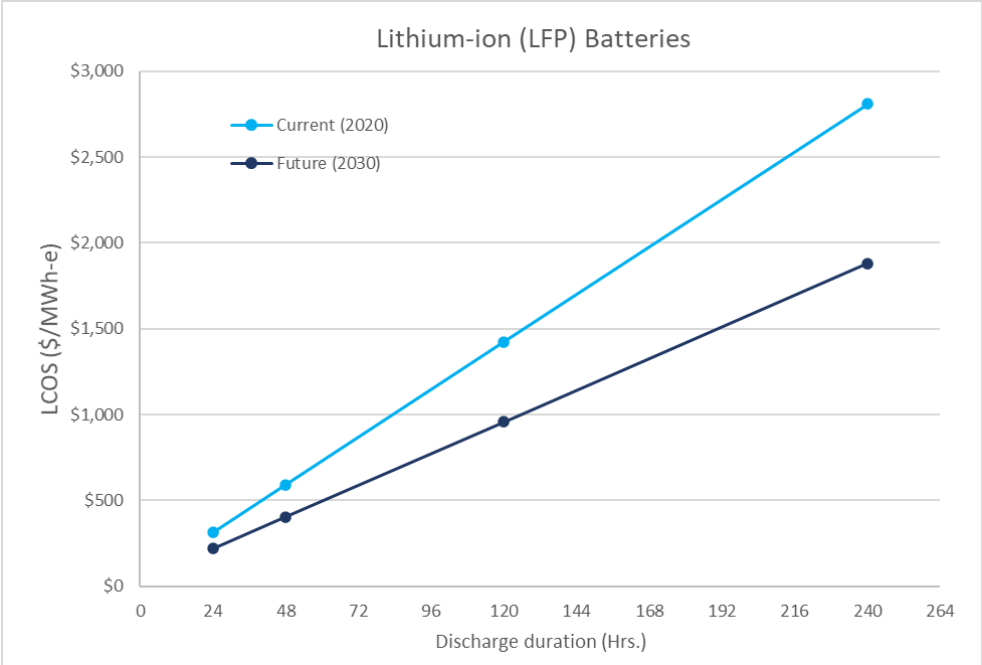

Figure 9. LCOS for Lithium-ion LFP batteries.

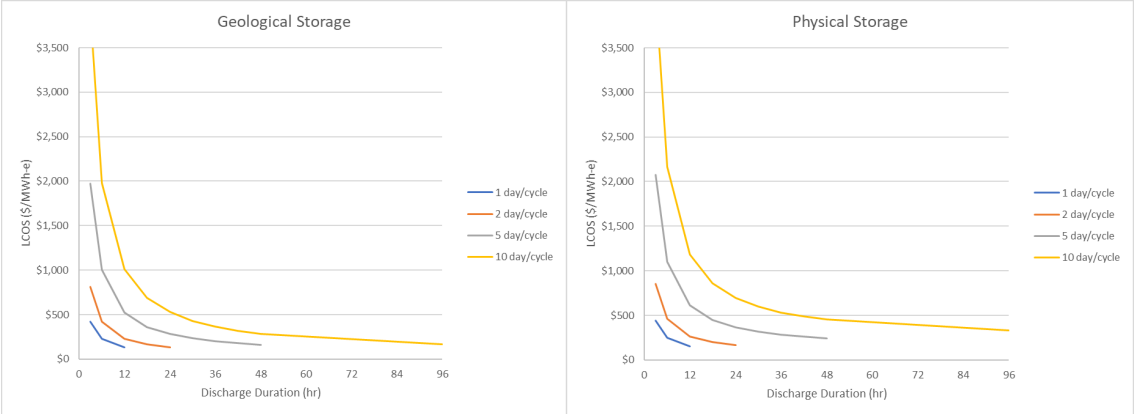

Figure 10. LCOS for Power-Hydrogen-Power (geological and physical storage). SOEC assumed for H_2 production and PEM for H_2 to power.

Figure 11 shows the LCOS as a function of the electricity charging cost for hydrogen geological and physical storage systems for storage durations of 6 and 12 hours.

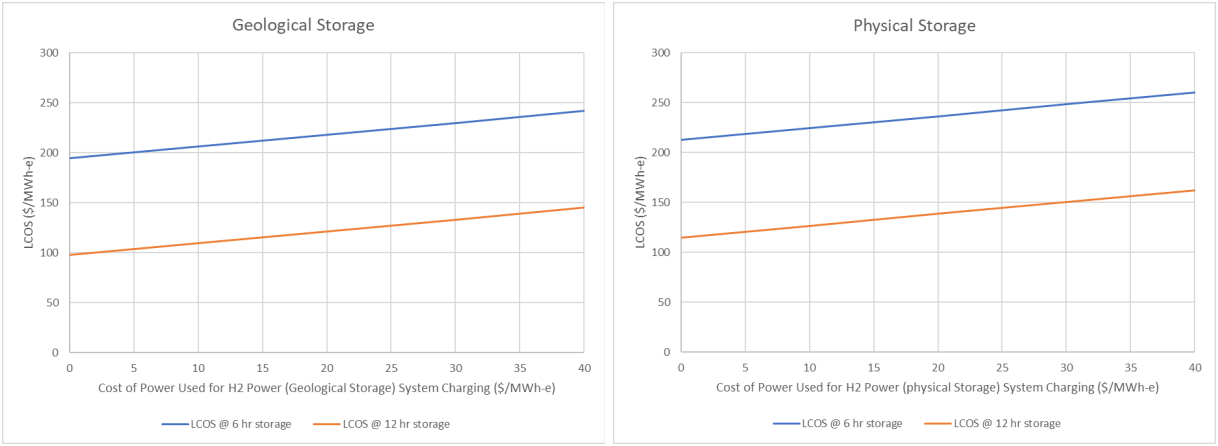

Figure 11. LCOS of hydrogen to power (geological and physical storage) as a function of the charge mode power cost (electricity cost). SOEC is assumed for H_2 production and PEM for H_2 to power.

A detailed LCOS comparison for hydrogen power (geological and physical storage) systems operating with selected discharge intervals/durations and charging costs are shown in Figure 12. The data series shown in blue is representative of hydrogen power systems operating with a constant charging energy cost of $30/MWh-e. The data series shown in orange is representative of a hydrogen power storage system with a rough average forecast time-dependent charging electricity cost based on the 2030 hourly energy market prices projected for the Palo Verde Hub as represented in the public Arizona Public Service 2020 integrated resource plan. As can be seen, the forecasted average data lowers the LCOS for each case due to the larger spread between the highs and lows and the electricity market price valleys being predicted to be consistently lower.

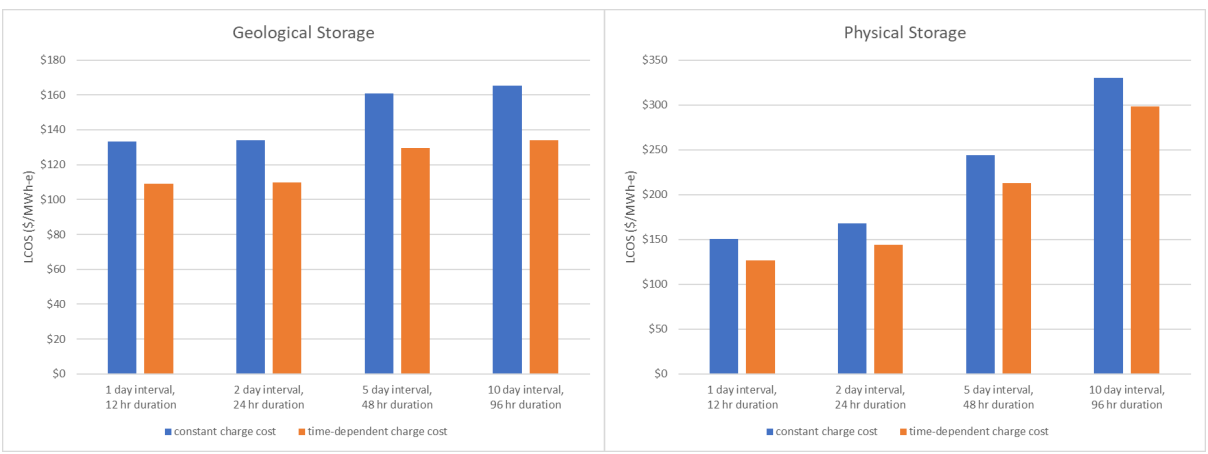

Figure 12. LCOS comparison for hydrogen to power (geological and physical storage) systems operating with selected discharge intervals/durations and charging costs. SOEC assumed for H_2 production and PEM for H_2 to power.

A sensitivity analysis shown in Figure 13 was performed on LCOS by varying various selected parameters (i.e. charging cost, total capital investment, DOD, debt fraction, cost of equity, cost of debt, and system efficiency).

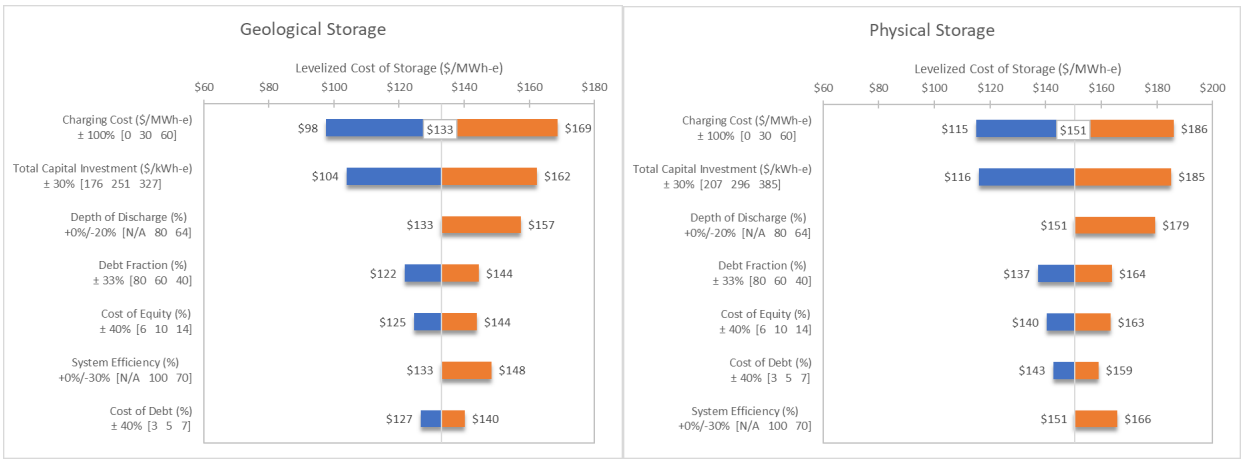

Figure 13. Tornado chart illustrating sensitivity of hydrogen to power (geological and physical storage) LCOS to selected parameters. SOEC assumed for H_2 production and PEM for H_2 to power.

2.3 Thermal Energy Storage

Thermal Energy Storage (TES) is a technology that accumulates and releases energy by heating, cooling, melting, or solidifying a storage medium so that the stored energy can be used later by reversing the process for various application, including power generation. TES could also provide a buffer between the NPP and the grid.

To enable TES integrated with LWRs, multiple studies [29, 30] have sought to understand the tie-in for thermal-power extraction (TPE) from an LWR for TES and other uses. The effects on the LWR have been analyzed to minimize impacts, such that LWR operations could continue without any impact to the LWR or its operating license. Given this new reality, innovations in energy storage via electrical, mechanical, chemical, electrochemical, and thermal means are under development globally in an attempt to achieve economic viability for these technologies. Of these, TES has long been viewed as a possible option for grid stability and integration of variable generators due to its low-cost potential, technology readiness level, and ability to be integrated with existing or future thermal power plants such as NPPs, natural gas combined cycle (CC) combustion turbines (CTs), etc.

To accommodate the vast array of possibilities, INL is developing a library of high-fidelity process models in the Modelica modeling language since early 2013. This repository, known as HYBRID, has dynamic thermal-storage models of concrete, phase-change materials (PCMs), thermoclines, and two-tank sensible heat systems. Additionally, a recent report[31] analyzed ten TES technologies for potential near-term coupling with LWRs, and used thirteen weighted figures of merit to rank them. This analysis concluded that sensible-heat TES systems that use concrete, molten salt, and thermal oil, as well as steam accumulators, ranked high for coupling with NPPs. The FOMs used in the analysis are presented in Appendix C-4.

Although several technologies are attractive candidates, the work presented herein focuses primarily on sensible-heat storage systems based on sand, molten salt, and thermal oil, as well as steam accumulators. SHS systems and steam accumulators are of high technology readiness level (TRL) and have been deployed at a large scale in concentrated solar-power plants and coal-fired power plants. This report also analyzes a novel system, ETES, currently under development. The following sections present the overview of those technologies, the operating conditions chosen, and assumptions made to conduct the analysis, as well as the results and conclusions acquired from the study. An overview of the state-of-the-art of several other existing TES systems is also included in an appendix to this report.

2.3.1 Echogen Electro Thermal Energy Storage

Echogen is a small business focused on innovative power systems. Echogen is developing an ETES[32,33,34] concept that converts electricity to thermal energy for storage. When needed the thermal energy is converted back to electricity. The conversions from electricity to thermal energy and back to electricity are done using a supercritical CO_2 power cycle. The charging cycle is essentially a heat pump cycle and the discharging cycle is a heat engine cycle. In charging, electricity is used to drive a compressor to produce heat for hot storage and expansion of the working fluid is used to produce cooling duty for cold energy storage. In discharging, thermal energy extracted from the hot reservoir is used as input to the heat engine for electricity generation while the cold reservoir improves the performance of the process. This process is illustrated in Figure 14.

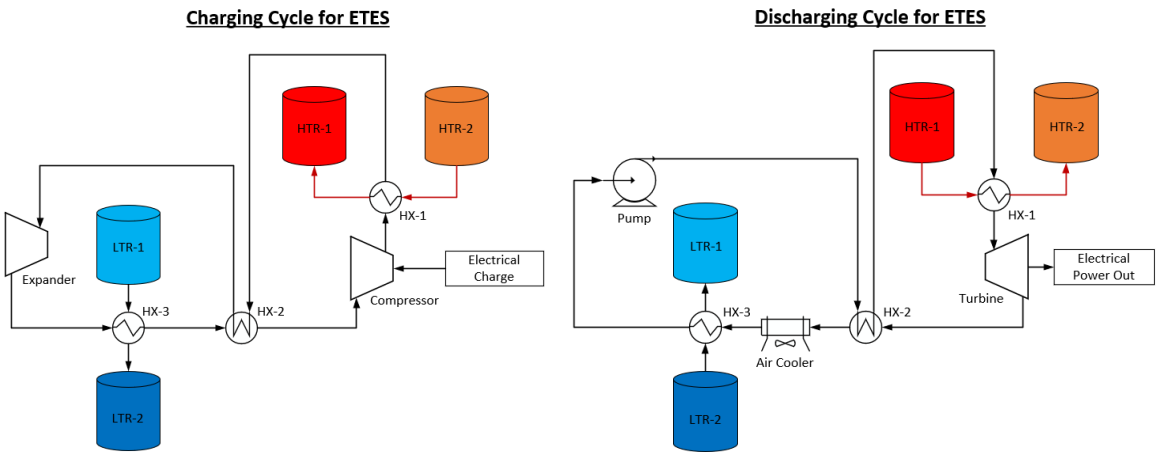

Figure 14. Process flow diagrams of the Echogen ETES charging and discharging cycles. Figure adapted from diagrams presented in Echogen technical documents[32,33].

The following analysis is not meant to be an exact analysis of Echogen's process. It is instead meant to be a preliminary high-level look to evaluate the potential benefits of this type of process. Some permutations to show the possibility of integrating nuclear heat are also shown.

2.3.1.1 System Performance Evaluation

A preliminary performance evaluation of an ETES system based on the Echogen process configuration was performed using AspenTech HYSYS process simulation software. Carbon dioxide was specified as the ETES system working fluid and the REFPROP Equation of State was used for the computation of fluid properties. Figure 14 illustrates the ETES flowsheet modeled in this analysis.

The preliminary process evaluation specifies the use of sand particulate TES media in the high-temperature reservoir (HTR). The HTR configuration evaluated includes separate high and low-temperature particle containment vessels or bins. The HTR high and low-temperature containment vessels store particles at temperatures of 390°C and 125°C, respectively.

The process evaluation specifies a 10% propylene glycol (PG) aqueous solution as the low-temperature reservoir (LTR) cold storage media. The LTR configuration evaluated is a single-tank configuration in which freezing/thawing of the 10% PG solution is used to store/release cooling duty. The LTR cold fluid temperature is specified as -3°C.

The assumptions used for the preliminary process evaluation of ETES technology are listed below:

- Steady state models of charging and discharging operating modes. No transient operations are evaluated. The charge level (energy content) of the HTR and LTR are not incorporated into the performance evaluation—i.e., the ETES process charging and discharging cycle performance is

evaluated based on specified HTR and LTR heat flow values. The effects of variation in HTR and LTR charge level (including heat/cold storage media temperature and/or heat transfer rate) are not considered in the system evaluation.

- No heat loss from system piping or system components to ambient.
- No heat loss from HTR and LTR during the charge cycle, discharge cycle, and/or system standby mode.
- System operation can alternate between charging and discharging mode.
- Rigorous evaluation of the fluid pumping, compression, and expansion equipment configurations was not performed i.e., operational issues associated with compression/expansion of CO_2 in the liquid vs dense (supercritical) state were not considered. Similarly, compression/expansion equipment that could accommodate the specified pressure ratios was not identified.
- Parasitic loads associated with the transport of the HTR and LTR TES media (energy required for circulation of the hot and cold energy storage media) were not considered.
- No cost is associated with the heat sink used for low-grade heat rejection during operation in either the heat pump or power generation mode. If air at ambient conditions is used for this purpose, then the low-grade heat-rejection costs would be represented by the air-cooler capital and operating costs.
- An ETES system with a generation capacity of 500 MWe was evaluated. Since economies of scale for many of the individual process equipment components are maximized in systems with approximately an order of magnitude smaller generation capacity (50 MWe), the capital costs per unit capacity and LCOS for ETES systems with generation capacity ranging from 50 MWe to 500 MWe could be similar to those for the 500 MWe system evaluated.

Performance Metrics

Key metrics for evaluating ETES system performance are described in the following paragraphs:

RTE is defined as the ratio of the discharge cycle power output to the charge cycle power input:

$$RTE = \frac{W_{discharge}}{W_{charge}}$$

For the ETES system the rate of heat flow to/from the thermal storage medium must be equal to accurate calculate RTE. In cases where the charge and discharge cycle heat flow are not equal, the RTE can be calculated as the product of the heat pump mode CoP and the power generation mode thermal efficiency:

$$RTE = CoP \times \eta_{thermal}$$

Where CoP is the coefficient of performance:

$$COP = \frac{Q_{hot}}{W_{charge}}$$

Round trip thermal-equivalent efficiency (RTQE) is defined as the ratio of the discharge cycle power output to the charge-cycle thermal-plus-electrical power input, where the electrical power input is converted to a thermal-equivalent through the use of a representative power plant thermal conversion efficiency:

$$RTQE = \frac{W_{discharge}}{Q_{equivalent,charge}} = \frac{W_{discharge}}{\left(\frac{W_{charge}}{\eta_{thermal}} + Q_{charge}\right)}$$

In cases where the charge and discharge cycle heat flow are not equal, the RTQE can be calculated as the product of the heat pump mode coefficient of performance, QoP and the power generation mode thermal efficiency:

$$RTQE = QoP \times \eta_{thermal}$$

where QoP is the coefficient of performance (ratio of heat input to the hot reservoir to the quantity of energy input) based on the thermal-equivalent energy input:

$$QoP = \frac{Q_{hot}}{\left(\frac{W_{charge}}{\eta_{thermal}} + Q_{charge}\right)}$$

In this analysis, a power plant thermal conversion efficiency of 33.3% was selected to be generally representative of an LWR nuclear power plant.

Charging Cycle (Heat Pump Mode)

A process flow diagram of the ETES system model, operating in charging (heat pump) mode, is shown below in Figure 15. Temperatures and pressures are shown were informed by process conditions reported by Echogen [35] (values marked with an asterisk indicate model-input specifications). The ETES charging cycle is further defined by the following operating-point specifications: HTR temperature of 390°C, LTR temperature of -3°C, ΔP of 100 kPa for all heat exchangers, compressor/expander isentropic efficiencies of 85%, and a supercritical CO_2 working fluid flow rate of 3842 kg/s (mass flow rate that results in HTR heat duty equal to the discharge cycle HTR heat duty required to support 500 MWe power output). The specified process conditions result in a maximum system pressure of 26.8 MPa and a compressor pressure ratio of ~10. The key performance metric for the ETES charging cycle is the CoP, defined as the quantity of heat input to the hot reservoir divided by the cycle net power input; a CoP of 1.6 is computed for the ETES charging cycle with the specified operating conditions.

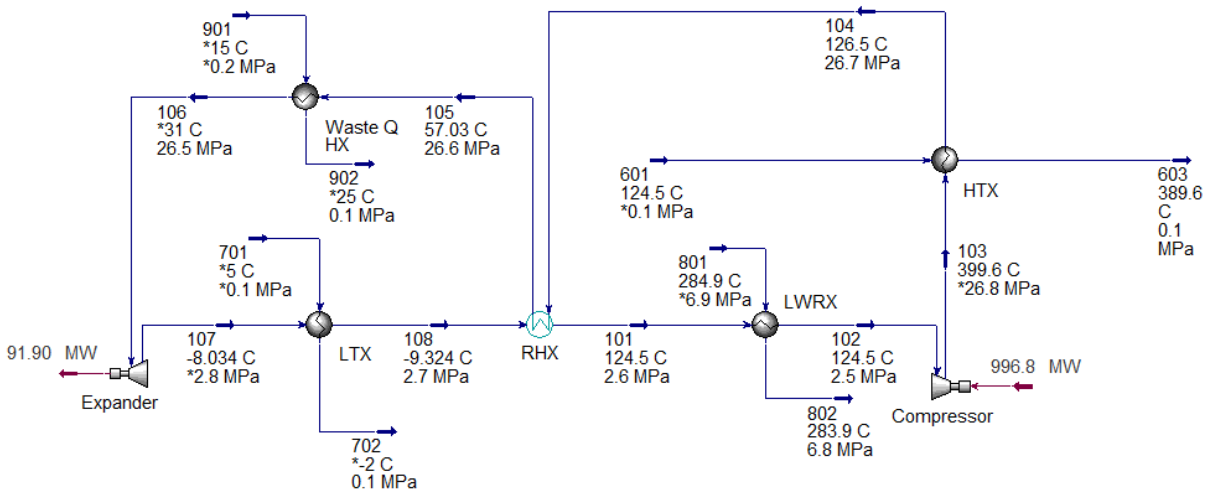

Figure 15. ETES charging cycle (heat pump mode) process flow diagram

Several observations can be made based on the ETES charging cycle process model results:

- The specification of heat exchanger ΔP of 100 kPa for all exchangers results in pressure drop ranging from 0.4% < ΔP < 3.5% of the stream inlet pressure. While heat exchanger pressure drops of this magnitude are believed to be generally representative for the application considered, future ETES process evaluation would benefit from rigorous heat exchanger modeling to improve the estimated pressure losses as well as exchanger heat-transfer performance and capital-cost estimates.
- In order to achieve the recuperator inlet/outlet conditions shown in Figure 15 a recuperator (RHX) minimum internal temperature approach (MITA) of 2°C is required. This small temperature approach specification has the effect of reducing the RHX log mean temperature difference (LMTD), which will result in a large exchanger surface area. It is expected that system capital costs (and actual exchanger pressure drop) could be decreased through the specification of a larger RHX MITA.
- Echogen's technical information [33,35] characterizes the ETES process as a supercritical CO_2 process. However, since $T_c = 31°C$ and $P_c = 7.4$ MPa for CO_2, the fluid is not in the dense (supercritical) phase at all points in the ETES process.
- A turboexpander is used to recover mechanical energy during the depressurization and cooling of the working fluid before heat exchange between the working fluid and the cold storage media (i.e., the PG solution). This equipment design for the expander should be evaluated in greater detail because the working fluid enters as a supercritical (dense phase) fluid and exits as a liquid. Possible issues associated with this mode of operation have not been investigated by the project team.

Discharge Cycle (Power Generation Mode)

A process flow diagram of the ETES system model operating in discharge (power) mode is shown below in Figure 16. Temperatures and pressures shown were based on process conditions reported by Echogen [35] (values marked with an asterisk indicate model input specifications). The ETES charging cycle is further defined by the following operating point specifications: HTR temperature of 390°C, LTR temperature of -3°C, ΔP of 100 kPa for all heat exchangers, compressor/expander isentropic efficiency of 90%, pump adiabatic efficiency of 90%, and a working fluid flow rate of 3865 kg/s (flow rate required to provide discharge mode net power generation of 500 MWe).

For the purposes of evaluating the ETES cycle performance, the charging cycle mass flow rate was set such that the HTR heat transfer rate matches the discharging cycle HTR heat transfer rate (which was in turn specified to provide 500 MWe of net power generation). However, it is expected that the system could be operated such that the thermal discharge rate differed from the charging rate, provided that the heat exchangers were appropriately sized/operated. One option for modulation of system power input/output would be the installation and operation of multiple smaller ETES units in parallel.

The ETES discharge cycle process configuration includes a "low-grade heat output" heat exchanger. The low-grade heat output exchanger is required to ensure that the ratio of the LTR and HTR heat duties is aligned with the ratio of the charging-mode. Specifically, discharge cycle low-grade heat output is required to match the charging cycle Qh/Ql=1.9. This specification is required to ensure that both reservoirs maintain similar charge levels throughout the charge/discharge operations.

The specified process conditions result in a maximum system pressure of 30 MPa and an expander pressure ratio of ~7.3. The key performance metric for the ETES discharge cycle is the thermal efficiency, defined as the quantity of net power output divided by thermal input; a thermal efficiency of 33.5% is computed for the ETES discharge cycle with the specified operating conditions.

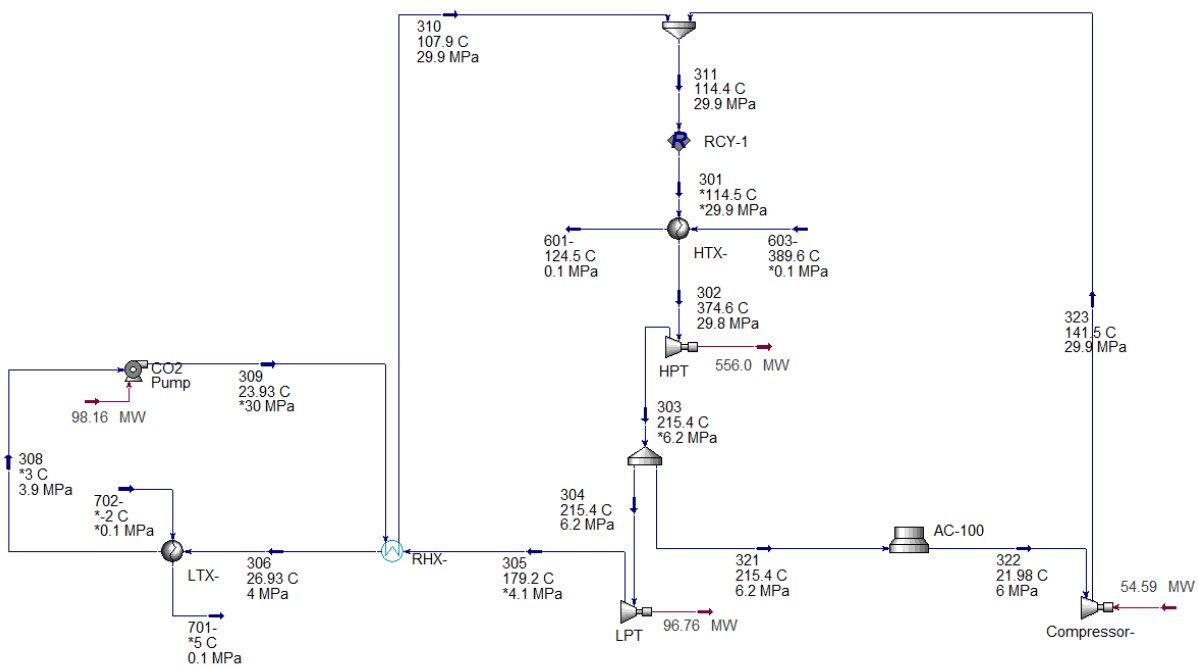

Figure 16. ETES discharge cycle (power generation mode) process flow diagram.

The following observations are made based on the ETES discharge cycle process model results:

- The specification of heat exchanger ΔP of 100 kPa for all exchangers results in pressure drop ranging from 0.3% < ΔP < 2.6% of the stream-inlet pressure. This pressure drop estimate is suitable for the preliminary analysis of the ETES discharge cycle. However, process evaluation should include advanced heat exchanger modeling to provide improved pressure drop (and heat transfer) performance estimates.
- Specification of the process conditions shown requires an RHX MITA of 3°C. Although this value is slightly higher than the charging-mode value, it is still indicative of a high-performance heat exchanger that may have a large surface area and/or high capital costs. It is recommended that the recuperator design be investigated in additional detail in future analyses of ETES technology.

- Similar to the charging-mode, the discharging mode also includes process conditions that are below the CO_2 supercritical temperature and pressure. Additionally, the LTX exchanger involves the condensation of a multiphase liquid/vapor mixture to a liquid phase. There is not a specific concern associated with these observations other than to note that they differ from the process characteristics described in available Echogen technical information [33,35], and the transition of the CO_2 working fluid in and out of the supercritical phase may complicate process control and operation, and the equipment design.
- During the discharge cycle, the CO_2 working fluid enters and exits the pump in the liquid phase. During the charging cycle, the CO_2 working fluid enters the expander (the rotational equipment that represents the reverse operation of the pump) as a supercritical fluid and exits as a multiphase vapor/liquid mixture. Because these process conditions differ substantially, it is not immediately clear that one pump/expander equipment component could accommodate the operating conditions associated with both the charge and discharge modes. Therefore, for economic modeling (discussed in a subsequent section) it is assumed that the charging cycle expander is an equipment component separate from the discharging cycle pump.

ETES system Heat Rejection

Heat rejection to ambient is required in the power generation operating mode to maintain the same ratio of HTR and LTR heat flow produced by the heat pump operating mode (the ratio of Qh/Ql must be equal during charge and discharge modes to maintain system heat balance throughout each and every charge and discharge cycle). However, the inclusion of heat rejection equipment for both operating modes increases the RTE while retaining the ability to maintain hot and cold storage inventory at equivalent levels during system operations.

Previous analysis of ETES technology (INL/EXT-21-62939, May 2021) identified the possibility that the system configuration shown in Echogen technical materials [33] may result in the requirement to reject waste heat from the power generation cycle at very low temperatures (which for the case of heat rejection to ambient may not be consistently available in most geographic locations). The current analysis of ETES technology is based on an ETES system configuration that enables waste heat rejection at elevated temperatures for both charging and discharging operating modes. In power generation mode (i.e., discharging), heat rejection is accomplished by cooling a slipstream of working fluid that is withdrawn between the high- and low-pressure turbines; the cooled slipstream is recompressed and reintroduced upstream of the high-temperature heat addition step (HTX). Heat pump mode (charging) heat rejection occurs between the hot side of the recuperator and the expander.

The use of these process locations for heat rejection allows the system to reject heat to ambient at reasonable temperatures (working fluid cooler outlet temperatures up to 60°C were evaluated). Heat rejection at elevated temperatures (during periods when the ambient temperature is high) has a negative impact on system performance, as shown by the plot of RTE versus heat rejection temperature shown in Figure 17; the current analysis uses the simplifying assumption that the same heat rejection temperature is used for both the charge and discharge cycles (due to the sequential nature of the charge and discharge cycle operations, it is unlikely that the ambient temperature would remain constant for the full duration of the charge and discharge cycles).

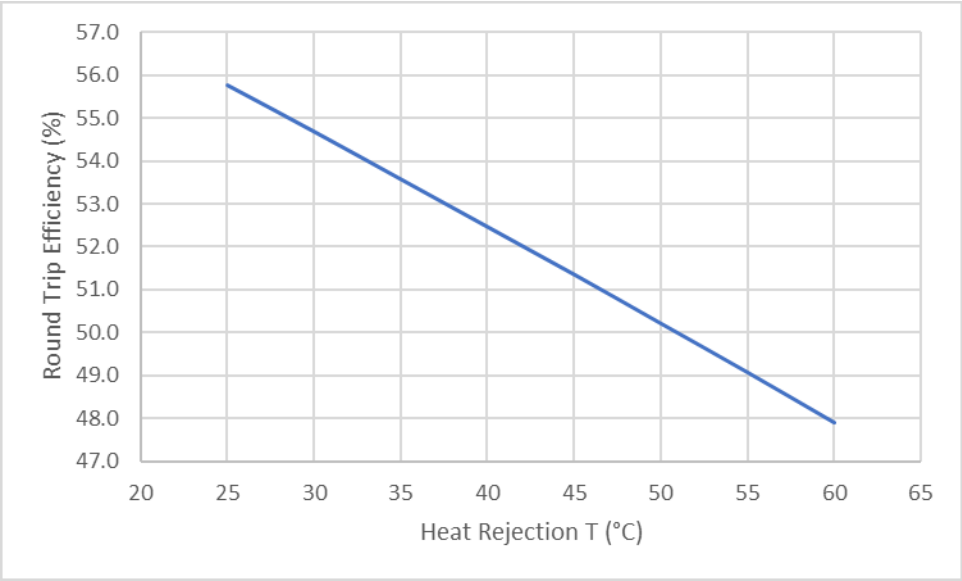

Figure 17. RTE as a function of process waste heat rejection temperature; standalone ETES process configuration (electrical power input only).

ETES Performance Evaluation Summary

The ETES performance evaluation indicates that a charge cycle CoP of 1.9 and a discharge cycle thermal efficiency of 33.5% result from the operation of the ETES system (with heat pump mode waste heat rejection) at the specified conditions. An RTE of approximately 55% would be possible by coupling charge and discharge cycle operations. However, per the stated assumptions, this calculation does not include system heat losses, detailed heat exchanger design and simulation, parasitic loads associated with the transport of the energy-storage media, or effects from transient system operation. Further evaluation of the ETES process is necessary to address the impacts of these items.

2.3.1.2 System Costs

A preliminary ETES system cost evaluation was performed. Capital costs were estimated based on the charging cycle process configuration; additional costs may be associated with the inclusion of discharge cycle specific equipment. The cost evaluation estimated capital costs for major process equipment items and the hot/cold TES media and associated containment infrastructure. Because rigorous heat exchanger modeling of the HTX has not been performed, an estimate of the overall heat transfer coefficient for a particle to sCO_2 heat exchanger was obtained from the literature [36]. An estimate of the heat exchanger area was then obtained based on the relation $Q = U \cdot A \cdot \Delta T_{LM}$ where Q is the heat transfer rate, U is the overall heat transfer coefficient, A is the heat transfer surface area, and ΔT_{LM} is the log mean temperature difference. The inputs and outputs for the particle/sCO_2 heat exchanger area calculation are shown in Table 9, sizing calculations correspond to power generation operating mode.

Table 9. Particle/sCO_2 heat exchanger sizing calculation input/output for the high temperature exchanger.

Parameter	Value	Unit	Notes
Q	1491	MW-t	HTX heat duty at charge cycle design point operating conditions
T_s,in	389.6	°C	Exchanger hot side (sand particulate media) inlet temperature
T_s,out	124.5	°C	Exchanger hot side (sand particulate media) outlet temperature
T_CO_2,in	114.5	°C	Exchanger cold side (CO_2 working fluid) inlet temperature
T_CO_2,out	374.6	°C	Exchanger cold side (CO_2 working fluid) outlet temperature
ΔT_LMTD	12.3	°C	LMTD
U	144	W/m²K	Overall heat transfer coefficient reported for particle/sCO_2 heat exchanger with 250 µm particle diameter; 6 mm plate spacing [36]
A	839,650	m²	Calculated heat transfer area
Amax	1672	m²	Aspen Process Economic Analyzer max plate-and-frame exchanger size
N	500		Number of units required to obtain required surface area

The results from the HTX heat transfer surface area calculation served as the basis for estimating the capital costs for a plate-and-frame heat exchanger using Aspen Process Economic Analyzer (APEA) capital cost estimation software. The HTX configuration described by Echogen would also require an elevator to circulate the sand TES media between the high and low-temperature containment vessels. The mass flow rate of the sand TES media was calculated, and this value was used as the basis for the APEA estimate of HTX elevator capital costs. The HTX exchanger and elevator estimated costs are listed in Table 10. This table also includes estimates of other major ETES heat pump and power generation equipment based on AspenTech HYSYS process model data, Exchanger Design and Rating heat exchanger equipment costs (an installation factor of 3.3 was assumed for estimation of heat exchanger installed costs) and APEA estimated equipment costs (for rotational equipment and material transport equipment cost estimation). The capital costs listed in Table 10 are for the energy conversion process equipment only; the capital costs for the full ETES system also include the energy storage media and containment vessel costs, which vary with the specified energy storage capacity and are discussed further in the subsequent text.

Table 10. Estimated equipment costs for an ETES system with 500 MWe net power generation capacity.

Equipment Component	Capacity	Unit	Equipment Cost	Installed Cost	Cost per kW-e	Notes
Pump	110	MW	$17,315,062	$26,931,100	$54	Based on APEA sizing calcs
Expander	92	MW	$41,195,000	$54,653,000	$109	70 units × 1315 kW; system operating P exceeds APEA allowable range, input P specified at max APEA input value
Compressor /Turbine	910	MW	$58,394,398	$68,169,000	$136	Assume that compressor is run in reverse to provide expander capability during power gen mode operations; compressor inlet T exceeds APEA allowable range, input T specified at max APEA input value
LTX	32,250	m²	$6,803,280	$22,450,820	$45	TEMA BEM exchanger; 20 shells in parallel
RHX	68,340	m²	$62,547,840	$206,407,870	$413	TEMA BEM exchanger; 60 parallel × 3 series config
LWRX	0	m²	$0	$0	$0	
HTX	840,000	m²	$61,700,000	$224,780,000	$450	APEA Plate & Frame exchanger mapping; system operating temperature and pressure exceed APEA allowable range, input temperature and pressure specified at max APEA input values
Sand Elevator	24,400	tonne /hr	$14,112,000	$17,375,000	$35	APEA "CO CONT BKT L" model; 140 units × 175 tonne/hr
Waste Q HX	3,040	m²	$3,374,440	$11,135,650	$22	TEMA BEM exchanger; 20 shells in parallel; 15°C cooling water heat sink
Discharge compressor	55	MW	$6,519,739	$7,469,200	$15	APEA GC CENTRIF sizing calcs based on simulator data file
AC-100	19,120	m²	$11,482,750	$37,893,075	$76	EDR Air Cooled Exchanger design based on process simulation data
Total				$677,264,723	$1,355	

The costs of the hot/cold TES media and the associated containment vessels vary as a function of the system energy storage capacity. The basis for energy storage media cost estimates is included in Table 11. This table provides an estimate of the energy storage media costs on a per kWh-t and kWh-e of energy storage capacity basis (the ETES system thermal efficiency is used to convert between thermal and electrical energy). The energy storage media costs shown in this table are used to estimate costs for systems with varying energy storage durations.

Table 11. Energy storage media estimated costs.

	Sand	10% PG aq. solution	Unit
Calculated Discharge Cycle Efficiency	33.5%	33.5%	
Q	1491	788	MW-t
Storage Time	1	1	hr
Storage Capacity	1491	788	MWh-t
	500	500	MWh-e
Th	390	-3	°C
Tc	125	-3	°C
Cp	830 (1)		J/kg-C
ΔH_{fusion}		325 (2)	kJ/kg
ρ		1012	kg/m³
$\dot{m}$	6776	2425	kg/s
m	24,394,520	8,728,620	kg
Unit Cost	$0.04 (3)	$0.20 (4)	$/kg
Total Cost	$941,160	$1,753,580	
Total Cost per unit Thermal Energy Storage	$0.63	$2.23	$/kWh-t
Total Cost per unit Electric Energy Output	$1.88	$3.51	$/kWh-e

Notes:

1. Sand Cp reference: https://www.engineeringtoolbox.com/specific-heat-capacity-d_391.html
2. PG solution ΔH_{fusion} reference: https://doi.org/10.1016/j.ijrefrig.2006.07.008
3. Sand cost reference: https://doi.org/10.1016/j.est.2020.101382
4. PG solution cost: 90% water @ $1/m³ (estimated); 10% propylene glycol @ $2/kg (Alibaba)

Particle TES media containment capital cost estimates are based on values reported in [36]. Particle containment cost data applicable to the current analysis is reproduced in Table 12. The calculated ETES system efficiency is used to estimate the particle containment CAPEX on a $/kWh-e basis.

Table 12. Particle containment CAPEX.[37]

Component	Cost	Unit
Tanks	$6.00	$/kWh-t
Foundations	$0.70	$/kWh-t
Piping/valves	$1.00	$/kWh-t
I&C	$0.50	$/kWh-t
Spare Parts	$1.00	$/kWh-t
Contingency	$4.00	$/kWh-t
Total (thermal)	$13.20	$/kWh-t
Total (electric)	$39.36	$/kWh-e*

* Based on 33.5% power generation cycle (discharge mode) thermal efficiency

The containment vessel for the PG solution cold-storage media is specified as a single-tank for storage of the liquid and solid slurry (the solid fraction of the mixture increases as the charge cycle progresses and more cold energy is stored in the form of latent heat of fusion). APEA was used to estimate capital costs for a multiwall vertical storage tank as a function of the calculated cold storage fluid volume required for systems of varying energy storage capacity. For the large-scale system considered, multiple 50,000 m³ tanks are needed to achieve the required cold storage capacity. Table 13 lists the estimated cold storage fluid containment-vessel capital costs as a function of ETES system energy storage capacity.

Table 13. Estimated costs for liquid/solid slurry tank with varying cold storage capacity.

Volume (m³)	Multi-wall vertical vessel direct cost	storage capacity (MWh-e)	$/kWh-e
1,000	$1,373,500	58	$23.69
2,000	$2,283,400	116	$19.69
5,000	$5,059,200	290	$17.45
10,000	$6,855,100	580	$11.83
15,000	$8,432,400	870	$9.70
20,000	$10,202,700	1,159	$8.80
30,000	$13,385,100	1,739	$7.70
40,000	$16,473,400	2,319	$7.10
50,000	$20,863,300	2,899	$7.20

The ETES system costs, including the heat pump/power conversion cycle, hot and cold TES media, and hot and cold TES media containment vessels were computed for a range of system energy storage capacities. An indirect cost adder of 50% was applied to the direct capital costs to obtain an estimate of the project total capital investment (TCI). Figure 18 shows the ETES unit capital costs ($TCI/kWh-e) as a function of the number of hours of storage. The plot indicates that the unit capital costs decrease exponentially as the number of hours of storage increases; this is attributed to the fact that the majority of the system costs are associated with the heat pump/power generation cycle, and increased energy storage

capacity only requires the additional costs associated with the relatively low-cost energy storage media and accompanying containment vessels.

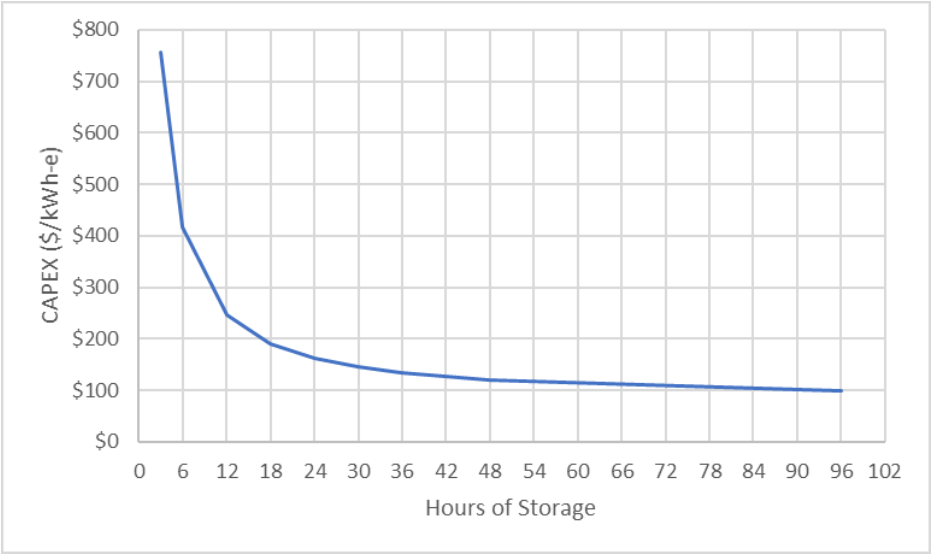

Figure 18. Estimated ETES capital costs (per unit of electrical energy storage capacity) as a function of storage capacity.

Figure 19 includes the ETES capital costs calculated in this analysis compared against capital costs reproduced from available Echogen technical information [33]. It is apparent from Figure 19 that while both analyses predict the same trend of decreasing capital costs). The battery costs reported by Echogen are higher than the cost of $427–356/kWe for a 100 MWe Li-ion battery system with 2–10 hours of storage, as reported in Table 5 of this report. The preliminary ETES capital costs calculated in this analysis are uncertain due to the use of generalized cost-estimating tools (i.e., APEA) and data reported in the literature, which are not expected to provide highly accurate cost data for supercritical CO_2 ETES systems (a specialized process application). Further analysis is recommended to refine capital-cost estimates and increase the certainty of the economic analysis.

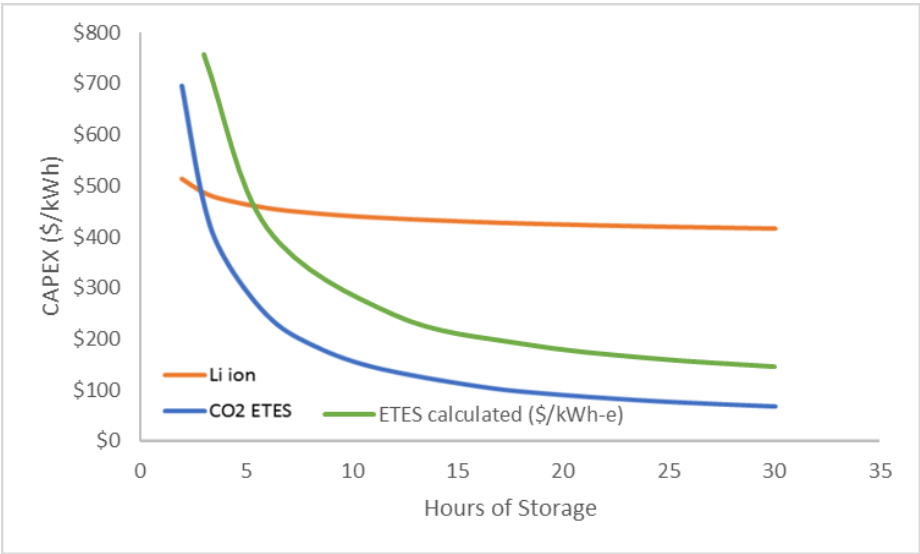

Figure 19. Comparison of estimated ETES and Li-ion battery capital costs. Lithium-ion battery energy storage costs (orange) and CO_2 ETES costs (blue) are reproduced from available Echogen technical information [33]. ETES costs (green) estimated in this report are included for comparative purposes.

2.3.1.3 ETES Levelized Cost of Storage

A LCOS calculation for the stand-alone ETES process was completed using the methodology described in Lazard LCOS v6.0 [38]. A summary of the LCOS analysis input parameters and key results are listed in Table 14. As shown in Table 14 a stand-alone ETES system with an energy storage duration of 12 hours and a one-day interval between the commencement of discharge cycles, the TCI (including a 50% adder for indirect costs) is $258/kWh-e. Using a cost of $30/MWh-e for the electricity used to charge the system, as specified in Table 14, the LCOS for the stand-alone ETES system was calculated as $141/MWh-e.

Table 14. Summary of ETES system LCOS analysis input parameters and key results.

System Design		**Units**
Power Rating	500	MWe
Duration	12	hr
Usable Energy	6,000	MWh-e
Interval between start of discharge cycles	1	day(s)
Depth-of-Discharge	100%	
Operating days/yr	350	
System Performance		
Round Trip Efficiency	55%	electric basis
Degradation	0.00%	per annum
CAPEX		
Total Capital Investment	$1,483,445,432	
Total Capital Investment Unit Cost	$247.24	$/kWh-e
OPEX		
Electricity Charging Cost	30	$/MWh-e
Charging Cost Escalation	2.50%	per annum
O&M, general	1.50%	% of CAPEX
General O&M Cost Escalation	2.50%	per annum
Calculated Levelized Cost of Storage		
LCOS (12 hr discharge capacity)	$141.21	$/MWh-e

Additional characterization of the ETES LCOS is provided in Figure 20, which maps ETES LCOS as a function of the discharge cycle duration and the interval between the initiation of the discharge cycles. The LCOS data plotted in Figure 20 is based on a standalone ETES process configuration (no thermal input) with heat pump mode waste heat rejection and a charge cycle power input cost of $30/MWh-e. Two trends in LCOS can be observed in Figure 20. First, increasing the ETES storage duration decreases the LCOS. Since the hot/cold energy storage media capital costs are relatively low in comparison with the heat pump/power generation cycle capital costs, increasing the system energy storage capacity effectively decreases the capital costs per unit of energy output (which also decreases LCOS). Second, increasing the interval between initiation of discharge cycles decreases the frequency with which the system can be discharged to generate revenue from power sales, which ultimately leads to increased LCOS to recover capital expenses (increasing the frequency of the discharge cycles is analogous to decreasing the capacity factor of a conventional power plant).

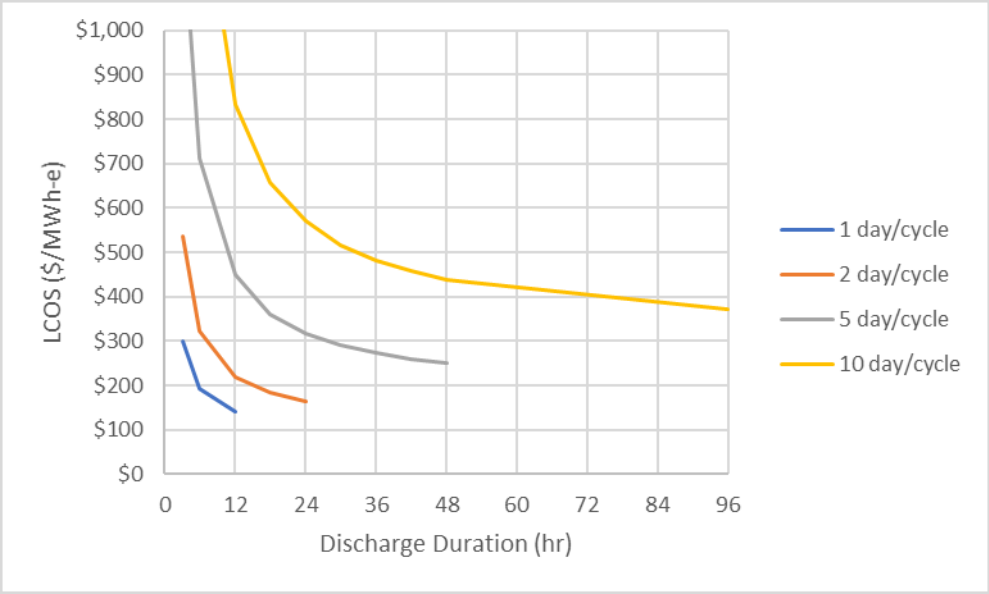

Figure 20. LCOS as a function of discharge cycle duration with the interval between initiation of discharge cycles as a parameter (standalone ETES process configuration with heat pump mode waste heat rejection).

Figure 21 is a tornado chart that illustrates the sensitivity of the ETES LCOS to selected parameters. The parameters that have the greatest impact on the LCOS are listed at the top of the chart. For the range of ETES sensitivity parameters evaluated, the charging cost, total capital investment, and system efficiency have the greatest impact on the LCOS. Additional observations regarding sensitivity parameters considered for this analysis are listed below:

- A wide range (±100%) of charging costs was evaluated to capture the wide range of costs associated with different possible operating scenarios (e.g., use of power purchased at an LWR O&M cost versus purchase of grid power during off-peak periods). The sensitivity analysis is based on specification of constant charging costs (i.e., the charging cost does not vary during the charging period in response to energy market pricing or other factors).
- The range of ±30% considered for total capital investment sensitivity analysis is representative of the probable error associated with a Class 5 cost estimate (the type of estimate presented in this analysis). An ETES system design that differs from that evaluated in this analysis would be expected to have capital costs that vary accordingly.
- The range of ±30% considered for the system efficiency is beyond the range of variation in this parameter expected from further evaluation of steady-state operating conditions. However, the inclusion of dynamic operating conditions such as startup/shutdown and partial load operation, as well as rigorous evaluation of thermal energy losses associated with the energy storage media may result in the realization of round-trip efficiency values that vary considerably from the value specified in the baseline case.
- The baseline case specified a 100% depth-of-discharge for every cycle. However, it is unlikely that electricity market pricing would remain at peak values for the duration of every discharge cycle in actual operating scenarios. It is also probable that operational considerations may restrict the system from releasing all stored energy during the discharge cycle. Therefore, less than 100% depth-of-discharge would be expected in actual operations.

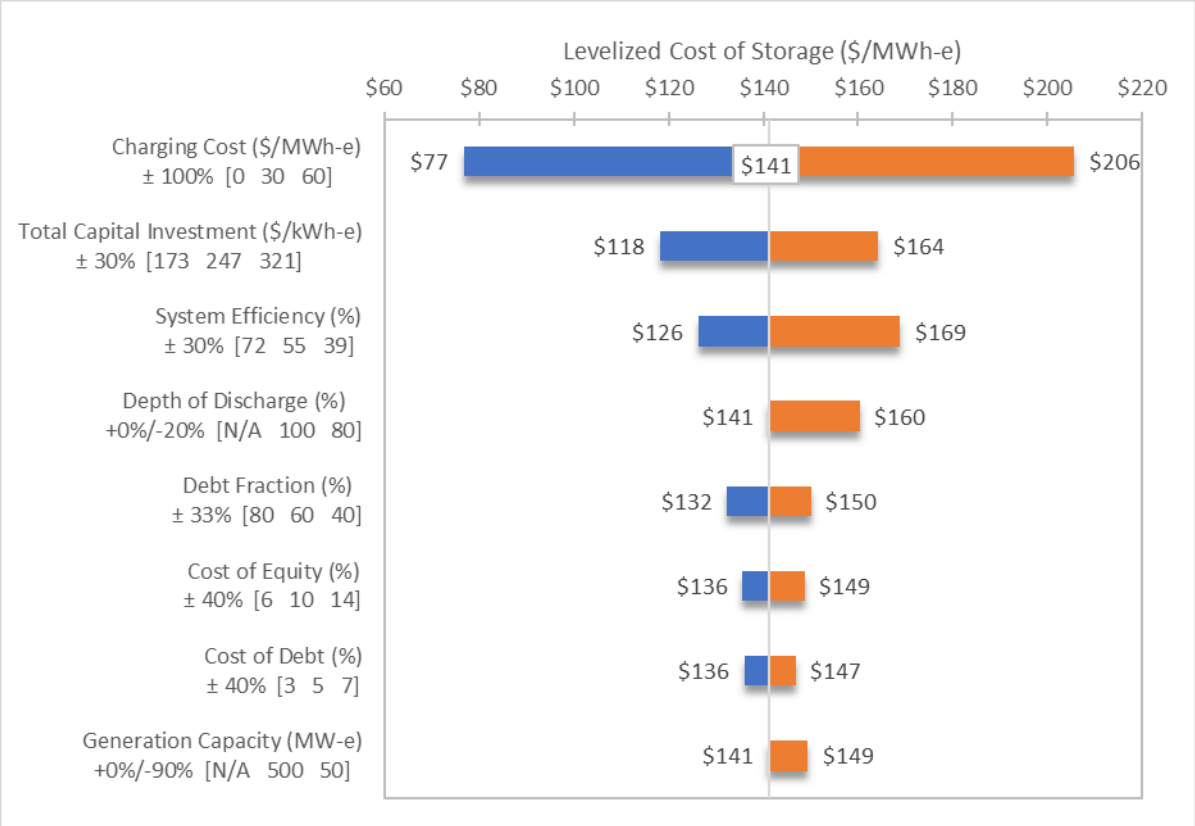

Figure 21. Tornado chart illustrating sensitivity of ETES LCOS to selected parameters.

As noted above, a wide range of charging costs was evaluated in the sensitivity analysis, which results in a large delta between the upper and lower LCOS values associated with this parameter. The most cost effective ETES operating strategy would involve charging the system when energy costs are low and discharging when energy costs are high. Therefore, a charging cost between the low and baseline values of $0/MWh-e and $30/MWh-e, respectively, is expected to be more representative of the charging costs for a potential ETES deployment than the high charging cost of $60/MWh-e (which is included primarily to indicate the sensitivity of the LCOS to the charging cost parameter). The O&M costs for the current fleet of LWRs are generally reported to be $30/MWh-e or lower, such that this energy cost could be considered an upper bound for the cost of charging an ETES system (e.g., for a hypothetical case in which the ETES system charge cycle energy is purchased directly from an LWR instead of from the grid). A cursory evaluation of recent historical locational marginal pricing data from the PJM and Electric Reliability Council of Texas Energy Markets indicates that energy prices of around $15/MWh-e to $20/MWh-e have been representative of the lowest 6 to 12 hours of energy pricing each day.

Additional details regarding the effect of charging cost on LCOS are provided in Figure 22 and Figure 23. Figure 22 plots LCOS as a function of charging cost for ETES configurations with 6 and 12 hours of energy storage (both cases assume daily charge/discharge cycle frequency). As expected, increasing charging cost results in increasing LCOS, and increasing the ETES storage duration decreases the LCOS (since the energy storage media capital costs are relatively low in comparison with the heat pump/power generation cycle capital costs). Figure 23 provides an LCOS comparison for selected combinations of discharge interval and duration. For each interval/duration two charging cost scenarios are evaluated: (1) the data series shown in blue is representative of an ETES system operating with a constant charging energy cost of $30/MWh-e, and (2) the data series shown in orange is representative of an ETES system with a time-dependent charging energy cost based on the 2030 hourly energy market prices projected for the Palo Verde Hub (Arizona Public Service). The time-dependent charging cost

scenario accounts for the hourly variation in energy prices expected in actual energy markets; as the charging duration increases the average charging price also increases since the minimum energy price on a given day occurs at only a single point in time (each incremental increase in the charging duration requires a corresponding quantity of energy to be purchased at a progressively higher cost).

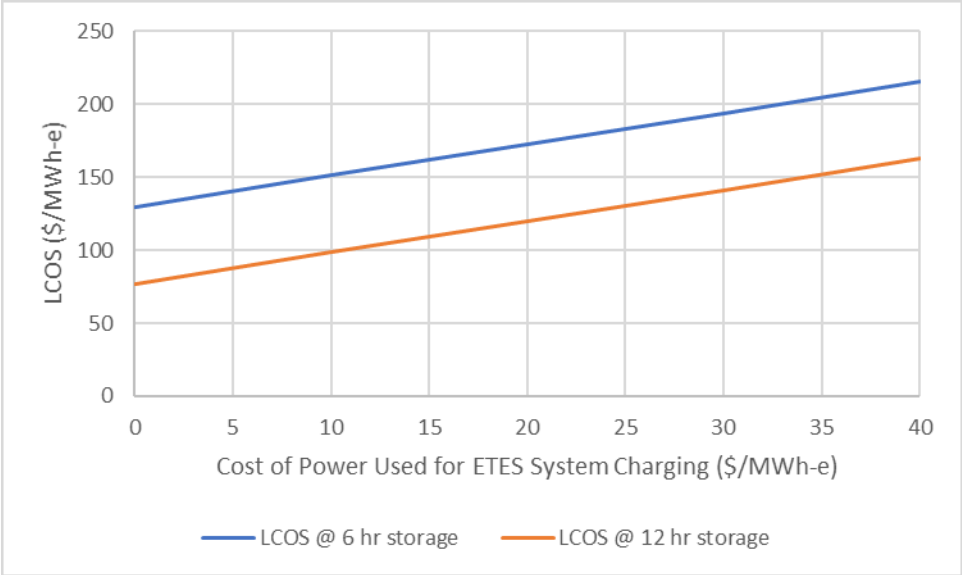

Figure 22. ETES LCOS as a function of the charge mode power cost (electricity cost) for a non LWR integrated ETES system configuration.

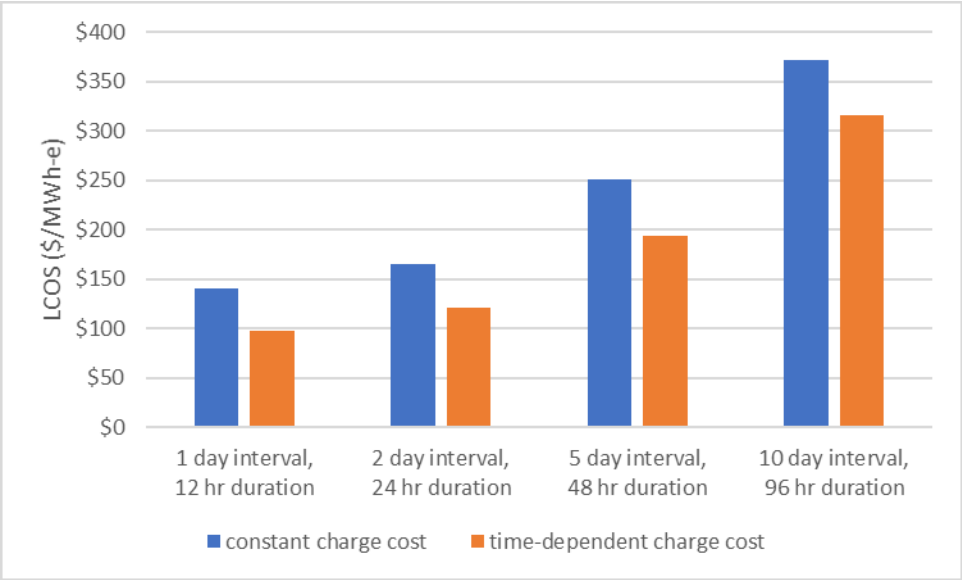

Figure 23. LCOS comparison for ETES systems operating with selected discharge intervals/durations and charging costs.

2.3.1.4 Alternate Flowsheet Analysis of ETES with Nuclear Heat Addition

The effect of nuclear heat addition on ETES process performance was evaluated for two process configurations: (1) heat addition to ETES SCCO2 working fluid, and (2) heat addition to ETES particulate TES media (HTR). The first configuration involves nuclear process heat upstream of the heat pump cycle compressor (and downstream of the cold side outlet of the working fluid recuperating heat exchanger) as shown in Figure 24. The second configuration includes nuclear process heat addition to the

particulate TES media (sand) upstream of the CO_2 to sand heat exchanger (HTX) as shown in Figure 25. The nuclear integrated ETES heat pump cycle and power generation cycle HYSYS model process flow diagrams are shown in Figure 26.

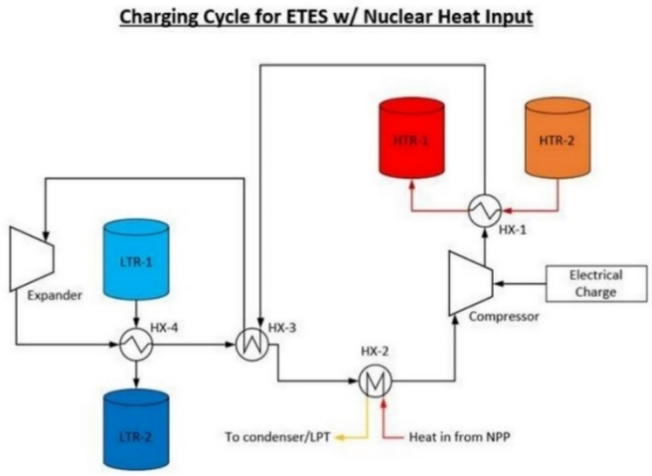

Figure 24. ETES heat pump cycle with nuclear process heat input (CO_2 working fluid heating).

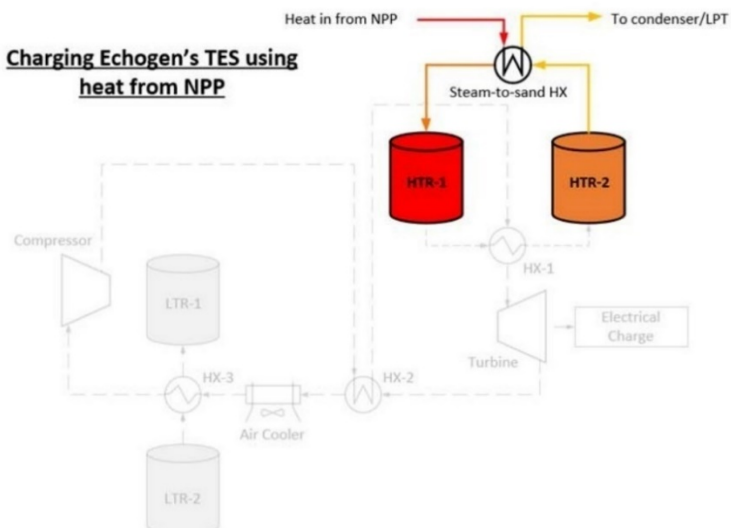

Figure 25. ETES heat pump cycle with nuclear process heat input (HTR media heating).

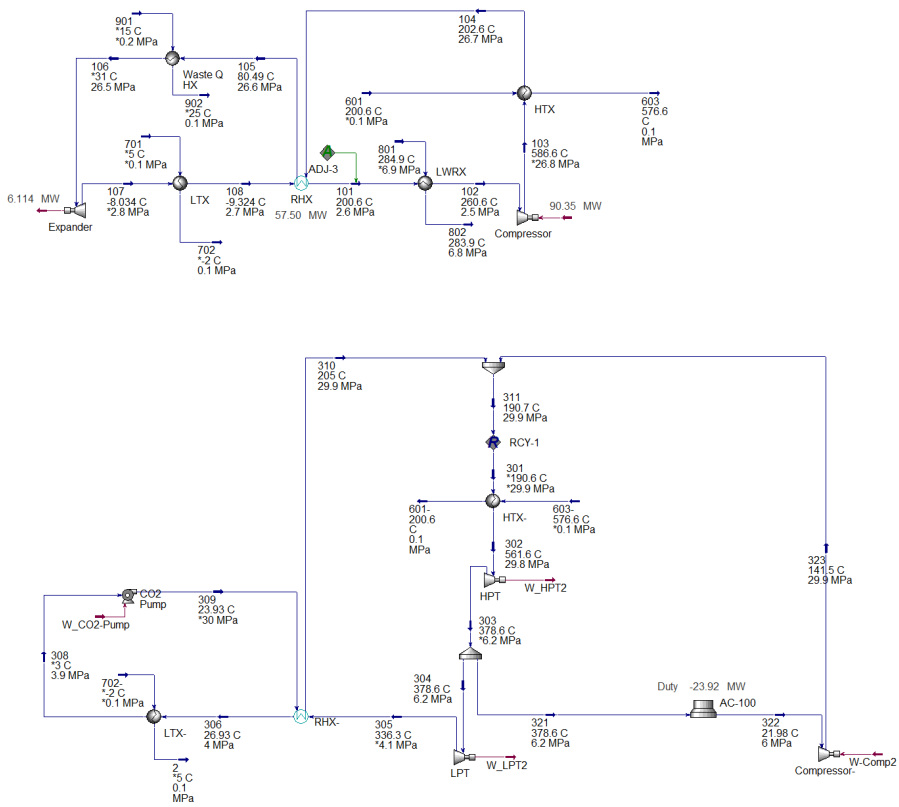

Figure 26. LWR-integrated ETES process configuration and operating conditions. Heat pump mode (charging cycle) shown in top diagram and power generation mode (discharge cycle) is shown in bottom diagram.

Although nuclear process heat from an LWR is limited to adding heat to the ETES process at temperatures of approximately 260°C or less (after accounting for heat losses in the thermal delivery loop to transport the nuclear process heat from the LWR site to a theoretical ETES process site), the addition of nuclear process heat results in increased HTR operating temperatures and associated increases in the operating temperatures of the associated equipment (heat pump mode compressor, power generation mode turbine, recuperator hot side inlet temperature, etc.).

Process evaluation using HYSYS process modeling software indicates that nuclear process heat addition to the ETES cycle working fluid results in the highest round-trip thermal efficiency system operation. Additionally, it is expected that the design and operation of a heat exchanger to transfer nuclear process heat into the CO_2 working fluid would result in a more conventional (also potentially less costly) heat exchanger design than a process configuration in which the nuclear process heat was added to the HTR particulate TES media (sand). Figure 27 illustrates the effect of nuclear process heat addition to the ETES process CO_2 working fluid for ETES process configurations with and without heat pump mode waste heat rejection as pictured in Figure 28 (both cases require waste heat rejection in the power generation operating mode to synchronize the charge levels of the hot and cold storage reservoirs throughout the charge/discharge cycle).

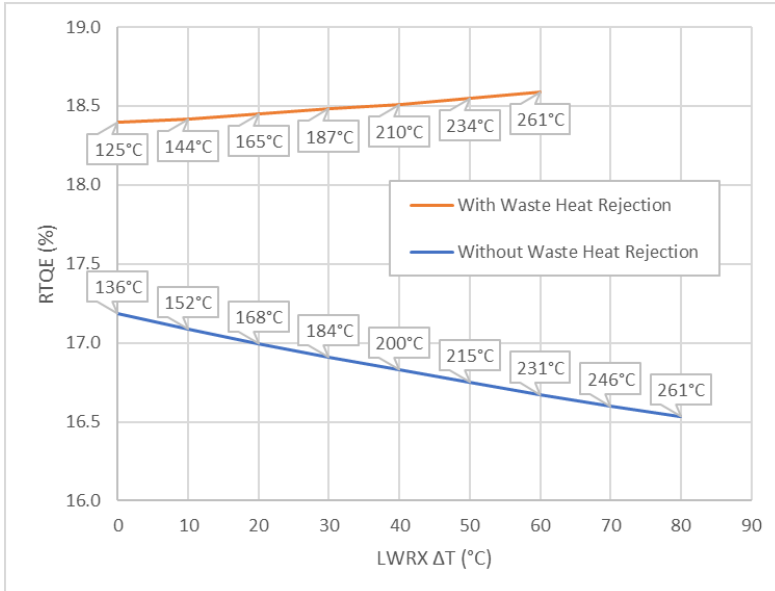

Figure 27. Effect of nuclear heat addition to ETES process working fluid for configurations with and without heat pump mode waste heat rejection. Data labels indicate LWRX heat exchanger cold side (CO_2 ETES working fluid) outlet temperature.

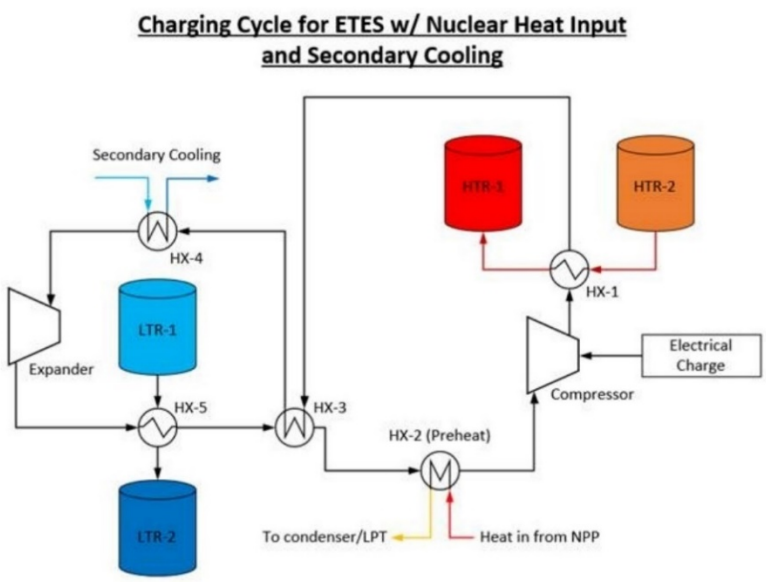

Figure 28. ETES process configuration with heat pump mode LWR thermal integration and waste heat rejection (denoted as "secondary cooling" in the diagram).

Although the increase in the hot reservoir temperature associated with LWR thermal integration enables the ETES power generation mode (discharge cycle) to operate with higher thermal efficiency, the increased compressor inlet temperature decreases the heat pump mode (charge mode) QoP. The net effect is that the LWR integration provides only a modest increase in the ETES process RTQE (18.4% for the ETES process with zero LWR heat addition versus 18.6% for the ETES process with LWR heating of the CO_2 working fluid to approximately 260°C). A plot of the heat pump mode thermal-equivalent coefficient of performance (QoP), power generation mode thermal efficiency ($\eta_{thermal}$), and system RTQE versus the LWRX CO_2 temperature increase from nuclear process heat addition for the ETES system with waste heat rejection (charging cycle) is shown below in Figure 29. The RTQE, which is the product of QoP and

$\eta_{thermal}$, is not a strong function of the LWR heat addition and does not change significantly over the range of ETES working fluid ΔT associated with zero LWR heat addition to maximal LWR heat addition (up to approximately 260°C).

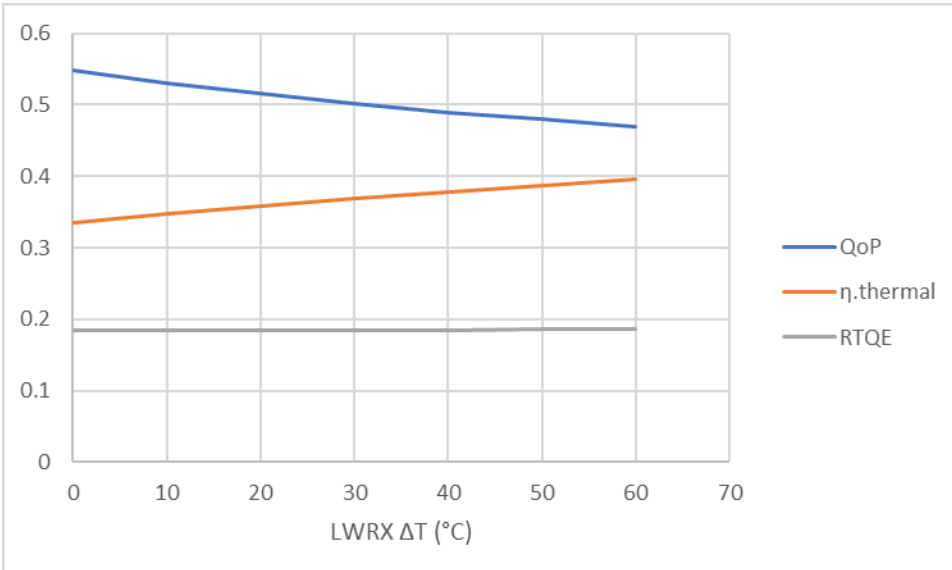

Figure 29. LWR integrated ETES process QoP (heat pump mode with waste heat rejection), $\eta_{thermal}$ (power generation mode), and RTQE (inclusive of charge and discharge mode system operations).

2.3.1.5 Summary and Recommendations

Summary

Preliminary process modeling has been performed to estimate the performance of stand-alone and LWR-integrated ETES process configurations. An initial economic analysis has been completed to determine the LCOS for the standalone ETES process. Results of the process and economic analysis are summarized in Table 15.

Table 15. ETES Process Performance Summary (LWR-integrated process configuration with heat input to CO_2 working fluid; standalone and LWR-integrated processes based on charging cycle with waste heat rejection).

	Stand-alone ETES (electric input only)	LWR-integrated ETES (electric and thermal input)
Capacity (discharge mode)	500 MWe	500 MWe
Heat pump mode CoP	1.65	N/A
Heat pump mode QoP	0.55	0.47
Power generation mode η_{th}	33.5%	39.6%
RTE	55.3%	N/A
RTQE	18.4%	18.6%
ETES system energy conversion equipment installed cost	$695 million ($1400/kWe)	TBD
Materials: 10% PG aqueous solution Sand Containment (tanks and silos)	 $3.51/kWh-e (Table 11) $1.88/kWh-e (Table 11) $50-60/kWh-e depending on energy storage capacity (Table 12 and Table 13)	 $3.51/kWh-e (Table 11) $1.88/kWh-e (Table 11) $50-60/kWh-e depending on energy storage capacity (Table 12 and Table 13)
Total Capital Investment 6 hr capacity 12 hr capacity	 $1,310 million ($436/kWh-e) $1,550 million ($258/kWh-e)	TBD
Levelized Cost of Storage 6 hr capacity 12 hr capacity	 $200/MWh-e $145/MWh-e	TBD

Recommendations

Recommendations for further evaluation of ETES technology include completion of additional process analysis and a rigorous economic evaluation of both standalone and LWR-integrated ETES systems. Additional details are provided below:

Additional process modeling to evaluate effects of:

- External heat loss (especially from heat/cold storage reservoirs).
- Heat exchanger configuration (geometry, materials of construction, etc.) and operation (including investigation of heat transfer coefficients for working fluid and hot and cold energy storage media).
- Parasitic loads associated with the transport of hot/cold TES media.
- System transient operations (switching between charging/discharging mode, effects of HTR/LTR charge levels on system performance).
- Evaluation of solid-phase TES particle heat exchanger technology, including technology readiness, equipment and operating/maintenance costs, operational issues, and vendors.
- Identification of compression/expansion equipment that can operate at the required pressure ratios; identification of expander device/technology able to generate shaft power at operating conditions that include CO_2 working fluid at supercritical inlet conditions and multiphase gas/liquid mixture outlet conditions.

Completion of a rigorous economic evaluation

The economic evaluation presented in this analysis is based on preliminary/readily available equipment component cost estimates. The estimated costs are not based on detailed equipment

specifications, and do not include provisions for specific equipment designs necessary to mitigate potential operational issues associated with unique operating characteristics of the ETES system (transient operations, supercritical CO_2 working fluid, solid-phase particulate transport/heat exchange, etc.). A detailed evaluation of the system equipment, energy storage media, and energy storage containment equipment costs should be performed to increase the level of certainty associated with the system cost evaluation. It is recommended that the detailed cost evaluation involve communications with equipment and materials vendors to obtain application-specific cost data/estimates/quotations.

Evaluation of thermal energy storage options

While the performance of two ETES process configurations incorporating nuclear process heat integration has been considered, additional options remain for incorporation of supplemental TES with the ETES system. As an example, the ETES HTR operating temperature could be adjusted to match the temperature at which heat could be supplied by an LWR, which may provide operational flexibility in maintaining the charge level of the hot and cold reservoirs (and thereby reducing/negating the requirement for use of waste heat rejection to maintain similar charge levels in the hot and cold reservoirs). Additionally, the incorporation of an external refrigeration source (i.e. refrigerant capacity provided by a LWR power plant) could also be used to enhance ETES process performance and maintain similar charge levels in the hot and cold reservoirs. Further investigation of the use of both external heat and cooling sources on process performance and economics is therefore recommended.

2.3.2 Liquid-Based Sensible Heat Thermal Energy Storage

Liquid-based sensible heat thermal energy storage systems (SH-TES), which are a widely deployed technology, utilize a liquid medium to transport and store thermal energy. Primarily, there are two designs of SH-TES systems – a direct heating setup, in which the storage medium is heated directly by the heat source, and an indirect setup, wherein an intermediary heat transfer fluid is used to transfer the heat from the heat source to the storage medium. Due to the myriad of liquids that are available with high specific heat capacities, the operating temperature range for SH-TES system is 10°C – 550°C. The existing fleet of SH-TES systems that have been primarily coupled with tower- and trough-based concentrated solar plants (CSPs) use molten salt as the storage medium (see Figure 30). In the solar tower design, which is a direct heating setup, the working fluid temperatures can go up to 565°C. In comparison, for the trough-based design, which is an indirect heating setup, synthetic oil is used to heat up the molten salt and the temperatures can go up to 393°C. Solar salt (60% $NaNO_3$ and 40% KNO_3) has a melting point of about 220°C, and therefore the difference between the maximum operating temperature and the melting point allows for a significant amount of sensible heat storage capacity. These systems also operate at near-atmospheric conditions, while discharging at a constant rate, thereby maintaining high power cycle efficiency.

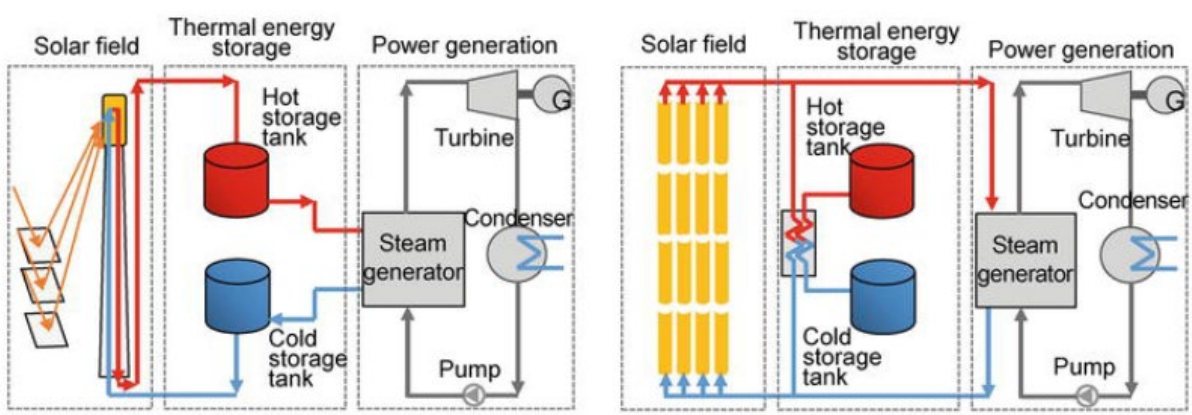

Figure 30. Solar power tower and parabolic trough concentrated solar power systems (CPSs) with integrated thermal storage systems.[39]

When compared to CSPs, LWRs have a steam outlet temperature of about 260 — 300°C, and therefore can heat up the solar salt only up to a maximum of 80 degrees above its melting point. Such a small temperature difference (ΔT) would result in a large quantity of salt requirement to store a certain amount of heat when compared to a medium that could provide a larger ΔT between the maximum operating temperature and its melting point. Therefore, SH-TES system designs with salts that have lower melting temperatures would be better options. Two candidate salts of particular interest are Hitec ($NaNO_3$-KNO_3-$NaNO_2$, 7-53-40) and Hitec XL ($NaNO_3$-KNO3-Ca(NO3)2, 7-45-48), whose melting points are 142°C and 120°C, respectively.

Similar to molten salts, synthetic oils are also good options for heat storage media. They do not have a low temperature operating constraint like their counterparts due to their very low freezing points[40,41]; their low vapor pressure eliminates the need for pressure vessels, and they are less corrosive when compared to molten salts. However, the costs for synthetic thermal oils are significantly higher than molten salts, and material cost for large storage systems contributes to a significant fraction of the capital costs of the SH-TES systems.

In order to quantify the best option for LWR, a simple technical-economic analysis was performed. Four fluids were chosen for this analysis Hitec and Hitec XL as the molten salt candidates, and two of the widely used synthetic oils, Therminol-66 and Dowtherm A. The generic properties of the chosen fluids are provided in Table 16[42,43,44].

Table 16. SH-TES storage media properties.

Storage Medium	Hitec	Hitec XL	Therminol-66	Dowtherm A
Melting Point (°C)	142	120	-32	15
Stability Limit (°C)	535	500	359	393
Density (kg/m^3) @ 300°C	1640	1992	809	815
Cp (kJ/kg-K) @ 300°C	1.56	1.45	2.57	2.32
Cost ($/kg)	0.93	1.19	6.72	3.96
Composition	$NaNO_3$-KNO_3-$NaNO_2$, 7-53-40	$NaNO_3$-KNO_3-$Ca(NO_3)_2$, 7-45-48	-	-

2.3.2.1 Modeling of Liquid-Based SH-TES

Steady-state process models of the SH-TES system were developed for the four SHS mediums using AspenTech HYSYS. The charging and discharging cycles were modeled separately as they require different components. Each of the components were sized appropriately to meet the discharge capacity of 500 MWe. The sized components were then used to estimate costs for the economic analysis using APEA.

To set a basis for SH-TES model development, the operating conditions of a typical NPP steam generator were used. Steam from the steam generator is used as the heat transfer fluid to heat the storage medium during the charging cycle. As the models are steady-state and focused primarily on the SH-TES system operation, the modeling of the NPP was not included. The steam conditions used for this analysis are listed in Table 17.

Table 17. Operating conditions of a typical nuclear power plant steam generators[45]

Parameter	Value
Mass flow rate (kg/hr)	7,420,000
Pressure (MPa)	6.9
Temperature (°C)	285

The synthetic oils and steam/water properties are readily available in HYSYS; however, the molten salts had to be modeled as hypothetical fluids. Temperature-dependent polynomials from the literature were used to generate tabulated data for density, viscosity, specific heat capacity and thermal conductivity, which were then imported into Aspen HYSYS46F46. This allowed for the calculation of the thermophysical properties of the molten salts at any point within the operating range used in the simulation. The temperature-dependent profiles of the thermophysical properties generated by HYSYS were compared to those provided in the literature for validation. The overall setup of the SH-TES models for all storage media to be analyzed is the same. During the charging cycle, steam from the NPP is condensed on the primary side of a set of heat exchangers and the condensate is returned to the NPP. On the secondary side, the heat-storage medium is pumped from the cold tank to the hot tank, absorbing the heat from steam condensation. Figure 31 shows a general schematic of the charging cycle for the SH-TES system and a process flow diagram (PFD) of its HYSYS equivalent.

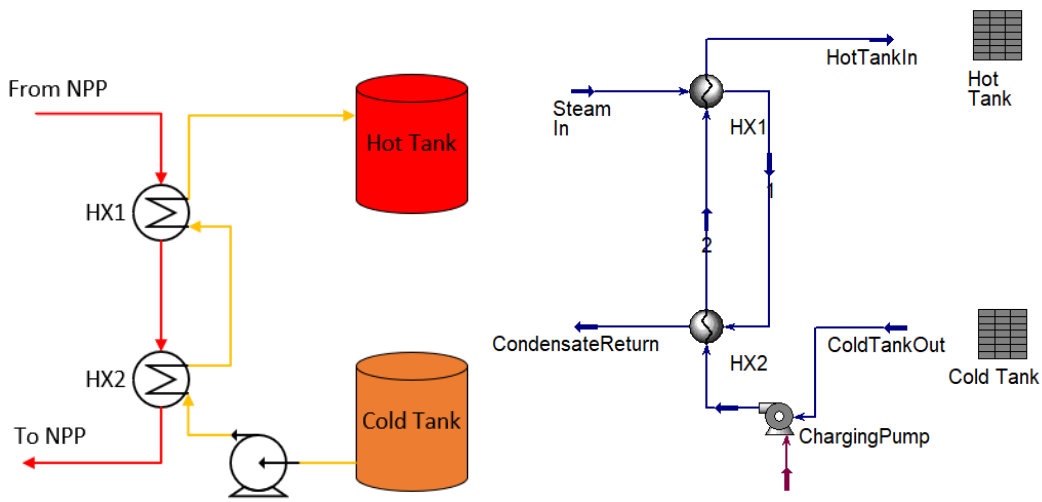

Figure 31. Schematic and PFD of SH-TES charge cycle.

During the discharge cycle, the fluid stored in the hot tank is pumped through another set of heat exchangers to produce steam for power generation purposes. The power cycle assumed for this analysis is a simplified Rankine cycle. The steam produced during the discharge cycle is routed to a secondary power cycle and not the primary Rankine cycle connected directly to the NPP. This secondary power cycle is an additional capital expense that is accounted for. Figure 32 shows a general schematic of the discharge cycle for SH-TES system and a PFD of its HYSYS equivalent.

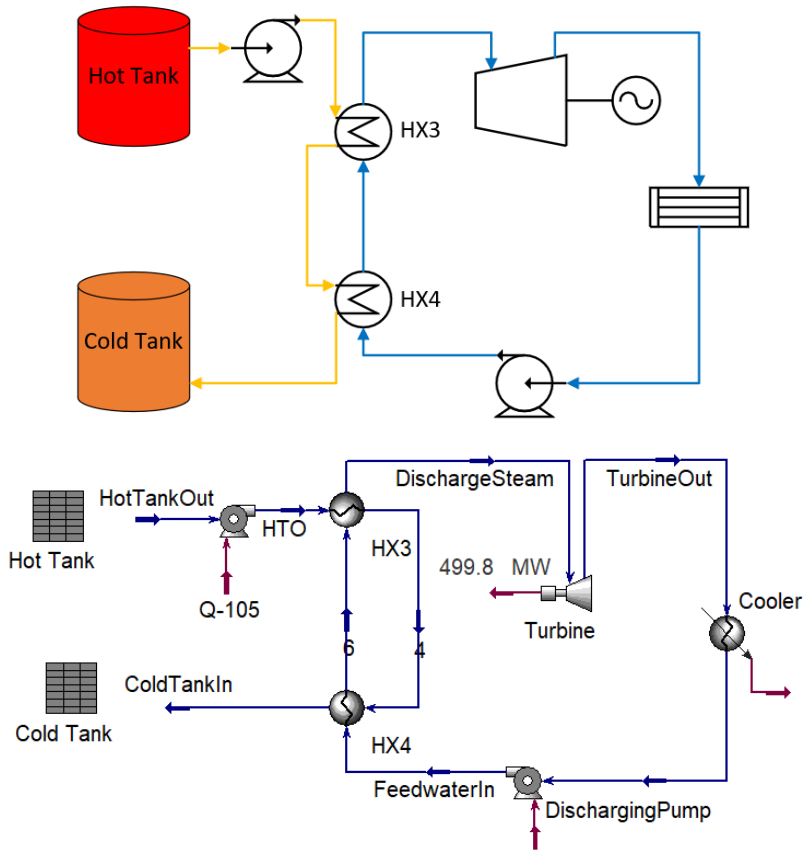

Figure 32. Schematic and PFD of SH-TES discharging cycle.

To simplify the analysis, the sizing of the tanks was conducted using embedded spreadsheets in HYSYS. The condenser in the Rankine cycle was modeled using a cooler. This was done to allow for better conversion of the simulation to temperature setpoints. However, to calculate the capital expenditures correctly, a stand-alone model for the cooler (condenser) was also modeled using a separate heat exchanger with feedwater streams and the exact inlet and outlet conditions from the cooler in the Rankine cycle. This stand-alone heat exchanger, along with all the other components from the charging and discharging cycle was sized appropriately and then the information was transferred to APEA to calculate the equipment costs.

The assumptions made to conduct the preliminary analysis of the SH-TES systems are as follows:

- All storage media operate with a cold tank temperature of 180°C and a hot tank temperature of 280°C.
- There is no heat loss from any components used in the analysis, including the storage tanks.
- All pumps and turbines have a 90% adiabatic and isentropic efficiency, respectively.
- No additional energy is required to maintain the entire system, particularly the discharge power cycle on hot stand-by mode.
- The turbine outlet pressure in the discharging cycle and the condensate return temperature are data points acquired from a generic pressurized water reactor (PWR).

Charging Cycle

While maintaining steam-inlet conditions constant during the charging cycle, the flowrates of the storage media required to produce a hot tank inlet temperature of 280°C were calculated. The upper limit for temperature was chosen such that a minimum approach temperature of 5°C could be maintained in HX1. The cold tank temperature was assumed to be 180°C, which is about 40°C higher than the melting point of Hitec salt. This is a safe ΔT that is assumed to prevent any solidification of the molten salts. These temperature limits were maintained for all the fluid sets to have the basis of equal comparison. As the model setup is similar for all the fluids, the PFDs of Hitec is used to represent the operation of the charging and discharging cycles.

Figure 33 shows the charging cycle with Hitec as the heat storage medium. HX1 is the heat exchanger wherein saturated steam from the NPP's steam generator undergoes condensation, while heating up the Hitec (Stream 2). Similarly, HX2 is the subcooler in which the condensed steam (Stream 1) is further subcooled before being sent back to the NPP. This subcooler acts as a preheater for the Hitec fluid being pumped from the cold tank. The input parameters provided to the model were the steam-inlet conditions, the Hitec-inlet temperature, the pressure drops across the heat exchangers, and the minimum approach temperature limit. The heat exchangers are initially modeled with a 2% pressure drop on each side. Based on these input parameters, the model calculates the flowrate required to match the Hitec outlet temperature at HX1 (hot tank inlet).

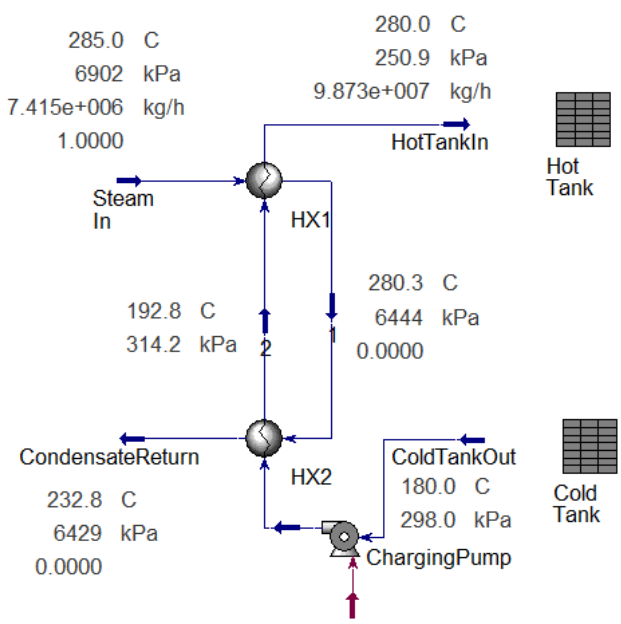

Figure 33. PFD of the charging cycle of SH-TES with Hitec as the storage medium.

The embedded spreadsheet uses operating conditions imported from the streams to conduct simple calculations to estimate the mass and volume of storage media required for different storage durations.

Discharging Cycle

The discharging cycle of the SH-TES system involves power generation with the help of a separate steam-Rankine cycle as previously described. Figure 34 shows the discharging cycle with Hitec as the heat storage medium. HX4 is the preheater for the feedwater in the Rankine cycle and HX3 is the evaporator and superheater. A HYSYS built in iterating tool called 'adjust' was used to ensure that appropriate flowrates for the feedwater and the storage media are calculated such that a net turbine power outlet of 500 MWe is generated. The turbine outlet pressure of 8 kPa is based on the condenser pressure

of a generic PWR design. This condenser is modeled as a cooler in the secondary Rankine cycle but is separately modeled with a standalone heat exchanger and feedwater streams (see Figure 35). As mentioned, the discharge cycle uses a separate power cycle and not the NPP's power cycle to generate electricity.

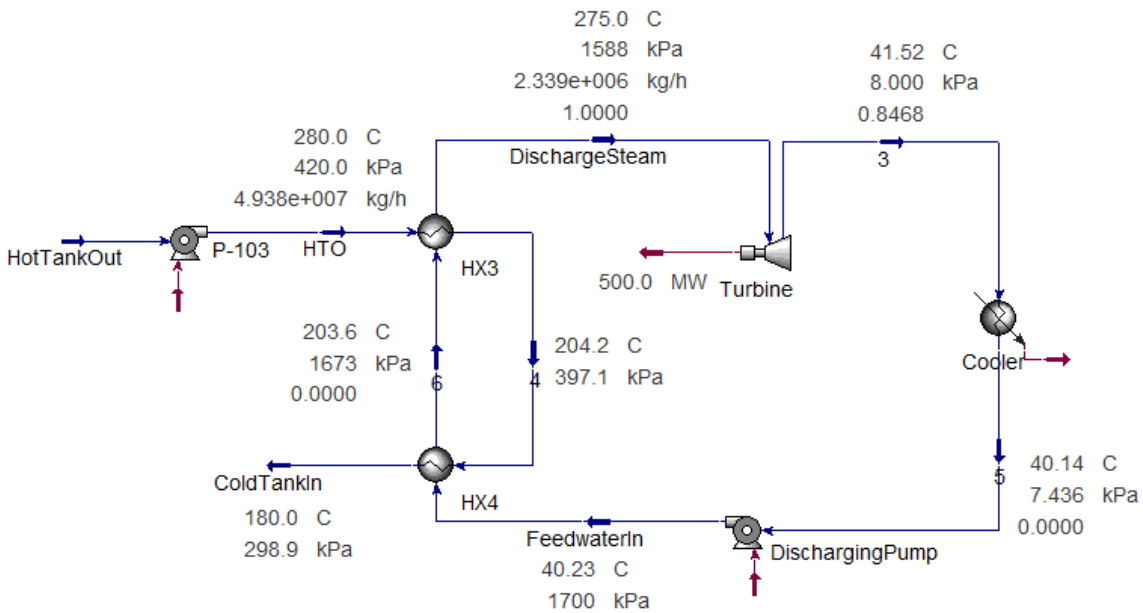

Figure 34. PFD of the discharging cycle of SH-TES with Hitec as the storage medium.

The feedwater-inlet temperature and pressure are assumed to be 15°C and 1 atm, and its outlet temperature is 35°C. Using these input parameters, and the flow conditions of the condensing steam from the turbine outlet, the feedwater flowrate is calculated, and the corresponding feedwater pump power.

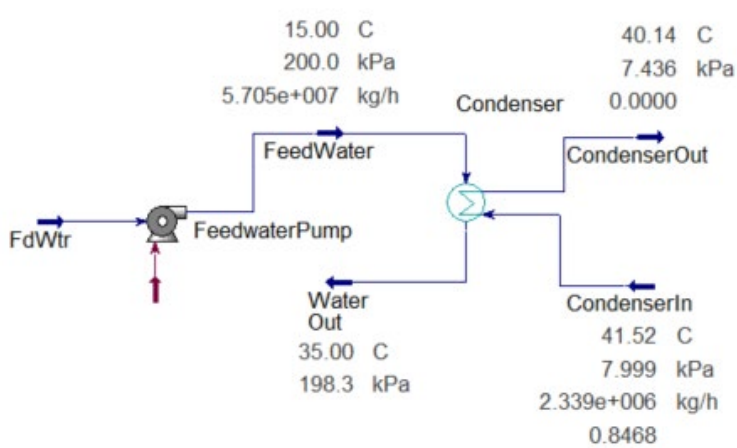

Figure 35. PFD of a standalone heat exchanger model for the condenser of Rankine power cycle.

Due to temperature and pressure limitations, the maximum conversion efficiency, which is the ratio of the net power out to the heat into the cycle, that could be achieved from the secondary Rankine cycle is 27%. This thermal-to-electric conversion efficiency multiplied by the 100% thermal efficiency of the

system provides a RTE of 27%. It should be noted that these calculations do not include heat losses or any other thermal-hydraulic-related parasitic loads.

The heat exchangers were next sized using Aspen Exchanger Design and Rating. This allowed for the acquisition of detailed heat exchanger designs and actual pressure drops across those designs. The pressure drops were then updated in the original Aspen HYSYS model to maintain consistency and improve accuracy. Details of the sized components, which include heat exchangers, pumps, and a turbine were then used in APEA to acquire the capital costs. The same procedure was followed for all storage media.

2.3.2.2 SH-TES System Costs

A preliminary SH-TES system cost evaluation was performed by estimating the capital costs of each component included in the charging and discharging cycles, as well as the cost of the storage media. As the models were sized to deliver 500 MWe for various durations, the estimated capital costs were broken down into two parts: costs that depend on the storage capacity and costs that are independent. Storage capacity-dependent costs include those of the storage tanks and the storage medium, while the heat transfer and thermal-hydraulic equipment are independent of the storage capacity. The independent component costs are further classified as equipment costs and the installed costs, both of which were acquired from APEA. The equipment and installed costs for an SH-TES system with Hitec as the storage medium are shown in Table 18.

Table 18. Estimated equipment costs for an SH-TES system with 500 MWe net power generation capacity with Hitec as a storage medium.

Equipment	Capacity	Unit	Equipment Cost	Installed Cost	Cost per kWe	Notes
HX1	3163	MW	$30,652,200	$37,516,888	$75	30 units in total - 3 series x 10 parallel.
HX2	482	MW	$6,945,800	$9,417,205	$19	7 units in total.
HX3	1371	MW	$4,836,200	$6,802,440	$14	20 units in total - 2 series x 10 parallel
HX4	453	MW	$16,649,300	$18,875,476	$38	36 units in total - 4 series x 9 parallel
Condenser	1326	MW	$38,040,000	$46,084,900	$92	90 units in total. Sizing limitations in APEA
Charging Pump	4.344	MW	$16,796,900	$18,532,595	$37	
Discharging Pump	3.519	MW	$7,118,000	$8,210,056	$16	
Power Cycle Pump	1.231	MW	$621,700	$743,330	$1	
Condenser Pump	1.758	MW	$1,740,000	$6,478,700	$13	90 units in total. To match the condenser quantities
			Total	$152,661,590	$305	

Although the system is charged with thermal energy, the costs per unit of energy are provided in an electric basis ($/kWe) since the final product of the system is electricity. The total cost of the storage medium required to discharge the SH-TES system for 1 hour was calculated using the flowrate and the cost of the medium per kilogram. This value was then divided by the total energy produced by the system i.e. 500 MWe. A similar calculation was performed to acquire the cost of the storage tanks, using the assumption that the thermal equivalent cost of the storage tank is $6/kWh-t47. The energy-unit costs ($/kWe) of the tanks and the storage medium were then multiplied with the amount of energy stored for different discharge durations to estimate the storage capacity-dependent costs. The calculation for the storage capacity-dependent costs for Hitec at 6 and 12 hours of storage is shown in Table 19.

Table 19. Estimated storage capacity dependent costs for Hitec at 6 and 12 hours of storage.

Component	Unit Cost ($/kWe)	Actual Cost ($M)
Hot Storage Tank	22	$66M (6h) $131M (12h)
Cold Storage Tank	22	$66M (6h) $131M (12h)
Molten Salt	92	$275M (6h) $551M (12h)
Total	136	$407M (6h) $813M (12h)

The sum of storage dependent and storage independent costs provides the total capital investment. A summary of the total capital investment for the various storage mediums for a 6 and 12 hours storage capacity is shown in Table 20.

Table 20. Estimated total capital investment costs for SH-TES system with 500 MWe net power generation for 6 and 12 hours.

Storage Medium	Equipment Cost ($M)	Storage-base Cost ($M)	Total Cost ($M)
Hitec	$152	407 (6h) $813 (12h)	559 (6h) $965 (12h)
Hitec XL	$169	429 (6h) $859 (12)	598 (6h) $1,028 (12h)
Therminol-66	$160	1376 (6h) $2,752 (12h)	1536 (6h) $2,912 (12h)
Dowtherm A	$154	966 (6h) $1,932 (12h)	1120 (6h) $2,086 (12h)

Based on the total capital investment cost, it is evident that the systems with synthetic oils as heat storage media are more expensive than those with molten salt, and within the salts, Hitec has the lowest capital investment costs. This pattern is true for all storage durations since the major contributor to the total costs is the cost of the storage medium. By dividing the total capital investment cost by the total amount of energy stored, the CAPEX per unit of energy stored is calculated in $/kWh-e. A plot of the variation of the CAPEX with respect to the storage capacity for all the storage mediums is shown in Figure 36. The plot indicates that the unit capital cost drops significantly for storage durations varying from 3 to 12 hours but then plateaus as the storage capacity increases further. This supports the fact that the storage capacity-dependent costs are a major contributor to the total capital investments, and they increase linearly with an increase in storage duration.

The detailed cost breakdown of the equipment costs and storage capacity-dependent costs for each of the fluids is provided in Appendix B.

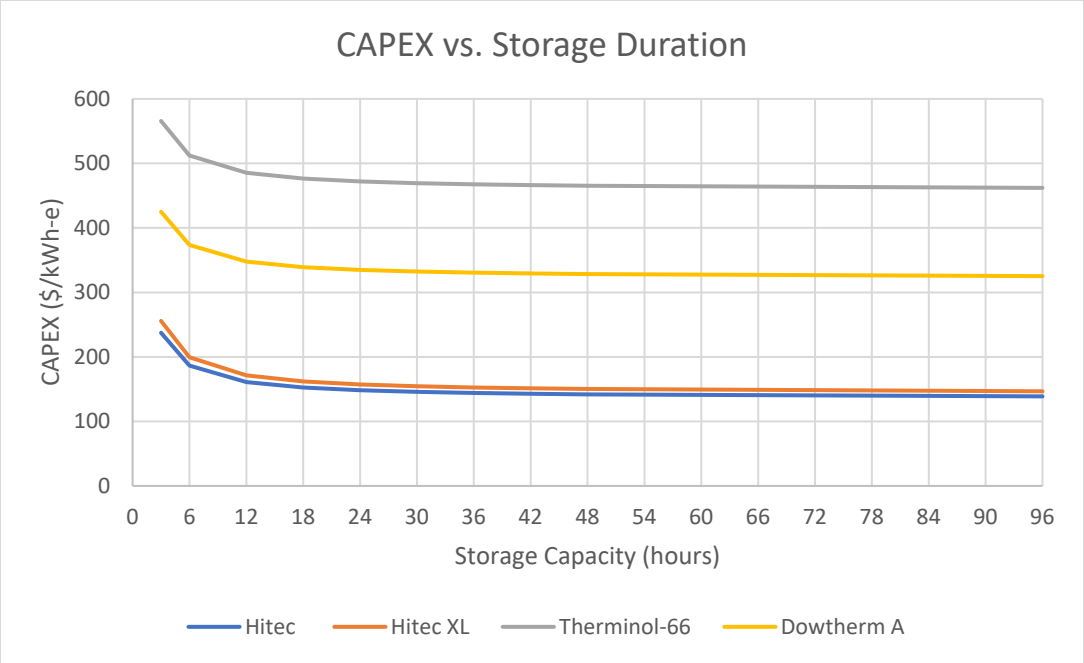

Figure 36. Estimated SH-TES capital costs (per unit of electrical energy storage capacity) as a function of storage capacity.

SH-TES Levelized Cost of Storage

The LCOS analysis conducted for the SH-TES system follows the same methodology as described in Section 2.3.1.3 and therefore, only the results of the analysis are presented in this section. Table 21 lists the input parameters used for the LCOS calculation for Hitec as the storage medium. For a power rating of 500 MWe, storage duration of 12 hours and a one-day interval between discharge cycles, the LCOS of the Hitec system is $93/MWh-e. It should be noted that the LCOS is a function of the charging cost, and therefore a variation in this cost depends on the source, application, location, etc. This variation for an SH-TES with Hitec as the storage medium for 6 and 12-hour storage duration is shown in Figure 37. The trend is similar to that of the ETES LCOS plot shown previously.

Additional analysis of the SH-TES LCOS system with Hitec as the storage medium is shown in Figure 37. This figure presents the LCOS as a function of the discharge cycle duration and the interval between the initiation of the discharge cycles. It is evident that increasing the storage duration does decrease the LCOS as expected, but the reduction is not so significant for storage capacities over 12 hours. This is primarily because the storage-dependent capital costs, which are the major contributor to the total costs, are a strong function of the storage durations. Therefore, a decrease in the capital costs per unit energy (CAPEX) is observed, but it is not significant. Another trend that can be observed is that increasing the interval between discharge cycles leads to an increase in the LCOS. This is because greater intervals between the discharge cycles lead to lower total discharge hours, thereby generating less revenue from the sales of electricity.

Similar analyses were conducted for systems with Hitec XL, Therminol-66 and Dowtherm A, the results of which are provided in Appendix B.

Table 21. Summary of LCOS analysis for SH-TES with Hitec as the storage medium.

System Design		**Units**
Power Rating	500	MWe
Duration	12	hr
Usable Energy	6000	MWh-e
Interval Between Start of Discharge Cycles	24	h
Depth-of-Discharge	100%	
Operating Days/yr	350	
System Performance		
Round Trip Efficiency	27%	total efficiency
Degradation	0.00%	per annum
CAPEX		
System CAPEX	$966	$M
Total Initial Installed Cost	$161.09	$/kWh-e
OPEX		
Electricity Charging Cost	30	$/MWh-e
Charging Cost Escalation	2.50%	per annum
O&M, General	1.50%	% of CAPEX
General O&M Cost Escalation	2.50%	per annum
Calculated Levelized Cost of Storage		
LCOS (12 hr discharge capacity)	$93.29	$/MWh-e

Note: The round trip efficiency is the product of the thermal efficiency of the SH-TES systems that is assumed to be 100% and the thermal-to-electric conversion efficiency of 27%, as calculated from the HYSYS models.

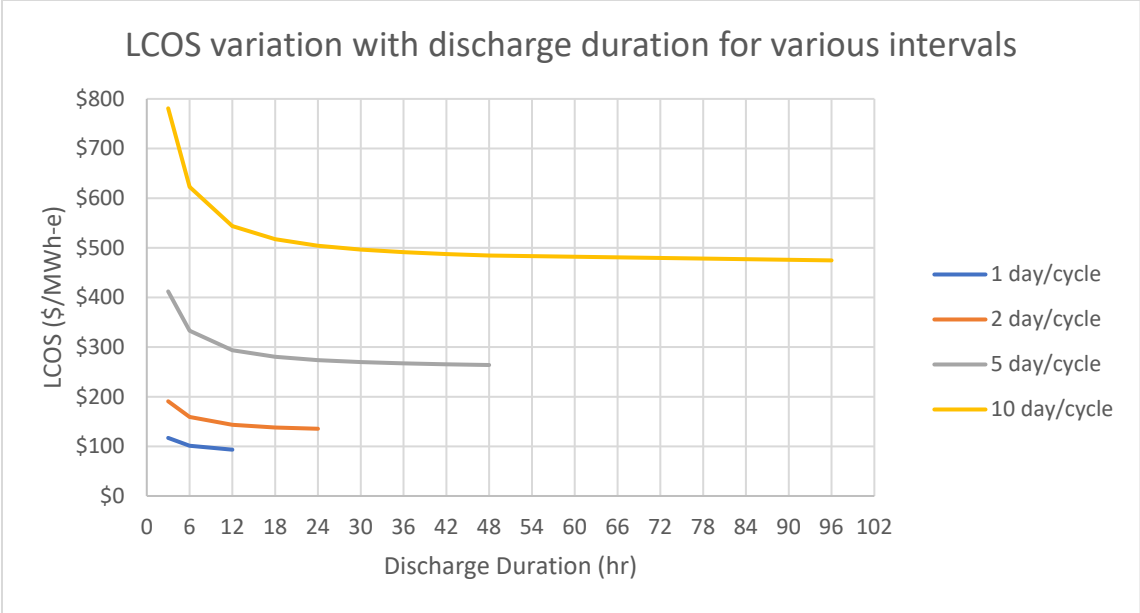

Figure 37. LCOS as a function of discharge cycle duration with an interval between initiation of discharge cycles as a parameter for Hitec-based SH-TES.

A sensitivity analysis was carried out for the SH-TES LCOS by varying 8 parameters, namely, the system efficiency, charging cost, total capital investment, cost of equity, cost of debt, debt fraction, DOD and generation capacity. The range of variance of the parameters and its effect is shown in Figure 38 using a tornado chart. It is evident that the charging cost, generation capacity and the total capital investment have the greatest impact on the LCOS of the Hitec-based SH-TES system.

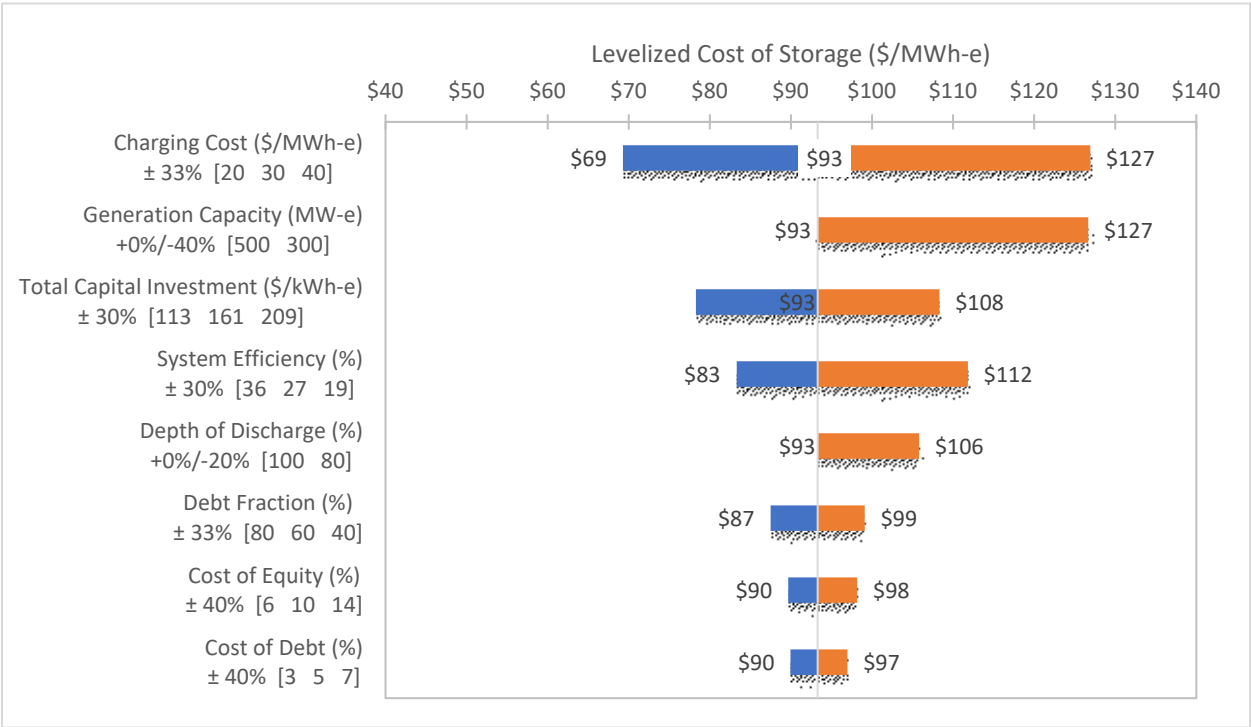

Figure 38. Tornado chart illustrating the sensitivity of Hitec-based SH-TES LCOS to selected parameters.

It is evident that varying the charging cost has the most amount of effect on the LCOS. It is obvious that for maximizing the profits, the system should be charged during the availability of the lowest electricity price and discharged during peak demand. The variation of the LCOS with charging costs for 6 and 12 hours of storage capacities is shown in Figure 39.

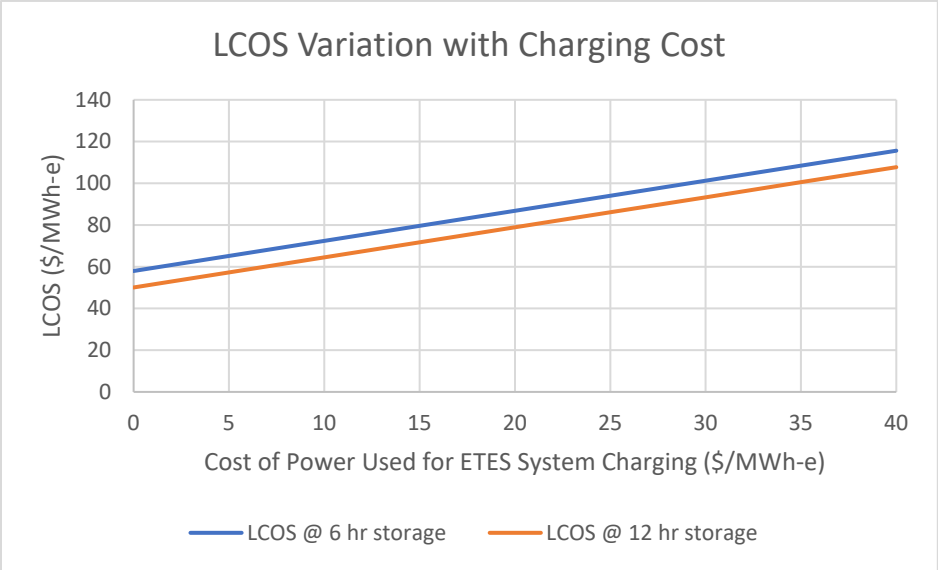

Figure 39. LCOS as a function of the charging electricity for an SH-TES with Hitec.

The above analysis uses a variety of fixed charging costs of electricity. Figure 40 shows the possible effects of variable charging costs based on average market electricity prices. The data series shown in blue is representative of an SH-TES system operating with a constant charging energy cost of $30/MWh-e. The data series shown in orange is representative of an SH-TES system with a time-dependent charging energy cost based on the 2030 average energy market prices projected for the Palo Verde Hub (Arizona Public Service) per the APS 2020 integrated resource plan.

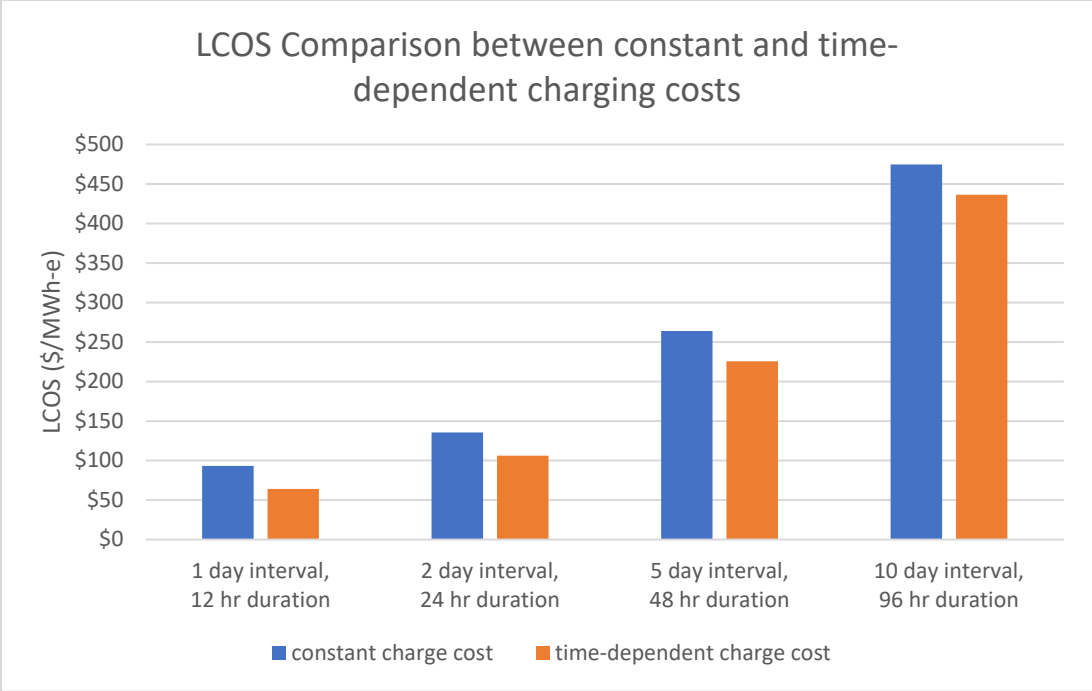

Figure 40. LCOS comparison for Hitec-based SH-TES systems operating with selected discharge intervals/durations and charging costs.

The LCOS behavior shown in Figure 37 – Figure 40 are all for the Hitec-based SH-TES system. Similar plots generated for Hitec XL, Therminol-66, and Dowtherm A are provided in Appendix B.

2.3.2.3 Summary of Liquid-Based SH-TES

Preliminary analysis of the liquid-based SH-TES systems has been performed for four fluid mediums, namely, Hitec, HitecXL, Therminol-66, and Dowtherm A. A techno-economic analysis focused on acquiring the LCOS of this technology was also carried out to conduct a relative comparison of this TES system, with other energy storage technologies. The results of this analysis are summarized below in Table 22.

Table 22. Summary of Liquid-Based SH-TES

System Design		**Comments**
Capacity (discharge mode)	500 MWe	
Thermal efficiency	100%	
Conversion efficiency	27%	Power cycle efficiency
RTE	27%	Product of thermal and conversion efficiency
Economics		
Equipment: Component costs (storage independent)	$152 million	
Storage & Material costs (storage dependent)	Hitec: $407 million (6h) $813 million (12h)	Calculated at $30/MWh-e charging cost
	Hitec XL: $429 million (6h) $859 million (12h)	
	Therminol-66: $1376 million (6h) $2752 million (12h)	
	Dowtherm A: $966 million (6h) $1932 million (12h)	
Total Capital Investment ($)	Hitec: $559 million (6h) $965 million (12h)	Calculated at $30/MWh-e charging cost
	Hitec XL: $598 million (6h) $1028 million (12h)	
	Therminol-66: $1536 million (6h) $2912 million (12h)	
	Dowtherm A: $1120 million (6h) $2086 million (12h)	
Levelized Cost of Storage ($/MWh-e)	Hitec: $101(6h) $93 (12h)	Calculated at $30/MWh-e charging cost
	HitecXL: $105 (6h) $96 (12h)	
	Therminol-66: $202 (6h) $194 (12h)	
	Dowtherm A: $159 (6h) $151 (12h)	

Conclusions

Based on the analysis conducted for the liquid-based SH-TES systems, it was evident that Hitec was the optimal choice as the storage medium. It has the lowest LCOS cost, and its melting point is fairly low to allow the coupling of the SH-TES to an existing LWR. The next best fluid is Hitec XL, with Therminol-66 being the most expensive of the four. Nevertheless, it should be noted that this analysis did not take into account several factors, the most important of which is heat loss from the system. This would play a crucial role as molten-salt-based systems require heat tracing along all of its components whereas oil-based systems do not. Furthermore, the oil-based systems could operate at a lower temperature, thereby increasing the available ΔT for operating. All of these factors need to be taken into account and more rigorous analyses, which include dynamic studies need to be conducted.

2.3.3 Steam Accumulators

Steam accumulators rank high incompatibility with existing LWR systems because they are charged directly with high-pressure steam, but the potential capacity low end. This technology has been around for decades and is used alongside industrial boilers. The first large steam accumulator built to produce peak electricity was the Charlottenburg Power Station built in Berlin in 1929 with a peak electricity output of 50 MWe and a storage capacity of 67 MWh. The steam was provided by a coal-fired boiler and the accumulator had a separate turbine. This accumulator had 16 tanks each 4.3 meters in diameter and 20 meters high (~290 m^3 each)[48]. Steam accumulators have also been coupled with CSPs that work on the principle of direct steam generation[49]. One of the most recent installments of a solar tower-based CSP plant with steam accumulator storage is the Khi Solar One in Upington, South Africa. This facility has the capability of storing super-heated steam for up to 2 hours in 19 steam accumulator tanks[50]. During normal operational hours, superheated steam is generated and sent directly to the power block to generate electricity. The condensate is cooled and returned to the solar power receiver. During off-peak hours, the superheated steam is used to charge the steam accumulators. During hours of high demand, the relief valve on the steam accumulators is opened and saturated steam leaves the system to be is used to produce additional power.

The idea of coupling steam accumulators with an NPP has been studied[48]. In that study, researchers discuss a high-pressure accumulator charged with fresh steam drawn via the turbine by-pass valve and a low-pressure accumulator charged by steam exiting the high-pressure turbine. The discharge from both accumulators is diverted to an auxiliary turbine during hours of additional demand. In a more recent analysis, the coupling of a steam accumulator to an LWR has been modeled, the discharge from which was used in the feedwater heaters and moisture separators[51]. This reduces the amount of steam drawn from the high-pressure turbine, thereby increasing the turbine power.

It should be mentioned that the current steam accumulator designs only produce saturated steam and at a sliding pressure. This is detrimental because the efficiency of the power cycle will decrease as more steam is released from the steam accumulator. Furthermore, steam accumulators are pressure vessels and therefore, they have physical constraints dictated by operating pressure. This limits the storage capacity of a steam accumulator. Using the numbers from Khi Solar one, 19 steam accumulators can provide 50 MWe, which is about 15% of a 1 GW NPP with a conversion efficiency of 33%. Although the amount of energy stored and recovered from the steam accumulators is significant, the number of storage tanks required to provide 500 MWe for 6-12 hours is very large. Based on another recent analysis [52], the pressure vessel's cost accounts for about 60-70% of the total TES cost. Nevertheless, steam accumulators can be discharged rapidly and have a RTE ranging between 60 and 80%. The discharged steam can either be superheated using electrical topping heat before its delivery to the power block, or it can be introduced into a low-pressure turbine in a Rankine power cycle. Due to this flexible nature and ease of use of steam accumulators, they are an attractive TES option for coupling with existing LWRs in small amounts. The feasibility of coupling steam accumulators with LWRs is briefly evaluated in the following section.

2.3.3.1 Steam Accumulator Sizing Analysis

A simplified model was built to determine the number of steam accumulator units that would be required to store 500 MWe for various discharge periods. In this analysis, the inlet steam conditions as provided were used. The volume of the steam accumulator is based on this storage capacity as well as the required discharge pressure required by the component or customer downstream of the steam accumulator. In this modeling effort, it is assumed that the discharged steam is sent to a similar secondary power cycle as discussed in Section 2.4.2. As shown in Figure 34, the design inlet pressure to the turbine is 1.59 MPa, however, the operating discharge pressure is chosen to be 1.69 MPa. This decision was made to provide an adequate steam flashing capacity for the steam accumulator, and an assumption was made that the pressure could be controlled using a throttling valve. The pressure at the outlet of the turbine is 8 kPa and the flow rate of steam through it is 2.339E6 kg/hr. To calculate the volume of the

steam accumulator, the flash steam generation amount needs to be calculated. Using the steam accumulator charging pressure (P1) and the design discharge pressure (P2), the amount of water required to flash and produce steam can be calculated using as,

$$m_{flash} = \frac{h_{liq}@P_1 - h_{liq}@P_2}{h_{vap}@P_2}$$

Herein, h_{liq} is the liquid enthalpy at the corresponding pressures, h_{vap} is the heat of vaporization and m_{flash} is the mass of steam flashed per unit mass of saturated water. Using the charging pressure of 6.902 MPa as P_1, the discharge pressure of 1.69 MPa as P_2, and their corresponding enthalpies, the ratio of steam flashed to the amount of water required is calculated to 0.14 kg steam/kg water.

Based on the calculated mass flow rate of steam required for the turbine, the amount of steam required for different storage capacities is calculated. Using the mass of steam required and the flash steam ratio, the mass of water required for the respective storage capacities is calculated. In most steam accumulators, a fully charged steam accumulator has 90% of its volume occupied by the liquid phase. Based on this information and knowing the density of water at the charging pressure, the volume of the steam accumulator is calculated. A steam accumulator storage tank volume of 290 m^3 is used and the number of steam accumulators is calculated. The calculated values are provided in Table 23.

Table 23. Steam accumulator sizing analysis results

Storage Durations (hours)	3	6	12	18	24	30	36
Mass of steam required (kg)	7.02E+06	1.40E+07	2.81E+07	4.21E+07	5.61E+07	7.02E+07	8.42E+07
Mass of water required (kg)	5.00E+07	1.00E+08	2.00E+08	3.00E+08	4.00E+08	5.00E+08	6.00E+08
Volume of water (m^3)	6.24E+04	1.25E+05	2.50E+05	3.75E+05	4.99E+05	6.24E+05	7.49E+05
Volume of tank (m^3)	6.94E+04	1.39E+05	2.77E+05	4.16E+05	5.55E+05	6.94E+05	8.32E+05
Number of tanks required	239	478	957	1435	1913	2392	2870

It is evident from Table 23 that the number of steam accumulators required to store very large quantities of energy is not feasible based on the assumed volume of the storage system. For a discharge period of 30 mins alone, the system would require about 40 such tanks. Although larger tanks can be built, the storage tanks would turn out to be expensive due to the high-pressure safety requirements. Therefore, it can be concluded that steam accumulators are not practical as a large-scale energy storage option that could be paired with an LWR with the purpose of using off-peak nuclear energy but they could be beneficial in small amounts up to 15% (150 MWe) of the energy a 1GW NPP.

2.4 Lifecycle Analysis of Energy Storage Options

Life cycle emissions for energy storage options were evaluated using a well-to-plug (WTP) analysis with the Argonne National Laboratory's (ANL's) Greenhouse gases, Regulated Emissions, and Energy use in Technologies (GREET) 2020 model. WTP greenhouse gas (GHG) emissions for electricity production using LWRs and natural gas generators (simple and combined cycle) include Uranium mining and natural gas extraction to power production and transmission of produced electricity to the demand location.

For natural gas combined cycle (NGCC) plants with carbon capture and storage (CCS) 90% of the carbon capture was assumed.

Figure 41 shows the GHG emissions per kWh for storing LWR energy using batteries, hydrogen and thermal options compared with electricity from natural gas generators simple cycle (SC), CC and CC with CCS. The electricity from LWR energy storage scenarios have emissions of 8-20 gCO_{2e}/kWh whereas electricity from natural gas generators is between 112-727 gCO_{2e}/kWh.

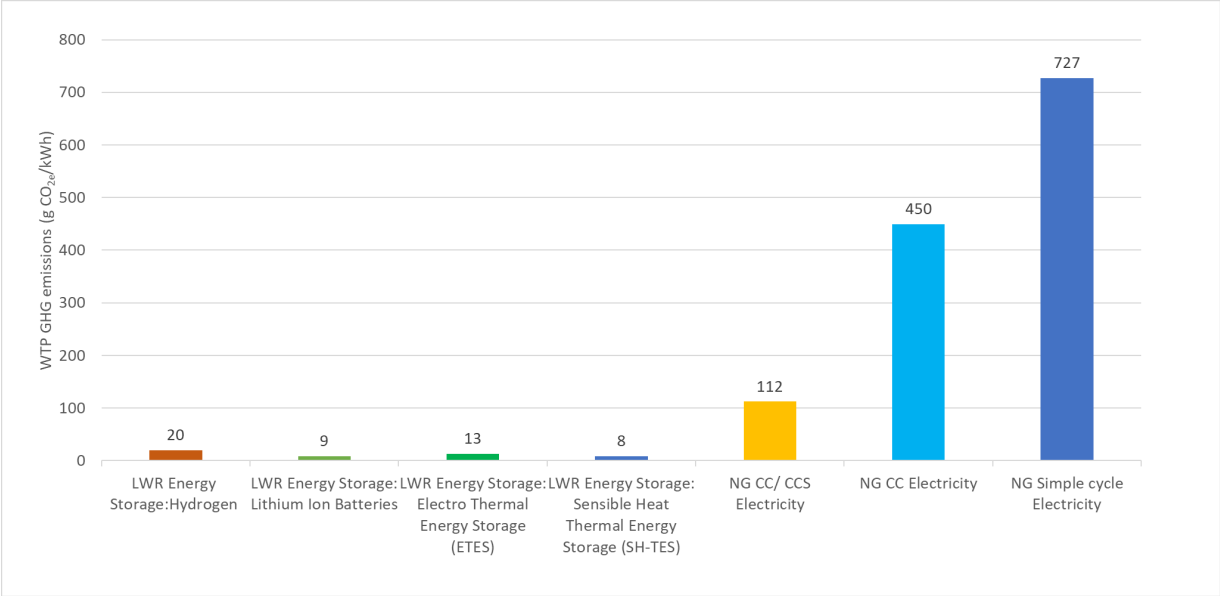

Figure 41 Life cycle GHG emissions for electricity from energy storage compared to electricity generated from natural gas.

2.5 Summary of Nuclear Power Energy Storage Options

Table 24 provides a comparison of the different energy storage technologies analyzed in this section. The assumptions made to conduct this comparative analysis are as follows:

- Cost of power production by an LWR - $30/MWh
- Selling price of electrical power during period of high demand - $80/MWh
- Period of energy discharge at 500 MWe – 6 and 12 hours
- DOD – 100%
- Number of days for arbitrage - 365
- 5% – cost of debt on capital loan.

Table 24. Comparison of energy storage options for power arbitrage discharge capacity of 500MWe and charging cost of $30/MWh.

Storage Option	Input Operating Temperature Range	Capital Cost per unit of stored energy ($/kWh)[a]	Capital Cost ($M)	Cost of Debt ($M/yr)	RTE (%)	Total Revenue ($M/yr)	LCOS (breakeven) ($/MWh-e)
Li-ion LFP Batteries	NA	828 (6 & 12 h)	2484 (6h) 4967 (12h)	119 (6h) 239 (12h)	88	300 (6h) 600 (12h)	357 (6 & 12 h)
H_2-Geological Storage, SOEC / PEM FC	NPP heat to SOEC	500 (6h) 251 (12h)	1500 (6h) 1507 (12h)	72 (6h) 73 (12h)	38	193 (6h) 224 (12h)	230 (6h) 133 (12h)
H_2- Physical Storage, SOEC / PEM FC	NPP heat to SOEC	548 (6h) 296 (12h)	1644 (6h) 1777 (12h)	79 (6h) 86 (12h)	38	209 (6h) 253 (12h)	248 (6h) 151 (12h)
H_2 Physical Storage, PEM to H_2 to Gas Turbine	NA	301 (6h) 238 (12h)	902 (6h) 1429 (12h)	423 (6h) 668 (12h)	61	148 (6h) 262 (12h)	135 (6h) 120 (12h)
Thermal (ETES)	-3°C to 390°C	417 (6h) 247 (12h)	1250 (6h) 1483 (12h)	60 (6h) 71 (12h)	55	204 (6h) 297 (12h)	194 (6h) 141 (12h)
Thermal (sensible / Hitec)	142°C to 535°C	186 (6h) 161 (12h)	559 (6h) 966 (12h)	26 (6h) 46 (12h)	27	106 (12h) 195 (12h)	101 (6h) 93 (12h)
Thermal (sensible / Hitec XL)	120°C to 500°C	199 (6h) 171 (12h)	598 (6h) 2912 (12h)	28 (6h) 49 (12h)	27	212 (6h) 202 (12h)	105 (6h) 96 (12h)
Thermal (sensible / Therminol-66)	15°C to 393°C	512 (6h) 485 (12h)	1536 (6h) 3174 (12h)	74 (6h) 140 (12h)	27	407 (6 h) 611 (12h)	202 (6h) 194 (12h)
Thermal (sensible / Dowtherm A)	-3°C to 359°C	373 (6h) 347 (12h)	1120 (6h) 2086 (12h)	54 (6h) 100 (12h)	27	167 (6h) 317 (12h)	159 (6h) 151 (12h)

a. The cost of storage includes the capital to convert the stored media back to power.

Table 25 below shows an overall comparison of the various energy storage technologies when the charging cost is varied between 0 and 40 $/MWh. Although an in-depth dynamic electric market analysis was out of the scope of this report, this analysis gives an indication of LCOS for a variety of possible market conditions.

Table 25. Summary of sensitivity of LCOS to charging cost for the various energy storage technologies. 500MWe discharge capacity

Technology		Charging Cost ($/MWhe)						
		0	15	20	25	30	35	40
Li-ion LFP Battery	LCOS ($/MWhe)	322 (6h & 12h)	339 (6h & 12h)	345 (6h & 12h)	351 (6h & 12h)	357 (6h & 12h)	363 (6h & 12h)	369 (6h & 12h)
H_2 Geological Storage, SOEC / PEM FC		194 (6h) 98 (12h)	212 (6h) 115 (12h)	218 (6h) 121 (12h)	224 (6h) 127 (12h)	230 (6h) 133 (12h)	236 (6h) 139 (12h)	241 (6h) 145 (12h)
H_2 Physical Storage, SOEC / PEM FC		213 (6h) 115 (6h)	231 (6h) 133 (12h)	237 (6h) 139 (12h)	242 (6h) 145 (6h)	248 (6h) 151 (12h)	254 (6h) 156 (12h)	260 (6h) 162 (12h)
H_2 Physical Storage, PEM EC / Gas Turbine		86 (6h) 71 (12h)	110 (6h) 95 (12h)	119 (6h) 103 (12h)	127 (6h) 112 (12h)	135 (6h) 120 (12h)	143 (6h) 128 (12h)	151 (6h) 136 (6h)
Thermal (ETES)		129 (6h) 77 (12h)	-	172 (6h) 120 (12h)	-	194 (6h) 141 (12h)	-	215 (6h) 163 (12h)
Thermal (sensible / Hitec)		58 (6h) 50 (12 h)	80 (6h) 72 (12h)	87 (6h) 79 (12h)	94 (6h) 86 (12h)	101 (6h) 93 (12h)	108 (6h) 101 (12h)	116 (6h) 108 (12h)
Thermal (sensible / Hitec XL)		62 (6h) 53 (12h)	84 (6h) 75 (12h)	91 (6h) 82 (12h)	98 (6h) 89 (12h)	105 (6h) 96 (12h)	112 (6h) 104 (12h)	120 (6h) 111 (12h)
Thermal (sensible / Therminol-66)		159 (6h) 151 (12)	181 (6h) 172 (12h)	188 (6h) 180 (12h)	195 (6h) 187 (12h)	202 (6h) 194 (12h)	210 (6h) 201(12h)	217 (6h) 209 (12h)
Thermal (sensible / Dowtherm A)		116 (6h) 108 (12h)	138 (6h) 130 (12h)	145 (6h) 137 (12h)	152 (6h) 144 (12h)	159 (6h) 151 (12h)	167 (6h) 159 (12h)	174 (6h) 166 (12h)

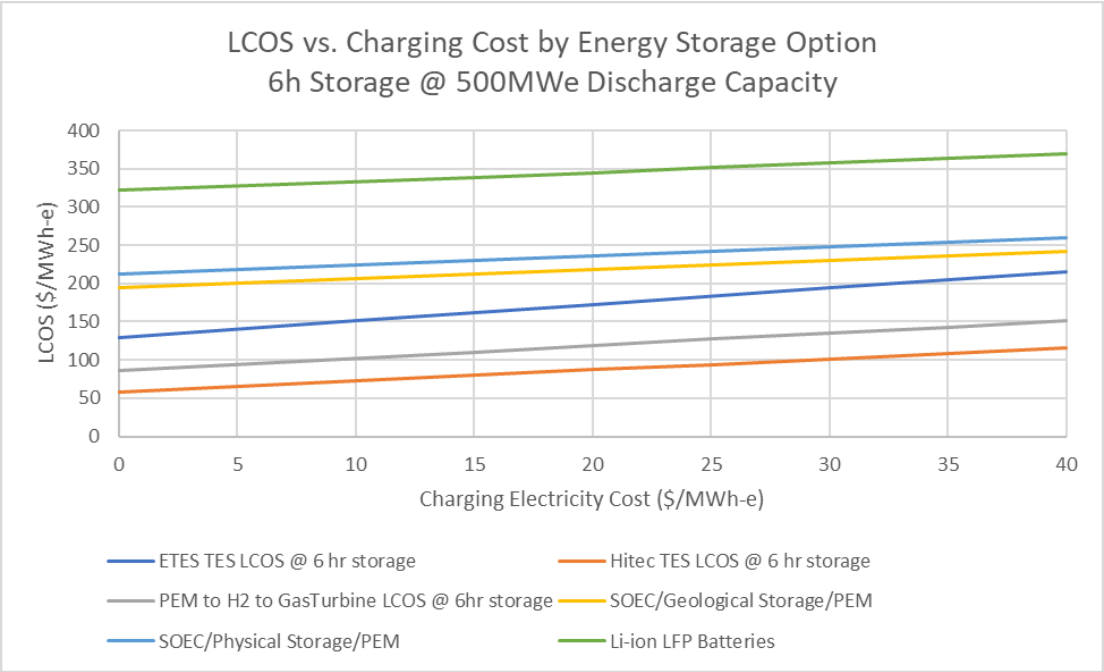

Figure 42 below plots a selection of the LCOS for the above options versus the charging cost to show what the LCOS would be depending on the electricity price that is able to be negotiated for the charging cost.

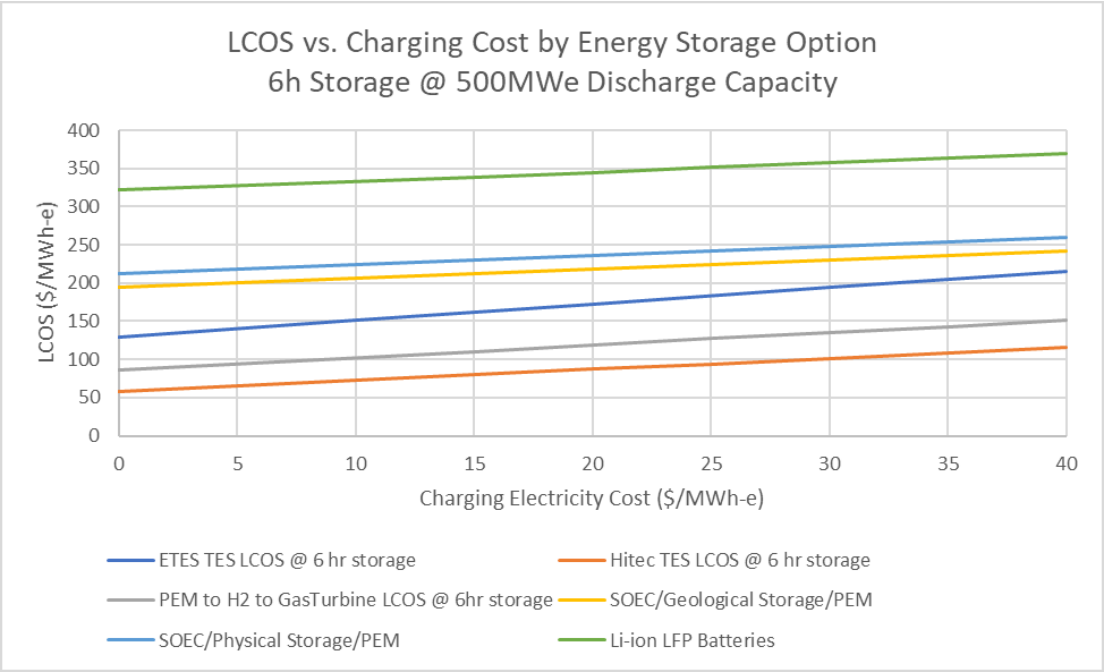

Figure 42. LCOS vs. Charging Cost by Energy Storage Option.

This section has presented a variety of TES systems that are currently being used in industry, as well as under development. The most widely deployed sensible heat-based systems are promising options for coupling with existing LWRs. Latent heat-based systems are not discussed in this report but may also be attractive due to their high gravimetric densities; however, their low thermal conductivity is a significant

barrier to efficient heat transfer. Significant research is being conducted to enhance this heat transfer rate with the help of advanced materials as well as efficient heat exchanger designs.

Although cheap storage material can be used to store thermal energy, efficient heat exchangers are required to transfer heat to and from these solid-state materials. Coupling different TES systems to take advantage of each individual's inherent properties is also a good option, along with using electrical topping heat to superheat the discharged steam.

3. DEMAND RESPONSE OPTIONS FOR INTEGRATION WITH NUCLEAR POWER

In this section, various demand-response options are analyzed for integration with NPPs. Demand response refers to dispatchable loads that are able to ramp up or down flexibly during off-peak grid demand periods. Pairing large dispatchable demand-response loads with NPPs allows reactors to maintain constant output while allowing variable generations of resources such as renewable energy to supply the grid and nuclear power to provide other valuable products and services. This is not meant to be an exhaustive analysis of all possible demand-response options but is a subset of the possibilities. The industries discussed are some that could have very large energy (electricity) demands; thus, these industries provide a large dispatchable load as a sink for off-peak nuclear energy while, at the same time, aiding in the decarbonization of these industrial sectors by providing low-carbon nuclear energy. Options discussed in this section include production of 1) liquid nitrogen via air separation and liquefaction, 2) liquefaction of hydrogen, 3) compressed hydrogen, and 4) cryogenic carbon capture.

Unlike the other options previously discussed in this report, these options do not entail conventional energy storage in the sense of regenerating electricity to support grid needs. The end result instead is demand dispatch to avoid power turndowns of nuclear power stations by having an alternative disposition for the electrical energy while producing marketable products. This is similar to the separately studied case of using off-peak nuclear energy to make hydrogen to sell into the market. Using nuclear energy also allows for increased decarbonization of the industrial sector.

3.1 Liquid Nitrogen

Liquid nitrogen is used for diverse applications such as providing the precooling needed for the first step of hydrogen liquefaction, a coolant for spray cooling, injection cooling, or immersion cooling. It could also be used in cryogenic carbon capture (discussed in a later section of this report). Increased use of liquid nitrogen as a refrigerant in areas such as medicine, industry, research, and cooking are expected to fuel the market growth[53].

Liquid nitrogen (LN_2) can be produced by cryogenic air separation and subsequent liquefaction. The LN_2 market size for the U.S. was estimated to be about 2.3 million MT in 2016. The energy required for separating pure N_2 from the air is about 0.162 kWh/kg-N_2, and for liquefaction of the separated nitrogen, the energy requirement is an additional 0.528 kwh/kg-N_2.[54]

Using these assumptions yields a power requirement of 181MWe to supply the U.S. LN_2 market for a year. This is only 18% of a generalized 1 GW NPP output so clearly the LN2 market alone will not make a large impact on demand response for NPPs.

Using nuclear electricity for nitrogen separation and liquefaction will reduce the emissions associated with this technology. The environmental benefits and life-cycle carbon analysis for these applications are shown in a subsequent life-cycle analysis section.

3.1.1 Liquid Nitrogen Market

Liquid nitrogen market price varies from \$0.3–2/gal, depending on the size of the production facility, utility price, and packaging and handling materials used[55]. For a delivered LN2 in volume (~5000 gal) the price is \$0.3/ gal LN_2.

3.1.2 Liquid Nitrogen Production Cost

To calculate the range of nitrogen production cost based on various sensitivities an existing rigorous process model for ammonia production was adapted and built-in Aspen process modeling software as a simplified model representing only the air separation unity (ASU) and associated heat and material balances.

Table 26 and Table 27 below show the design conditions assumed in the ASU modeling.

Table 26. Cryogenic ASU Design.

Cryogenic Air Separation Unit System
Evaluated includes N_2 compressor (42 bar)
Analysis based on data reported in Wood, R. "Nuclear-Integrated Ammonia Production Analysis" INL TEV-666, 2010
Total Energy Requirement of 23.2 MWe for 2532 tonne-N_2/day + 715 tonne-O2/day unit
9.2 MWe ASU compressors
14 MW N_2 product compressor

Table 27. ASU base case design conditions.

Base Case
ASU design capacity
2532 tonne-N_2/day
715 tonne-O_2/day
• N_2 product 99.9 mol% compressed to 42 bar
• CAPEX: $76.3 million ASU Tot Cap Inv includes: – water systems (7.1% adder) – piping (7.1% adder) – instrumentation and control (2.6% adder) – electrical systems (8.0% adder) – civil/structural/buildings (9.2% adder)
• OPEX – Electricity $30/MWh-e – Labor (1.15% of Total Capital Investment) – Maintenance (3.0% of Total Capital Investment) – Overhead (65% of Labor and Maintenance) – Insurance and Taxes (1.5% of Total Capital Investment)
• Revenues (base case approx. 50% of total revenue from N_2 sales and 50% from O_2 sales)
N_2 (production cost varied to set net present value = 0)
O_2 fixed selling price of $46/tonne-$O_2$

From this model, a sensitivity case study was run to find the nitrogen production cost. In Figure 43, it is shown that if oxygen can be sold, then it has the largest effect on nitrogen production cost, followed by the ASU plant capacity and the ASU CAPEX. Interestingly, electricity price affects nitrogen-production cost, but not as pronounced as other factors.

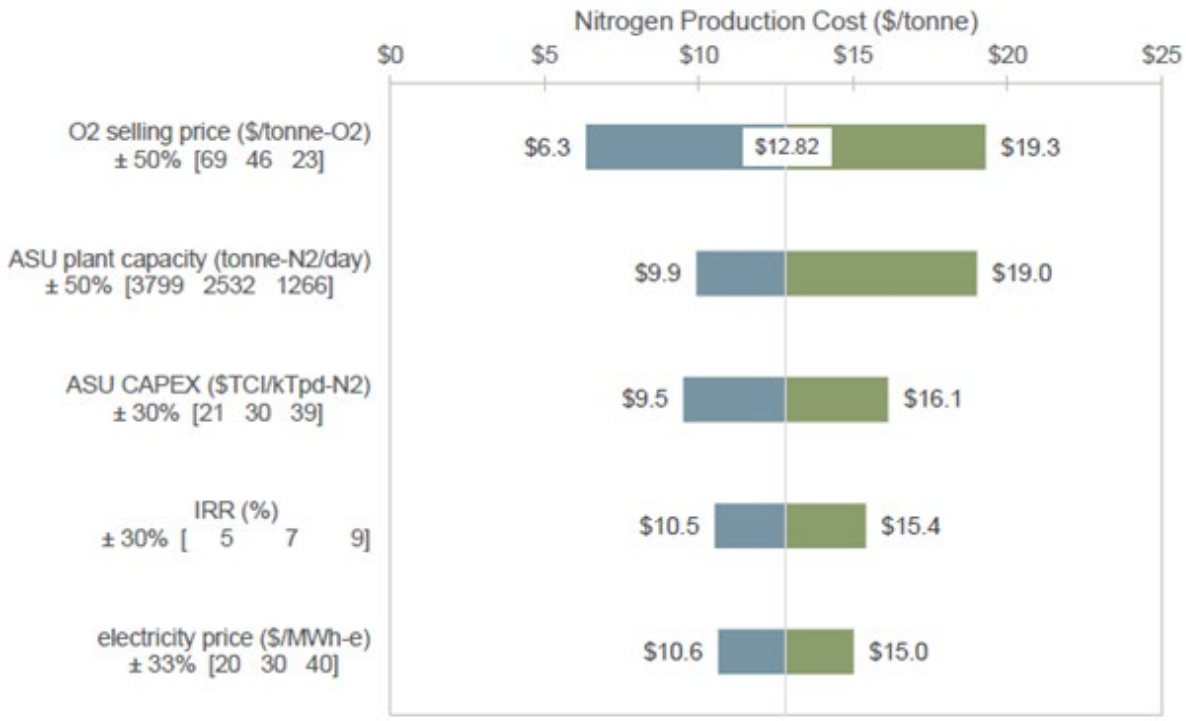

Figure 43. Sensitivity study on the effects of various factors on the cost of nitrogen production via air separation.

3.2 Liquid Hydrogen

Liquid hydrogen can be used as a refrigerant or as a means to provide compact transportation of hydrogen to high-value markets such as fueling fuel cell vehicles, or downstream chemicals, fuels, and materials manufacturing.

The hydrogen liquefaction process includes gas compression, cooling with water, and precooling with liquid nitrogen to cool the hydrogen below its inversion temperature. The inversion temperature for hydrogen is approximately -73°C and is defined as the temperature below which, upon expansion through a valve, hydrogen will cool rather, than warm. This cooling is known as the Joule–Thomson effect, and its exploitation is essential in the liquefaction of gases.

The liquid hydrogen (LH_2) market in the U.S. is about 261 MT/day[56] and will grow by 50% with the addition of new plants in the next 2–3 years. The installed capital cost of a 30 MT/day liquefier is approximately $100 million[57], and the corresponding electric energy requirement for liquefaction is 10-12 kWh/kg of hydrogen. Hydrogen liquefaction accounts for nearly half of liquid truck-delivery costs. The energy required for liquefaction of 261 MT/day of H_2 will be approximately 2.8 GWh/day (11 kWh/kg).

3.3 Hydrogen Compression

Gaseous H_2 (GH_2) requires compression from 20 to 350 bars; the electric energy required could be up to 2 kWh/kg (this value differs from a DOE recorded value of 1.05 kWh/kgH_2 in that the recorded value

is theoretical whereas this value is considered a practical value[58]). For fuel-cell electric vehicles (FCEVs) using GH_2, the energy required for 1 million cars using 0.5 kg H_2 per day would be 1 GWh/day, 1/24th the size of a generic 1GW NPP.

Figure 44 shows the H_2 compression and H_2 and N_2 liquefaction energy cost using nuclear energy, assuming an electricity cost of $20–60/MWh. The energy cost for hydrogen liquefaction is approximately 30% of total levelized cost of liquefaction at electricity cost of $60/MWh. The energy cost for hydrogen compression to 350 bars is approximately 10–20% of total levelized cost of hydrogen compression at electricity cost of $60/MWh.

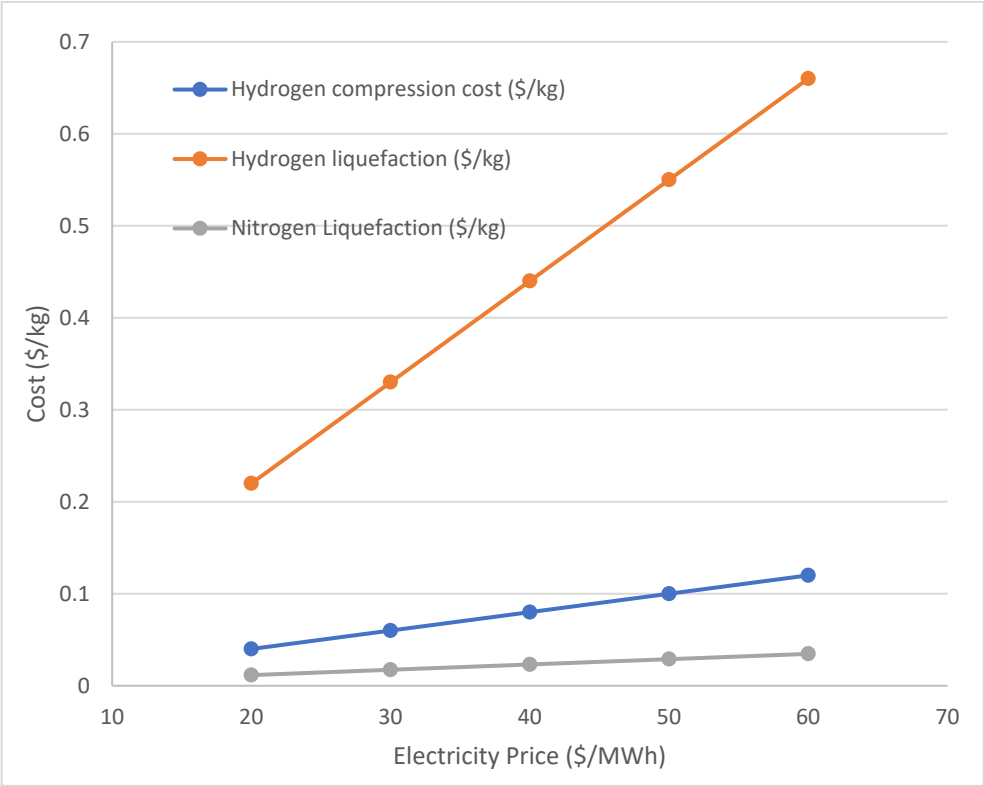

Figure 44. Cost of energy for H_2 compression to 350 bars and liquefaction at different electricity prices.

3.4 Liquid Nitrogen and Liquid Hydrogen Offsite Transportation

Hydrogen or nitrogen produced at a central production plant can be liquefied and loaded into liquid tankers for delivery to various end-users. A cryogenic pump draws liquid hydrogen or nitrogen from a cryogenic storage tank to the liquid tankers. A liquid tanker is transported to the demand location where it is emptied into a cryogenic storage tank and held until use. Cryogenic storage tanks at terminals near liquefaction plants usually hold 5–7 days' worth of typical demand for liquefied production, so approximately 150–210 MT/day of storage.

Hydrogen exists in a liquid state below 20 K at atmospheric pressure. Achieving these low temperatures is energy-intensive and expensive. Liquid hydrogen must be stored at 20 K in jacketed stainless-steel vacuum tanks. Liquefying hydrogen increases its volumetric mass and energy densities, thus improving the economics of delivery. The capacity of the liquid tanker is about 4 metric tons, 5–6 times the capacity of a composite tube-trailer and 15–20 times the capacity of a steel tube-trailer.[20 59]. Nitrogen is liquified below 77 K at atmospheric pressure and, like liquid H_2, needs to be stored and transported in a jacketed tanker. The production of liquid nitrogen via cryogenic ASU is less energy-intensive when compared to liquid H_2 production. Transporting a unit of mass of liquid nitrogen is less

costly than the transportation of liquid hydrogen due to the higher energy density of LN_2, as shown in Figure 45.

The Hydrogen Delivery Scenario Analysis Model (HDSAM) was used to calculate the transportation cost of liquid H_2 and the equivalent cost for liquid N_2. This transportation cost includes the terminal cost and liquid tanker/trailer costs.

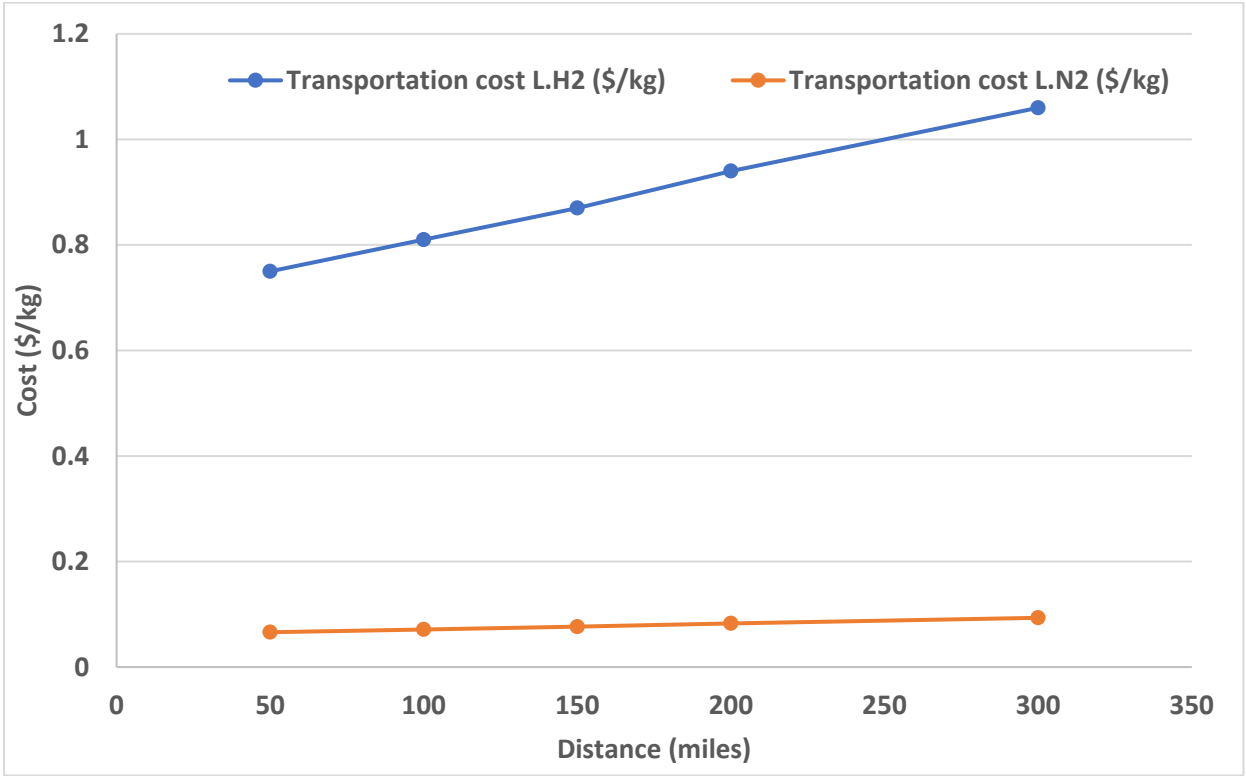

Figure 45. Cost of transporting liquid H_2 and liquid N_2 in liquid tankers.

3.5 Cryogenic Carbon Capture

Historically, CO_2 separation from industrial processes has been done using amine absorption. In new and innovative cryogenic CO_2 capture processes, CO_2 is separated by changing its phase from gas to liquid or solid. Unlike a conventional amine-based process, cryogenic processes do not require chemical absorbents. However, often cryogenic processes are thought to be highly energy-intensive due to the cooling duty required to separate CO_2 as a solid frost at the sublimation temperature (195 K) at atmospheric pressure. Two types of cryogenic CO_2 capture processes are summarized herein: the Sustainable Energy Solution (SES) cryogenic carbon capture (CCC)- external cooling loop (EL)[60] and the Advanced CCC (A3C) processes.[61] Other processes not analyzed include cryogenic capture with Stirling coolers.[62] The main objectives of these technologies are to reduce the cost and energy consumption of CO_2 separation. Using low-carbon-intensity energy from LWRs for CC operation would be beneficial for lowering overall carbon emissions while also potentially providing a large demand-responsive load to enable NPPs to maintain constant power while dispatching energy output to the demand-response load during off-peak grid-electricity demand periods.

3.5.1 Cryogenic Carbon Capture

The CCC technology developed by SES is designed to capture post-combustion CO_2 from large point sources such as power plants, cement kilns, steel mills, etc.[63] As shown in Figure 46, CCC technology involves multiple steps. Initially, the flue gas is cooled, and water is removed before it reaches 273 K.

Next the gas is passed through a desublimation column with a contact liquid, where the gas cools to ~154 K to form solid CO_2 in a slurry. The solid CO_2 is then separated and melted under pressure before it warms back to room temperature.

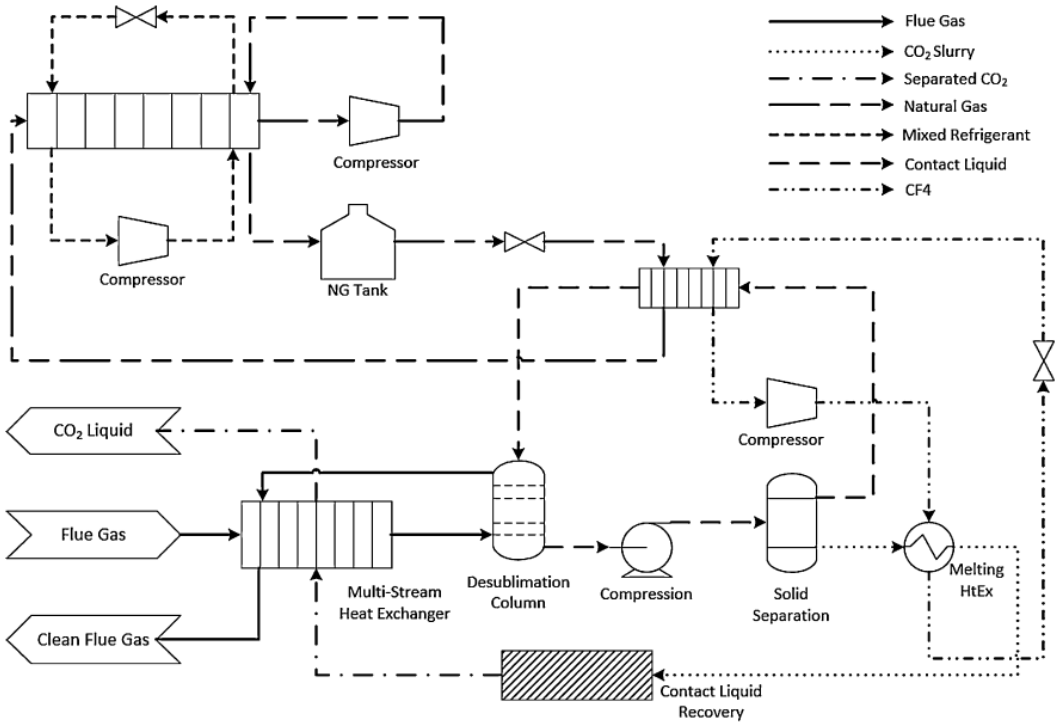

Figure 46 Outline of the simplified CCC process with EL [64]

SES claims that the CCC with ECL (EL) process costs \$45/tonne-CO_2 for a 550 MW coal power plant with a capture rate of 1 ton/day CO_2. For reference, the conventional amine process costs ~\$69/tonne of CO_2 captured for a coal power plant[60]. SES projects it may be possible to reduce the SES CO_2 capture cost further by implementing energy and cost savings from steam cycle improvements and offsetting costs and energy requirements for SOx, NOx, and mercury controls. Refrigerants used for the SES CCC process are CF4, LNG, L.N2, and mixed refrigerant. [65]

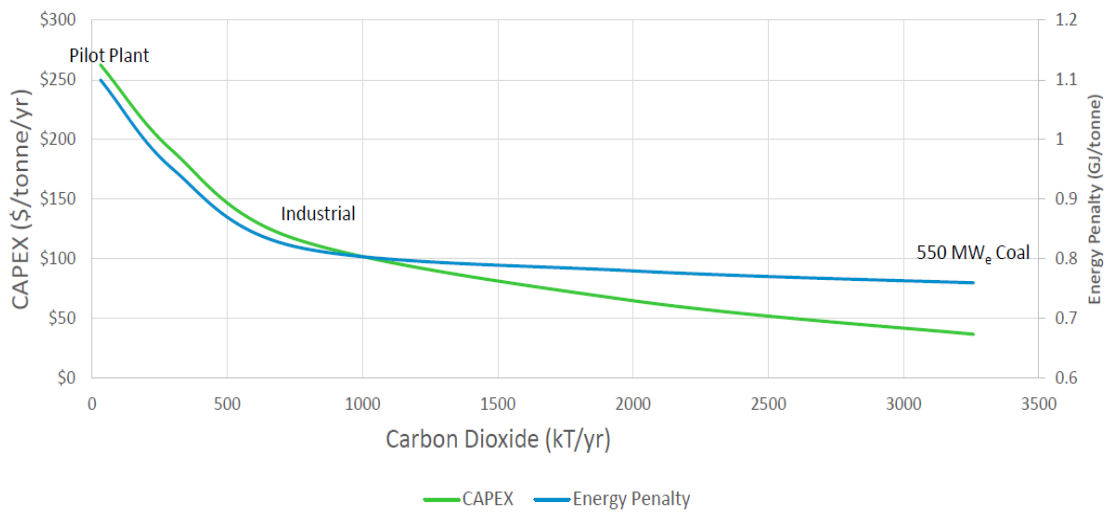

CAPEX numbers is the total equipment cost, not depreciated over any timeframe, and it does not include operating costs. These numbers assume a CO_2 composition of approximately 16% on a dry basis.

Figure 47. Cost and energy penalty of CCC process with plant size for coal power plant with 16 vol% CO_2 in the flue gas[66]

Figure 47 shows the CAPEX and energy penalty of SES CCC process with respect to the CO_2 capture rate. SES also provides the cost and energy penalty of CCC process versus the CO_2 concentration in the flue gas (Figure 48). Both CAPEX and the energy penalty of CCC process increase with the decrease in plant size and CO_2 content in the flue gas.

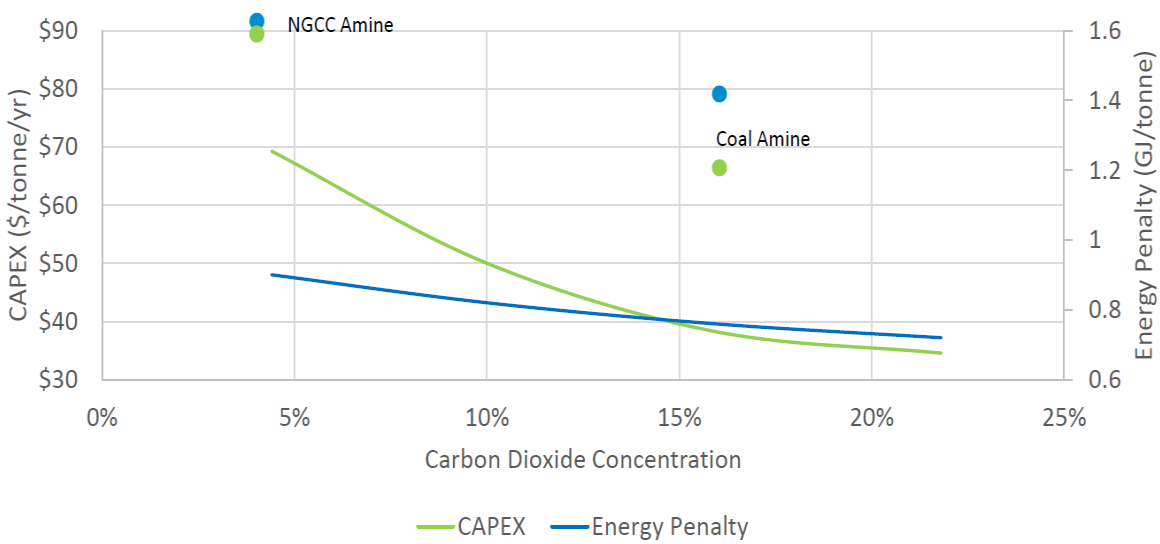

CAPEX numbers is the total equipment cost, not depreciated over any timeframe, and it does not include operating costs. These numbers assume large installations on the order of a power plant

Figure 48. Cost and energy penalty of SES CCC process with CO_2 composition in the flue gas[66]

3.5.2 A3C Carbon Capture Process

Willson et al. studied the technoeconomic viability of cryogenic CO_2 capture with the CO_2 content in the flue gas using the A3C process and compared it to mature mono-ethanolamine (MEA) technology.[61] The A3C process proposed by Willson et al. has two steps: a cooling drying step and a CO_2-separation step, as seen in Figure 49. Each step consists of a moving bed of metallic beads that are used as a heat-

transfer medium and frost-capture surface. In this process, the refrigeration system uses conventional components.

In the cryogenic CO_2 capture process, CO_2 is separated by changing its phase from gas to liquid or solid. Like the SES process, the A3C cryogenic process does not require chemical absorbents. As mentioned, cryogenic CO_2 capture processes have historically been considered highly energy consuming due to the large cooling duty required to separate CO_2 as a solid frost at below sublimation temperature (195 K) at atmospheric pressure. In this regard, Willson et al. aimed to reduce energy consumption and the cost of CO_2 separation with the A3C process.[61] The process has two steps: a cooling drying step and a CO_2-separation step, as seen in Figure 49. Each step consists of a moving bed of metallic beads which are used as a heat-transfer medium and frost-capture surface. In this process, the refrigeration system uses conventional refrigeration components.

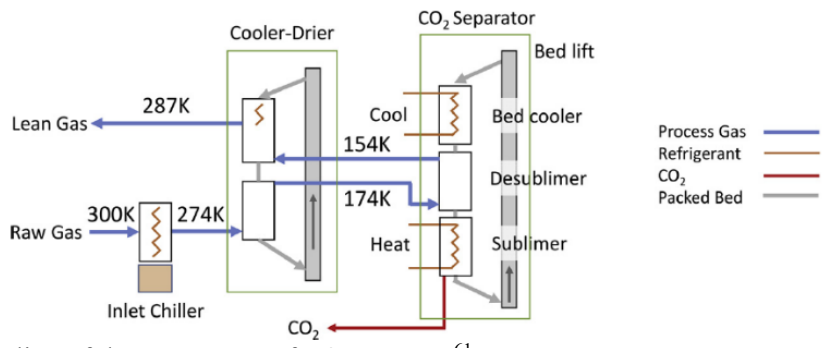

Figure 49. Outline of the two stages of A3C process[61].

Willson et al. estimated the energy consumption and costs to evaluate the process performance of A3C process. The energy consumption and costs to evaluate the process performance of A3C process for utility boiler and combined cycle gas turbine (CCGT) applications are tabulated in Table 29. The Aspen Plus modeling program was used to estimate the thermodynamic behavior of the A3C process. Assumptions and modifications were made to qualitatively represent the moving solid bed of A3C process in Aspen Plus. In the model, the moving solid bed was represented by a nonreactive liquid (such as heptane or dimethyl ether). The deposition of CO_2 on the solid bed was represented by the mixing of solid CO_2 with the liquid. For cost estimation, the heat-transfer area is manually calculated based on heat duties and temperatures generated from the Aspen model. For the MEA process, the conventional 30 wt% MEA solvent is used, and the efficiency of the pumps are assumed to be 80%. The APEA is used to estimate the direct equipment costs for the MEA technology. The levelized cost of carbon capture (LCCC) in A3C and MEA for the different application are tabulated Table 29.

Table 28. Comparison of LCCC for MEA and A3C for the different applications at baseline energy cost (Willson, Lychnos et al. 2019).

	Utility Boiler		CCGT	
	MEA	A3C	MEA	A3C
Heat (MJ/s)	114	0	28.6	0
Power (MW)	12.2	34.4	2.95	17.2
Equivalent Power (MWe)	38.6	34.4	9.9	17.2
CAPEX ($M)	114.6	116.0	52.9	46.8
OPEX excluding energy ($M)	9.0	7.2	5.1	2.3
LCCC ($/tonne eq CO_2)	56.0	49.2	108.3	111.8

Generally, the CO_2 concentration in the flue gas and plant size are two important factors to determine the CO_2 capture cost.

A3C offers lower capital costs than MEA for CCGT applications. However, a better understanding of the operation of the A3C process is necessary for a wide range of applications.

Table 30 shows various processes and their corresponding flue gas concentration of CO_2 from highest to lowest. Also shown is the cost of CO_2 capture as reported by Zang et al67 for other industrial sectors (such as cement, hydrogen, and steel) along with the coal and natural gas power plants. The specific electricity consumption (kWh/kg) of the CO_2 capture increases with the decrease in the CO_2 concentration of the flue gas. Figure 50 shows a comparison between the LCCC of amine-based and cryogenic CO_2 capture process with the CO_2 concentration in flue gas.

Table 29. CO_2 capture cost from different process effluent sources with amine and cryogenic processes.

Sources	Conc. Of CO_2 (vol%)	Electricity Consumption (kWh/kg)		Thermal Energy (kJ/kg)		CO_2 Capture Cost ($/MT)		References
		Amine Process	Cryogenic Process	Amine Process	Cryogenic Process	Amine Process	Cryogenic Process	
Hydrogen	45	0.154	-	4454	-	82	-	Zang et al. [2021][67]
Iron/Steel	25	0.142	-	4441	-	111	-	Zang et al. [2021] [67]
Cement	22	0.142	-	4459	-	108	-	Zang et al. [2021] [67]
Coal Based Power Plant	16	0.291	0.242	0	0	69	45	SES CCC Baxter et al. [2019] [60]
	13	0.346	-	0	-	58	-	Zang et al. [2021][67]
Oil Fired Boiler	12	0.372	0.332	0	0	56	49	A3C Willson et al. [2019] [61]
natural gas Power Plant	4	0.303	-	0	-	80	-	Zang et al. [2021] [67]
	3	0.476	0.831	0	0	108	112	A3C Willson et al. [2019][61]

Willson et al. claimed that the cost analysis presented in their article is no better than Class 5 (concept screening) with an expected accuracy range of no less than +50%/-30%. The proposed A3C process is at TRL 2 or 3 (proof of principle and initial demonstration) while the MEA process is at TRL 9 (proven in a commercial application).

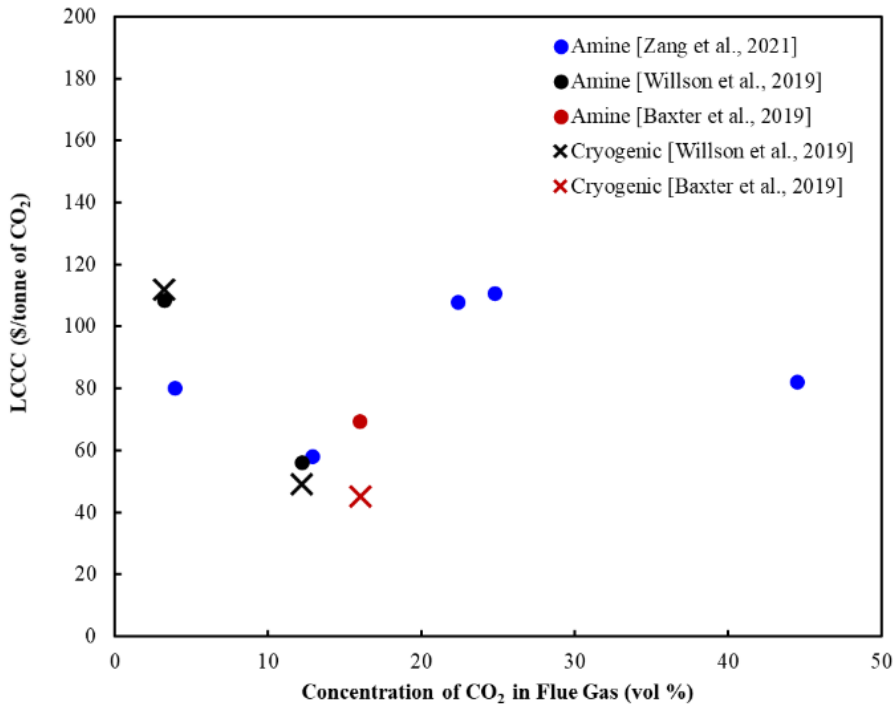

Figure 50. LCCC with the concentration of CO_2 in the flue gas for A3C and amine-based processes.

3.6 Lifecycle Analysis of Demand Response Options

Liquefaction of H_2 or N_2 or cryogenic capture of CO_2 can use large amounts of energy. These operations are evaluated here using the GREET life cycle analysis model to show the potential reduction of CO_2 emissions that could be realized if the energy required for these processes is provided by nuclear power plants.

Figure 51 shows GHG emissions from the liquefaction of N_2 and H_2 processes and cryogenic separation of N_2 using U.S. grid mix and nuclear electricity. As expected, the emissions for these operations using nuclear electricity are much lower than the U.S. grid mix. The emissions for the liquefaction of 1 kg of H_2 using the U.S. grid will emit 4.9 kg of CO_{2e} versus only 0.084 kg of CO_{2e} if nuclear electricity were to be used.

Figure 51. GHG emissions for utilizing LWR nuclear electricity for liquefaction and cryogenic seperation and compared to U.S. mix Grid.

CC processes using amine and cryogenic were discussed previously as well as the GHG emissions for both methods of CCC. Conventional amine CC process using the U.S. grid mix and nuclear electricity are plotted in Figure 51. These emissions were calculated using the energy requirements for these operations as shown in Table 30.

CO_2 capture with the amine or cryogenic process using nuclear electricity is about 2–4 g CO_{2e}/kg of CO_2 captured while, for using the U.S. electricity grid mix is 106–176 g CO_{2e}/ kg of CO_2 depending on the concentration of CO_2.

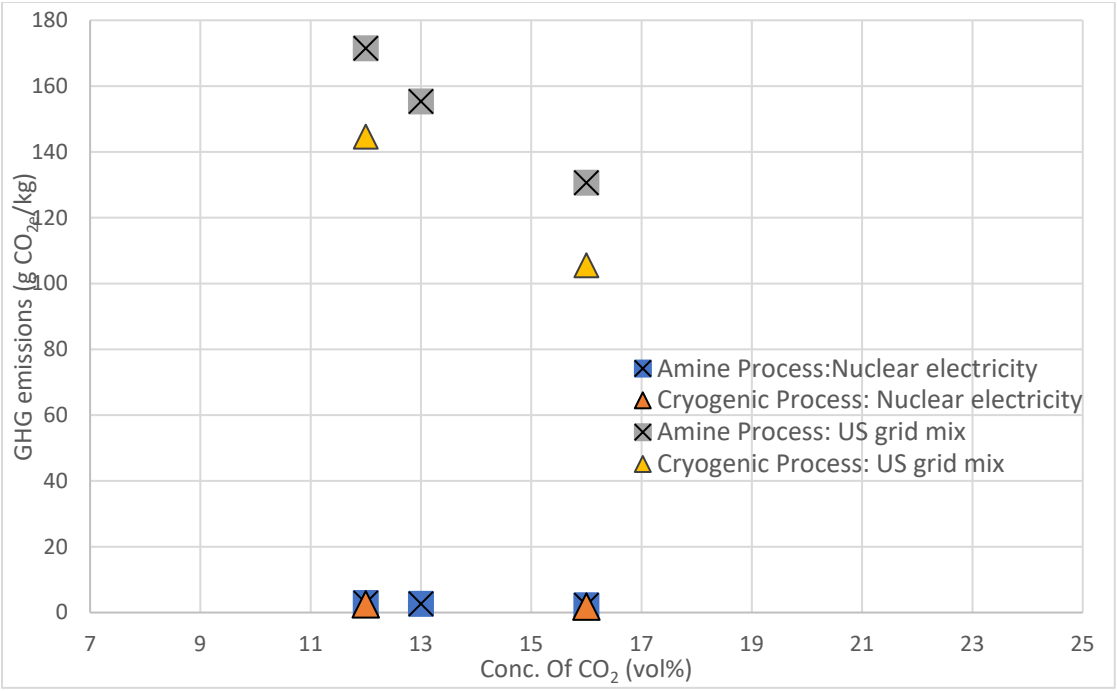

Figure 52 GHG emissions for CO_2 capture.

Natural gas CCGT is the most common electricity generation in the U.S. Combined with CCS, CCGT could reduce CO_2 emissions by 90%. CCS requires additional energy and reduces the overall efficiency of the power plant; it also uses fossil-based energy for CCS. This energy can be provided by NPPs, thus lowering the overall emissions for natural gas CC with CCS power generators. Figure 53 shows the WTP GHG emissions calculated using the GREET model for a) NGCC generators, b) NGCC generators with CCS, and c) NGCC generators with CCS using nuclear electricity.

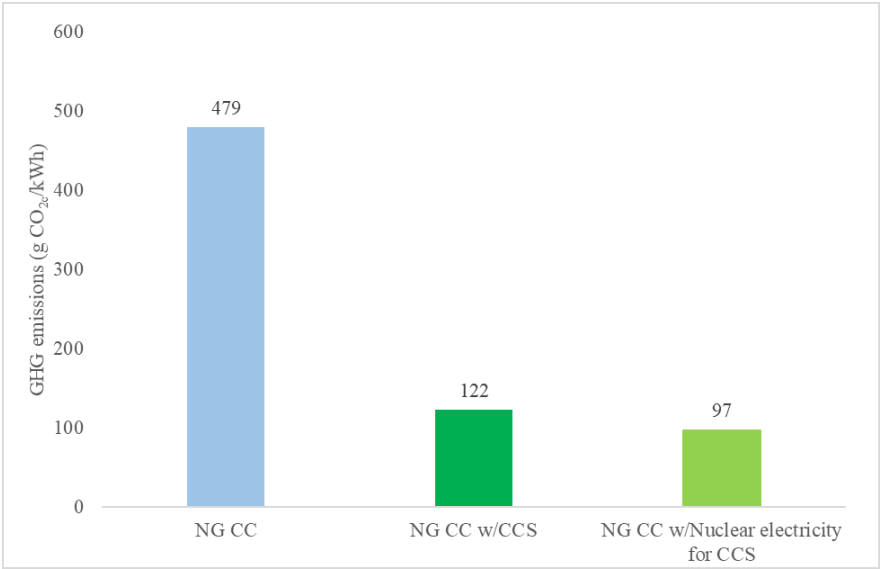

Figure 53 WTP GHG emissions for NGCC electricity generators.

3.7 Summary of Demand Response Options

For all the cryogenic demand-response options explored thus far, LWR energy may be well used due to the fact that all of these options are energy-intensive processes. Using a low-carbon energy source will benefit the decarbonization of these technologies. Nitrogen, carbon dioxide, and hydrogen are used in many different industries as refrigerants and energy sources. Their cost of production, capture, liquefaction, and transportation was explored, as shown in Table 30.

Table 30. Summary of compression and cryogenic options. Cost of nuclear electricity assumed at $30/MWh.

Technology		Energy Required (kWh/kg)	Cost	Efficiency
Hydrogen Compression (to 350bar)	Hydrogen	2	$60/MT [a]	
Liquefaction	Hydrogen	11	$330/MT [a]	
	Nitrogen	0.528	$16/MT [a]	
CO_2 capture	Cryogenic capture (A3C)	0.332 (for 12vol% CO_2) 0.831 (for 3 vol% CO_2)	$49/MT (for 12vol% CO_2) $112/MT (for 3 vol% CO_2)	90%
	Cryogenic Carbon Capture (SES)	0.242 (for 16 vol% CO_2)	$45/MT (for 16 vol% CO_2)	90%
	Amine (MEA)	0.372 (for 12vol% CO_2) 0.476 (for 3 vol% CO_2) 0.291 (for 16 vol% CO_2)	$56/MT (for 12vol% CO_2) $108/MT (for 3 vol% CO_2) $69/MT (for 16 vol% CO_2)	90%
Cryogenic Air separation	Nitrogen	0.162	$5/MT [a]	

4. CONCLUSION

The goal of this report is to analyze various options for the use of off-peak LWR nuclear energy in the realm of both energy storage and large demand-response loads. The use of utility-scale lithium-ion batteries and the production of hydrogen and its use in the generation of electricity, analyzed elsewhere, were summarized here in this report for comparison. Various sensible-heat thermal-storage systems have been explored and summarized—ETES, which uses sand as the heat storage media, and other liquid-based sensible-heat storage systems using storage media such as mixtures of molten salts and thermal oils. ETES technology converts electricity to stored thermal energy via a supercritical CO_2 heat-pump cycle and then back to electricity using a supercritical CO_2 heat-engine cycle.

This report presented a variety of TES systems that are currently used in industry, as well as some that are under development. The most widely deployed sensible-heat-based systems are promising options for coupling with existing LWRs. Latent-heat-based systems are not discussed in this report, but maybe attractive due to their high gravimetric densities; however, their low thermal conductivities are a significant barrier to efficient heat transfer. Significant research is being conducted to enhance this heat-transfer rate with the help of advanced materials as well as efficient heat-exchanger designs.

Although cheap storage material can be used to store thermal energy, efficient heat exchangers are required to transfer heat to and from these solid-state materials. Coupling different TES systems to take

advantage of the inherent properties of each is also a good option, along with using electrical topping heat to superheat the discharged steam.

Relative ranking of energy storage options was done using a LCOS metric which calculates a rough breakeven cost for the system taking into account the capital and operating costs as well as the revenue from arbitrage. Table 31 below shows the LCOS for each of the options energy storage options considered. First, in the table, LFP batteries are listed as the base case for comparison against the other options. Next is hydrogen storage where most of the hydrogen analyses assumed the hydrogen to be produced using solid oxide electrolytic cell (SOEC) HTSE. The others used existing models of PEM low-temperature electrolysis to produce hydrogen. HTSE performance parameters and costs were taken from existing INL models. Various means were assumed to convert the hydrogen to electricity, including PEM fuel cells (FCs) and a gas turbine mixed in a 30 vol% mixture with natural gas. Physical storage (pressure vessels) and geological storage (natural underground features) were used to store the hydrogen as noted. Geological storage is more economical, but the locations are limited which have pre-existing geological formations that will support storage. TES options were also analyzed including ETES and four different (Hitec, Hitec XL, Therminol-66, and Dowtherm A) liquid sensible heat TES storage media as noted. The ETES process uses a separate supercritical CO_2 charge and discharge cycle and uses sand as the heat storage media.

Table 31. Comparison of energy storage options for power arbitrage discharge capacity of 500MWe and charging cost of $30/MWh.

Technology		Charging Cost ($/MWhe)						
		0	15	20	25	30	35	40
Li-ion LFP Battery	LCOS ($/MWhe)	322 (6h & 12h)	339 (6h & 12h)	345 (6h & 12h)	351 (6h & 12h)	357 (6h & 12h)	363 (6h & 12h)	369 (6h & 12h)
H_2 Geological Storage, SOEC / PEM FC		194 (6h) 98 (12h)	212 (6h) 115 (12h)	218 (6h) 121 (12h)	224 (6h) 127 (12h)	230 (6h) 133 (12h)	236 (6h) 139 (12h)	241 (6h) 145 (12h)
H_2 Physical Storage, SOEC / PEM FC		213 (6h) 115 (6h)	231 (6h) 133 (12h)	237 (6h) 139 (12h)	242 (6h) 145 (6h)	248 (6h) 151 (12h)	254 (6h) 156 (12h)	260 (6h) 162 (12h)
H_2 Physical Storage, PEM EC / Gas Turbine		86 (6h) 71 (12h)	110 (6h) 95 (12h)	119 (6h) 103 (12h)	127 (6h) 112 (12h)	135 (6h) 120 (12h)	143 (6h) 128 (12h)	151 (6h) 136 (6h)
Thermal (ETES)		129 (6h) 77 (12h)	-	172 (6h) 120 (12h)	-	194 (6h) 141 (12h)	-	215 (6h) 163 (12h)
Thermal (sensible / Hitec)		58 (6h) 50 (12 h)	80 (6h) 72 (12h)	87 (6h) 79 (12h)	94 (6h) 86 (12h)	101 (6h) 93 (12h)	108 (6h) 101 (12h)	116 (6h) 108 (12h)
Thermal (sensible / Hitec XL)		62 (6h) 53 (12h)	84 (6h) 75 (12h)	91 (6h) 82 (12h)	98 (6h) 89 (12h)	105 (6h) 96 (12h)	112 (6h) 104 (12h)	120 (6h) 111 (12h)
Thermal (sensible / Therminol-66)		159 (6h) 151 (12)	181 (6h) 172 (12h)	188 (6h) 180 (12h)	195 (6h) 187 (12h)	202 (6h) 194 (12h)	210 (6h) 201(12h)	217 (6h) 209 (12h)
Thermal (sensible / Dowtherm A)		116 (6h) 108 (12h)	138 (6h) 130 (12h)	145 (6h) 137 (12h)	152 (6h) 144 (12h)	159 (6h) 151 (12h)	167 (6h) 159 (12h)	174 (6h) 166 (12h)

Figure 54 below is shows the data from the table above plotted in graphical form for a subset of the energy storage options.

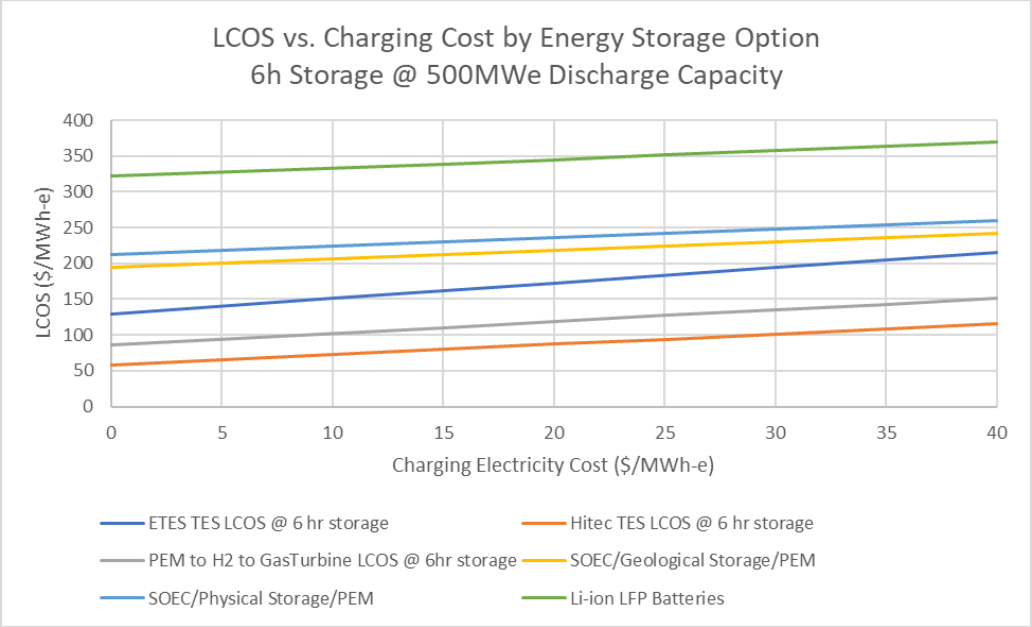

Figure 54. LCOS versus charging cost for various energy storage options.

From this analysis, the relative economic ranking of the energy storage options analyzed by LCOS for 6h of storage of 500MWe discharge capacity can be deduced from most economic to least as:

1. Liquid sensible heat thermal energy storage using Hitec fluid as the thermal media,
2. Power to H_2 via PEM/H_2 to electricity via mixing up to 30 vol% H_2 with natural gas in a gas turbine,
3. ETES with a supercritical CO_2 cycle and sand thermal storage media,
4. Power to H_2 via SOEC/Geological H_2 Storage/H_2 to electricity via PEM fuel cell,
5. Power to H_2 via SOEC/Physical H_2 Storage/H_2 to electricity via PEM fuel cell.

Other permutations of hydrogen production, storage, and H_2 to electricity not analyzed include reversible SOEC/FC which can operate either as an electrolytic cell to produce hydrogen using electricity or as a fuel cell to produce electricity using hydrogen. Reversible SOEC/FCs should be fully analyzed with the most up-t- date modeling in future work and compared to these results.

Steam accumulators were briefly analyzed but cannot meet the scale requirements to provide a disposition for large amounts of off-peak nuclear energy. Steam accumulators are pressure vessels and therefore, they have physical constraints dictated by operating pressure. This limits the storage capacity of a steam accumulator. Using the numbers from Khi Solar one, 19 steam accumulators can provide 50 MWe, which is about 15% of a 1 GW NPP with a conversion efficiency of 33%. Although the amount of energy stored and recovered from the steam accumulators is significant, the number of storage tanks required to provide 500 MWe for 6-12 hours is very large. Based on another recent analysis [71], the pressure vessel's cost accounts for about 60-70% of the total TES cost. Nevertheless, steam accumulators can be discharged rapidly and have a RTE ranging between 60 and 80%. The discharged steam can either be superheated using electrical topping heat before its delivery to the power block, or it can be introduced into a low-pressure turbine in a Rankine power cycle. Due to this flexible nature and ease of use of steam accumulators, they are an attractive TES option for coupling with existing LWRs in small amounts.

In addition, this study has applied the greenhouse gas (GHG) emissions uses the Greenhouse GREET model to analyze the low CO_{2e} emissions of the various arbitrage energy-storage options when integrated with nuclear power. This information is valuable for organizations that have set goals for staged decarbonization to understand the ranking and cost/benefit of various carbon reduction strategies. This

information in turn will be used to enhance the GREET model for the assessment of energy systems that include LWR energy inputs.

Figure 55 shows the GHG emissions per kWh kilowatt-hour for storing LWR energy using batteries, hydrogen and thermal options compared with electricity from natural gas generators with SC, CC and CC with CCS. The electricity from LWR energy storage scenarios have emissions of 8–20 gCO_{2e}/kWh whereas electricity from natural gas generators is between 112–727 gCO_{2e}/kWh..

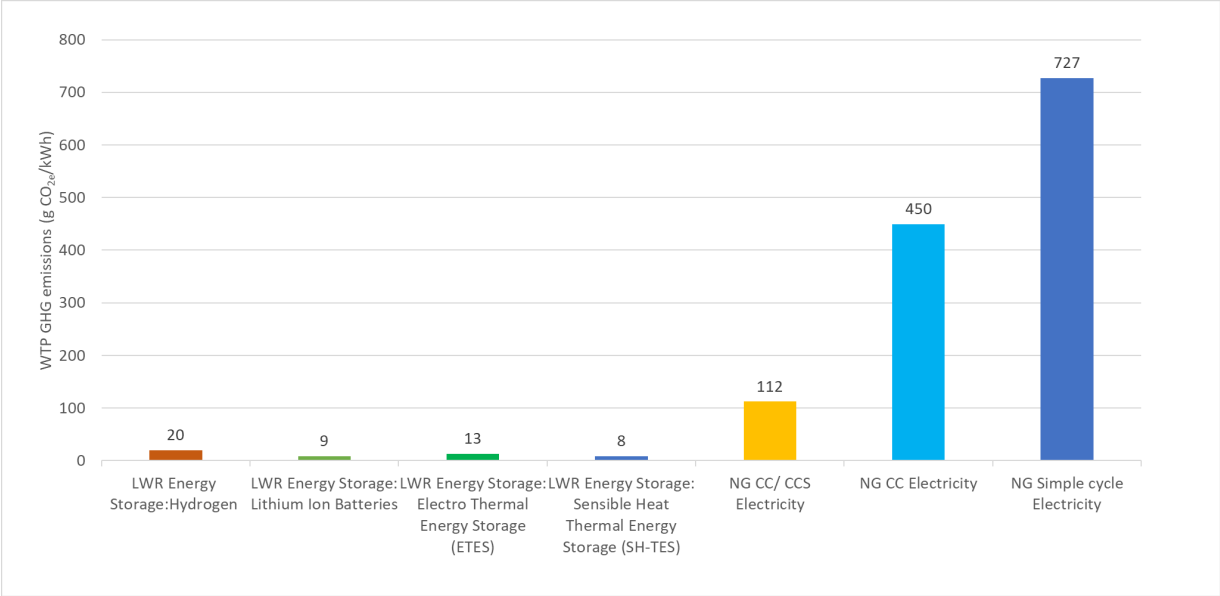

Figure 55. Life cycle GHG emissions for electricity from energy storage compared to electricity generated from natural gas.

Finally, large demand response options were analyzed, and a summary of these options considered is shown in Table 32. Separation and liquefaction of nitrogen is one of the lower cost options for demand response followed by new and innovative cryogenic carbon capture via the SES process. The analysis for these processes did not take into account at this time the sales revenue from each product and market analysis and pricing which could be done in future work.

Table 32. Summary of demand response options for compression and cryogenics. $30/MWh nuclear electricity cost is assumed in these calculations.

Technology		Energy Required (kWh/kg)	Cost	Efficiency
Hydrogen Compression (to 350bar)	Hydrogen	2	$60/MT [a]	
Liquefaction	Hydrogen	11	$330/MT [a]	
	Nitrogen	0.528	$16/MT [a]	
CO_2 capture	Cryogenic capture (A3C)	0.332 (for 12vol% CO_2) 0.831 (for 3 vol% CO_2)	$49/MT (for 12vol% CO_2) $112/MT (for 3 vol% CO_2)	90%
	Cryogenic Carbon Capture (SES)	0.242 (for 16 vol% CO_2)	$45/MT (for 16 vol% CO_2)	90%
	Amine (MEA)	0.372 (for 12vol% CO_2) 0.476 (for 3 vol% CO_2) 0.291 (for 16 vol% CO_2)	$56/MT (for 12vol% CO_2) $108/MT (for 3 vol% CO_2) $69/MT (for 16 vol% CO_2)	90%
Cryogenic Air separation	Nitrogen	0.162	$5/MT [a]	

APPENDIX A
STATE-OF-THE ART OF TES

Page intentionally left blank

APPENDIX A

STATE-OF-THE ART OF TES

A-1. HOT AND COLD WATER STORAGE

Thermal energy storage systems that employ water as the heat storage material can either be a single naturally stratified tank, a two-tank hot/cold water storage system, or a cascade of multiple tanks. Thermal energy, either in the form of hot or cold water, is produced during off-peak hours, collected in storage tanks, and then used for heating or cooling purposes during peak hours. For example, in a naturally stratified water-based TES system, chilled water circulated through facilities for cooling is then returned to the storage tank at the top because it has absorbed heat and is warm. The associated chillers and condensing equipment are deenergized during this time. This is the discharging cycle and it runs during peak hours. In comparison, during off-peak hours, the water returning from the facilities is cooled using the chiller system and is returned to the tank from the bottom (see Figure A-1).

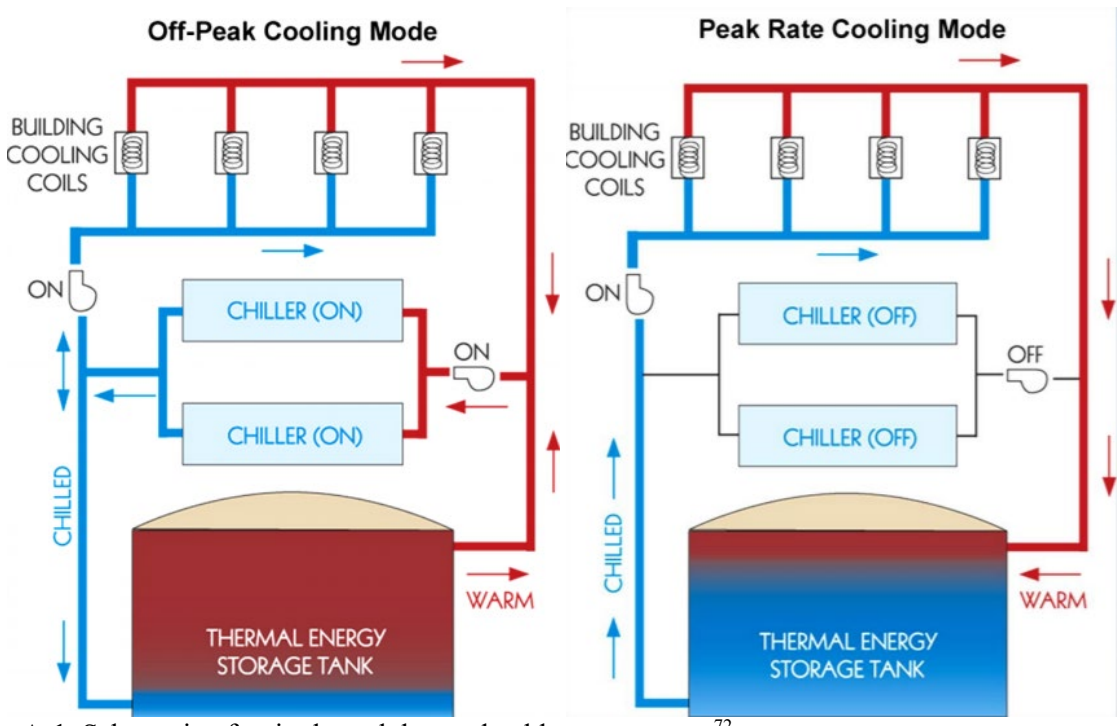

Figure A-1. Schematic of a single-tank hot and cold water storage[72].

A-2. UNDERGROUND THERMAL ENERGY STORAGE (UTES)

UTES systems store energy by pumping heat into underground locations such as boreholes, aquifers, and caverns, etc. Geothermal storage is a form of UTES storage. In most cases, the working fluid used is water, which transfers energy to and from the heat-storage medium. A borehole TES system consists of an array of drilled wells with U-bend thermal loops. These thermal loops transport the working fluid which transfers heat to and from the surrounding soil.[73] In comparison, aquifer TES systems need two thermal wells and are used during seasonal changes wherein water from a cold aquifer is used for cooling and then transferred to a warm aquifer, and the process reverses during the winter.[74] A cavern-based TES system would use large underground reservoirs or pits to store the working fluid.

Figure A-2 shows a schematic of a borehole TES system that is currently operational in the Drake Landing Solar Community, Alberta, Canada. Herein, a mixture of water and non-toxic glycol is pumped through roof-top solar collectors and heated when the sun is out. This mixture is then transferred to a district heating system where it transfers heat to water, which is then pumped into the boreholes for seasonal heat storage.

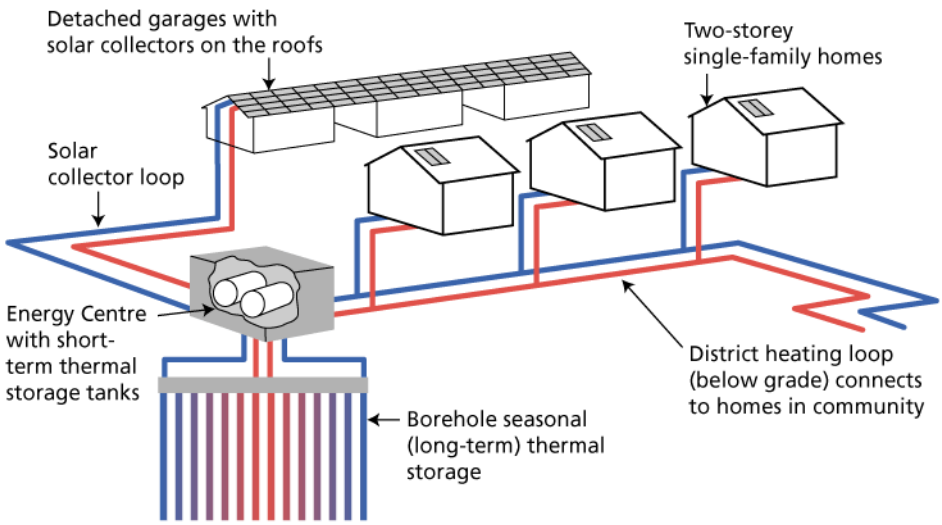

Figure A-2. Schematic of a district heating loop with an integrated seasonal borehole TES.[75]

A-3. THERMOCHEMICAL STORAGE

Thermochemical energy is a result of chemical reactions that release or absorb heat during exothermic or endothermic reactions. If such reactions are reversible, then those chemicals are used to store and release thermal energy. Although thermochemical storage systems have the highest energy density of all TES systems, significant challenges exist with regard to the cyclability of the chemical reactions.[76] Although several bench-scale thermochemical TES systems have been designed and developed, more-intensive study on charging- and discharging-cycle behavior in chemical reactors and their possible integration with other systems is required.

A-4. SENSIBLE HEAT STORAGE

Sensible-heat TES (SH-TES) systems store heat by the virtue of an increase or decrease in temperature. Herein, heat from a source is deposited either directly or indirectly into the storage medium. In direct systems, the heat-transfer fluid acts as the storage medium whereas, in indirect systems, the storage medium is different from the heat-transfer fluid. So far, the most widely adopted TES systems are deployed along with concentrated solar power (CSP) plants. In CSPs, radiative heat from the sun is concentrated using mirrors in solar fields to heat the working fluid, which flows to a power block where heat is extracted to produce steam for electricity generation. During hours of low energy demand, the working fluid flows through an intermediary loop and transfers heat to a storage medium. This thermal energy can be stored during the day and used for electricity production even when sunlight is not available.

Depending on the state of storage media, the SH-TES systems are classified as liquid- or solid-based. In liquid-based SH-TES systems, the storage medium is in liquid form throughout its operational life cycle and is transported to the heat source during the charging cycle and the power block during the discharging cycle. In solid-based SH-TES systems, the storage medium is solid while the heat transfer fluid is in a liquid state.

A-4.1 Two-Tank Sensible-Heat Thermal-Energy Storage

Currently, the two-tank SH-TES design is the only system to have been deployed on a gigawatt scale. This system has two tanks to store the hot and cold storage media, and an intermediary heat exchanger transfers heat to the heat-transfer fluid. Most designs currently deployed have molten salt as their storage medium while a few others have thermal oil. During the charging cycle, the storage medium is pumped from the cold tank, heated primarily using solar energy, and transferred into the hot tank. During hours of additional demand in electricity, the hot storage medium is run through a heat exchanger, where it transfers heat to the heat-transfer fluid, cools down, and returns to the cold tank. The heat-transfer fluid is then used to generate electricity. Figure A-3 shows a schematic of a two-tank SH-TES system coupled with a CSP.

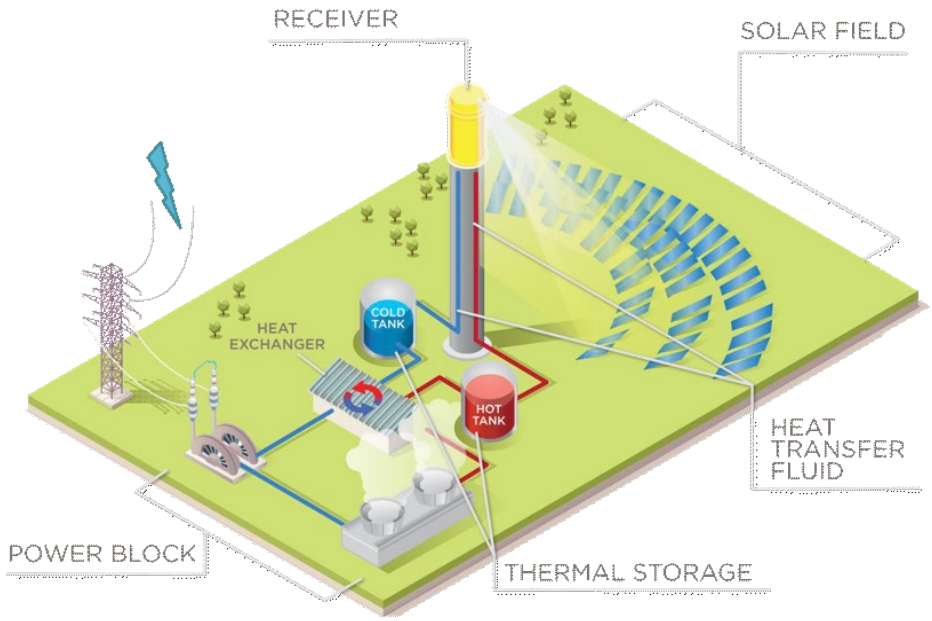

Figure A-3. Schematic of a CSP coupled with a two-tank SH-TES.[77]

Most of the existing SH-TES systems use solar salt—i.e., a salt mixture made up of about 60% sodium nitrate and 40% potassium nitrate. This composition is near the eutectic point and is thermally stable up to 600°C. There are other SH-TES systems that use thermal oil as the heat-transfer fluid as well as the storage medium.

A-4.2 Thermocline Thermal Energy Storage

Similar to the SH-TES, a thermocline also store sensible heat energy. Here, hot and cold fluids are separated due to thermal stratification caused by density differences. During the charging cycle in a thermocline, the heated heat-transfer fluid enters the tank from the top while, simultaneously, the colder fluid is withdrawn from the bottom and sent to the heat exchanger to be heated. The process is reversed during the discharging cycle. A schematic of a thermocline is shown in Figure A-4.

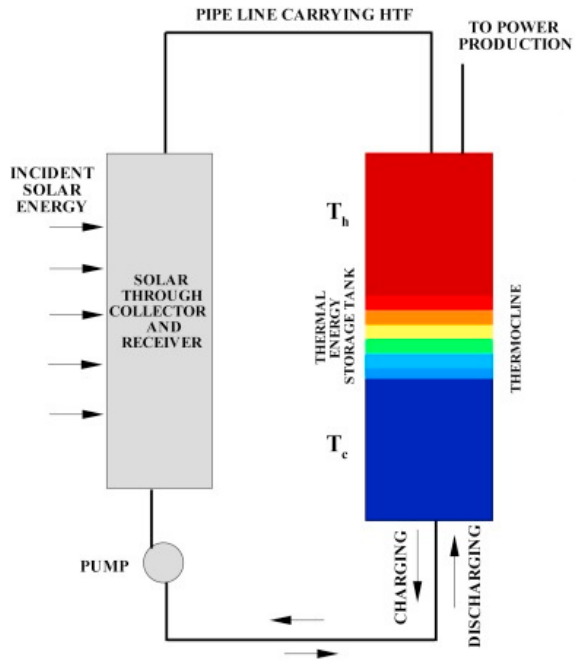

Figure A-4. Schematic of a single-tank thermocline TES.[78]

A-5. SOLID-MEDIA SENSIBLE-HEAT STORAGE

Commercially proven TES systems that are deployed on a large-scale are primarily limited to two-tank sensible-heat storage and steam accumulators. One approach to reducing capital costs of storage technology while simultaneously reducing its impact on the environment is to use low-cost solid-state materials. Examples of TES systems developed by using such materials are discussed as follows.

A-5.1 Concrete

Concrete TES is a simple, low-cost, SHS technology that can be coupled with medium to large-scale heat-producing systems. Significant research on this technology has been performed, with a few companies ready to deploy medium-scale concrete storage systems. In this technology, heat transfer between the heat-transfer fluid and the solid concrete media occurs through tubes that are embedded in the concrete block. Figure A-5 shows a schematic of EnergyNest's module, displaying a tube embedded in HEATCRETE, a proprietary concrete material developed by EnergNest.[79]

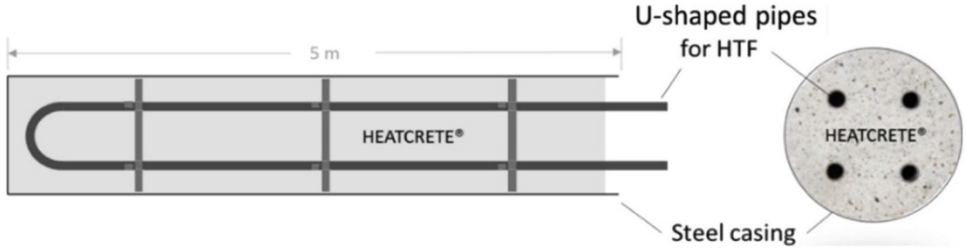

Figure A-5. EnergyNest's concrete thermal energy storage (module.

A-5.2 Firebrick

Firebrick resistance heat energy storage (FIRES) is a technology that stores thermal energy, generated using electrical heaters that are run during off-peak electricity. The FIRES system stores energy in ceramic bricks, operating between 1000 and 1700°C, and discharges it as a hot airstream to either heat industrial plants in place of fossil fuels or to regenerate electricity in a power plant.[80]

A-5.3 Ceramic Particle

Falling-particle receivers are currently being investigated to store thermal energy in ceramic particles which are heated by a CSP.[81] A solid-particle receiver is a central tower that allows the falling flow of a curtain of ceramic particles that are directly illuminated by a beam of concentrated sunlight from heliostats in a collection field. These heated particles can then be stored in an insulated storage tank or passed through a particle-to-working fluid heat exchanger, where the sensible heat from the solid material is used to produce energy.

A-6. LATENT-HEAT STORAGE

Latent-heat TES (LH-TES) systems store heat by the virtue of phase change. Although phase change can be from solid-solid, solid-liquid, solid-gas, and liquid-gas, most of the research focus is narrowed to technologies that employ solid-liquid and liquid-gas phase changes. Phase-change systems use the heat of fusion of material and, therefore, in theory, provide larger gravimetric densities while reducing the storage volumes.

The phase change materials (PCM) in LH-TES systems is held within a single container throughout its operational life cycle, and the heat-transfer fluid flows through a heat exchanger embedded within the system, transferring heat to and from the storage medium. This eliminates the need for an external heat exchanger as in the case of SH-TES systems. During the charging cycle, hot heat-transfer fluid flows through the embedded heat exchanger, transfers heat to the PCM, thereby melting it, and storing latent heat. During discharging, cold heat-transfer fluid flows through the system, absorbs heat, and in the process, solidifies the PCM. A schematic of charging and discharging cycles is shown in Figure A-6.

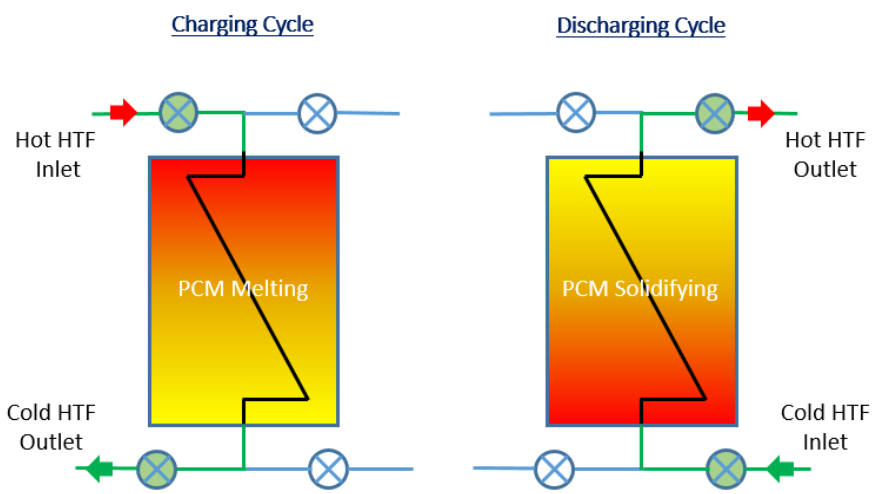

Figure A-6. Schematic of the working principle for a generic LH-TES system.[82]

A-7. STEAM ACCUMULATORS

Steam accumulators are insulated pressure tanks containing hot water and steam under pressure that can be released when the demand is high to produce electricity. The system is filled with water with pressurized steam at the top, both in equilibrium at saturated conditions. To charge the steam accumulator, steam is inserted into the liquid from the bottom via a perforated pipe. This allows some of the steam to condense and, while doing so, increases the temperature of the water as well as the pressure of the system. During the discharging cycle, a release valve at the top of the accumulator is opened, thereby releasing saturated steam and lowering the system pressure. This, in effect, causes some of the water to flash and produce additional steam. The working principle of a steam accumulator is shown in Figure A-7.

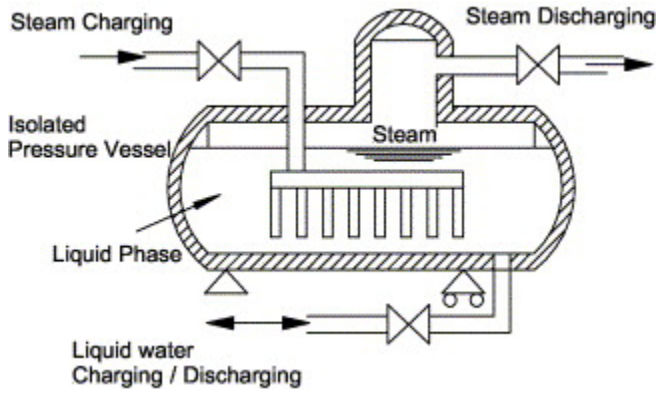

Figure A-7. Schematic of a sliding-pressure steam accumulator.

A-8. IDAHO NATIONAL LABORATORY (INL) PREVIOUSLY COMPLETED STUDIES

The Integrated Energy Systems (IES) program at INL has developed systems-level dynamic thermal storage models of concrete, PCM-based LH-TES, packed-bed thermocline, and two-tank sensible heat systems. These models are developed using the latest publicly available data and incorporate the possibility of control-strategy inclusion for use with the existing IES modeling, analysis, and optimization toolset. Details of the modeling work and preliminary simulation analyses are provided other works[83, 84, 85] and are outside the scope of this report, but are mentioned here to showcase the capabilities of the IES program.

A-8.1 Concrete TES

The Modelica-based CTES models are of two types: single pipe and dual-pipe. In the single pipe design, the heat transfer fluid flows through the same pipe during the charge and discharge cycles, whereas in the two-pipe design, separate pipes are used during the operational cycles. The models use concrete media from the TRANSFORM library, which has thermophysical state properties for density, thermal conductivity, and heat capacity of Heatcrete.[86]

The heat-transfer fluid used for charging is steam while that for discharging is water, and the heat-storage medium is concrete. The heat transfer between the heat-transfer fluid and the concrete occurs through stainless-steel pipes. For simplification, the model is primarily based on the energy equation, and the mass and momentum equations are ignored by assuming a fully developed flow. This assumption is made because low-flow or no-flow conditions increase the complexity of the model significantly. Both concrete models are built to interact within a Modelica thermofluid system via four fluid ports that match pressure with the outside fluid network connectors and match mass-flow rates and energy values at the

connectors. The charging and discharging modes should be connected at their labeled inlet and outlet fluid nodes for these models. A CTES model that allows for charging, discharging, and energy-storage analyses is shown in Figure A-8.

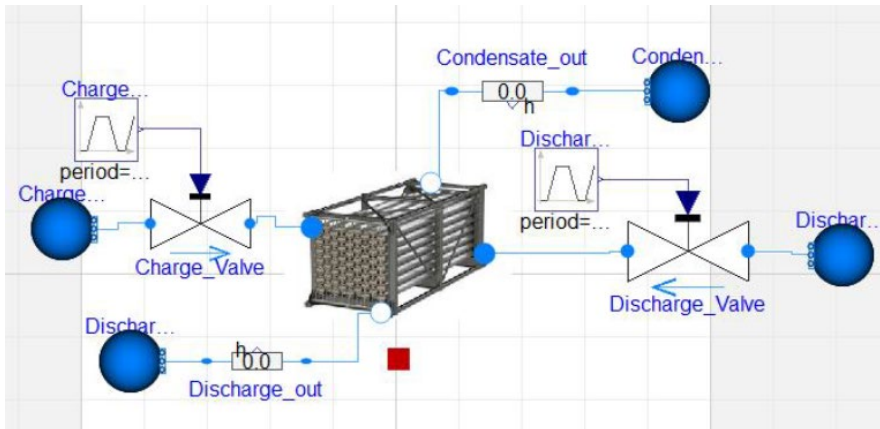

Figure A-8. Modelica-based CTES model for charging and discharging tests.

Figure A-9 shows the flowrates during the charge and discharge cycles. During discharge cycles, flow occurs in the opposite direction and is therefore indicated by negative values.

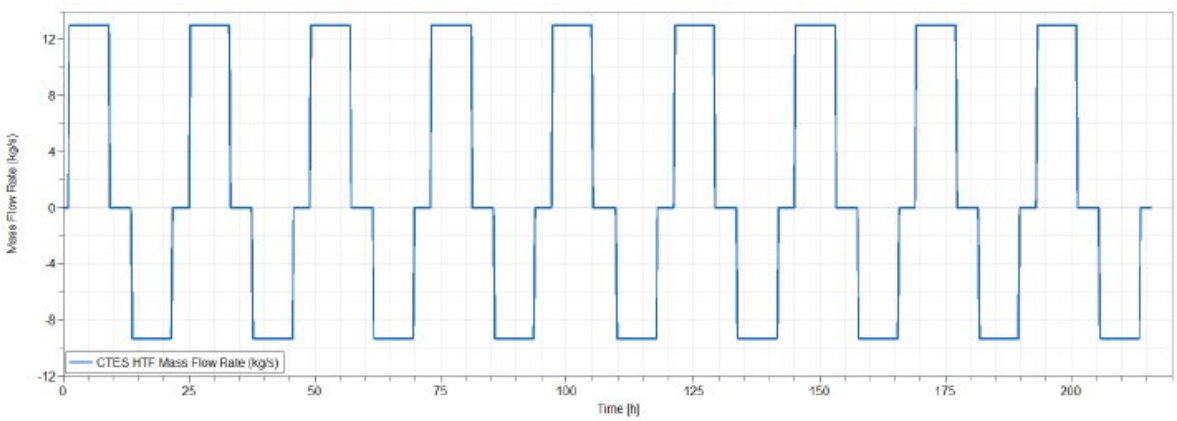

Figure A-9. Mass-flow rate during charging and discharging cycles.

A comparison of the energy stored over the period of 24 hours is shown in Figure A-10 for the single and dual-pipe models. It can be seen that the single pipe model allows higher energy to be deposited and discharged. Figure A-10 shows one possible advantage of one design over the other. However, each of the designs has pros and cons, which are provided in detail in the HYBRID repository[87] and are therefore not presented here.

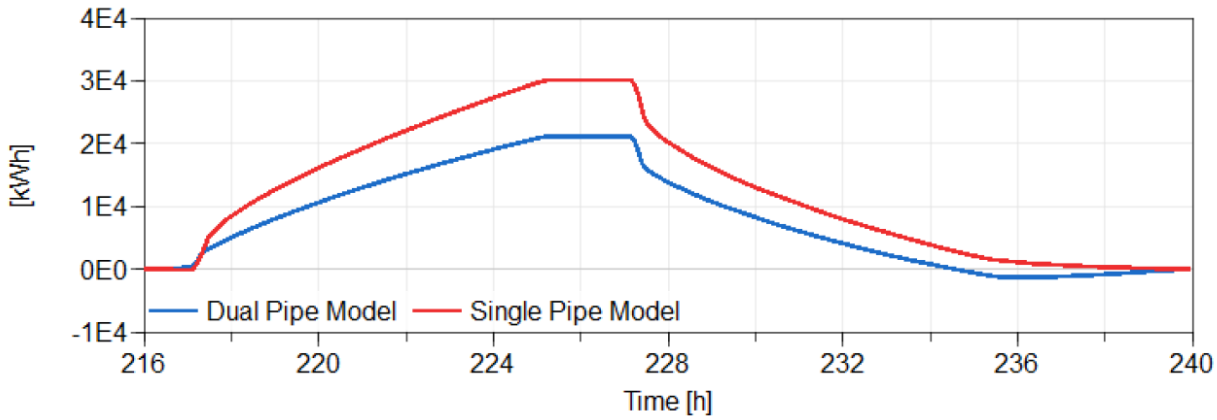

Figure A-10. Energy storage content over a 24-hour period for single- and dual-pipe configurations.

A-8.2 PCM-based LH-TES

The model developed is based on a study which employed n-Eicosane as the PCM and water as the heat-transfer fluid.[82] Herein, a numerical model was developed in MATLAB and computational fluid dynamics (CFD) analyses were conducted in STAR-CCM+ to understand the thermal-hydraulic behavior of the LH-TES. Furthermore, experimental studies were carried out on a bench-scale model to validate the numerical models. The MATLAB model was then converted into a Modelica model and is currently being modified to comply with existing models. Figure A-11 shows the charge and discharge cycle temperatures for the heat-transfer fluid, and Figure A-12 shows the corresponding nodal temperatures within the problem domain.

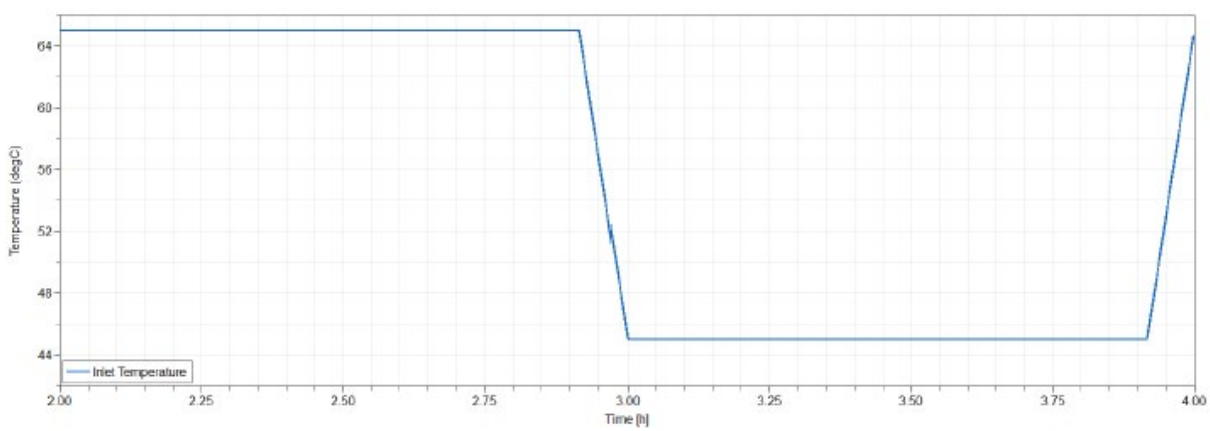

Figure A-11. Charging and discharging simulation for the LH-TES model.

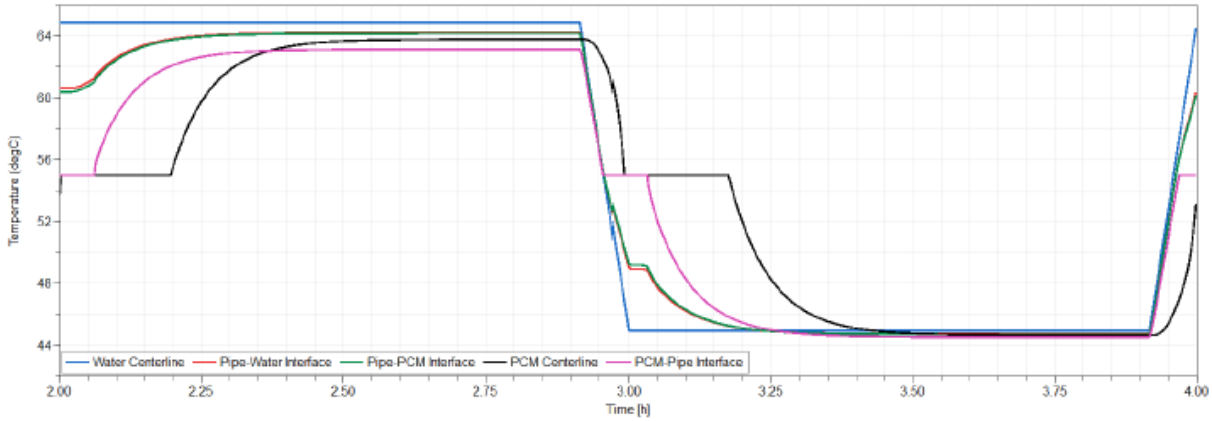

Figure A-12. Axial temperature profiles during a charge and discharge cycle.

The LH-TES model is still under development and will be further refined and validated based on the available experimental data. Additionally, experiments are being carried out at the University of Idaho to support the development of a LH-TES that is charged by steam and produces steam during the discharge cycle. As PCMs continue to be researched and new materials are provided, the modeling capabilities within the HYBRID repository will be expanded.

A-8.3 Therminol-based Thermocline

The thermocline model developed at INL is of a packed-bed design, with Therminol-66 as the working fluid and alumina beads as the filler material. The porosity of the system is set to 0.6, indicating that alumina beads make up 40% of the system's volume. The model uses a modified set of Schuman equations and neglects self-degradation in the axial direction. The problem domain is nodalized axially, with each node containing a fluid and solid component. During charging, hot Therminol-66 is flown from the top while, during discharging, cold Therminol-66 is flown from the bottom. Detailed analyses of this model are presented in [89] and are, therefore, not included here. The Modelica-based model for this TES is shown in Figure A-13.

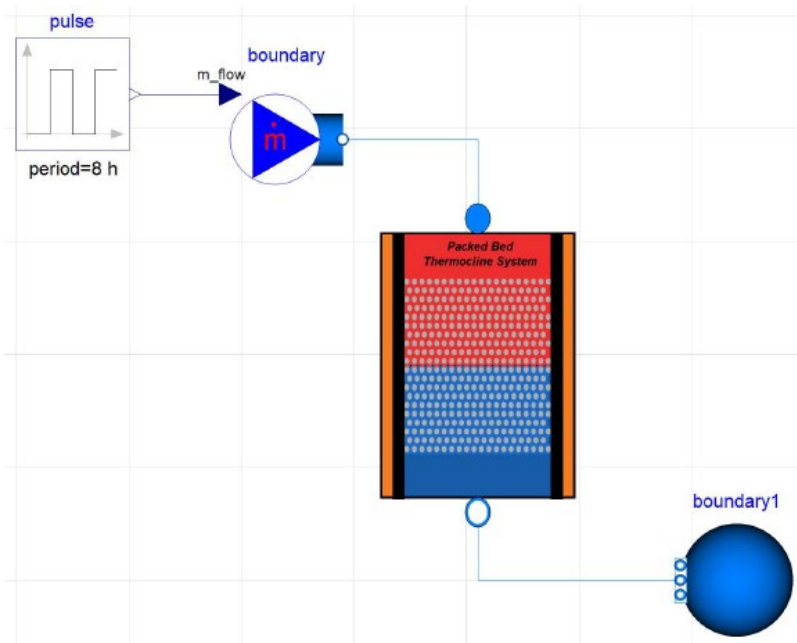

Figure A-13. Modelica-based model for a single-tank thermocline.

A-8.4 Therminol-Based SH-TES

The SH-TES model is a two-tank design with Therminol-66 as the storage medium and steam as the heat-transfer fluid. During the charging-mode, cold fluid is pumped from the cold tank through an intermediary heat exchanger (IHX) where it absorbs heat from the heat-transfer fluid and is then transferred to the hot tank for storage. During the discharging cycle, the process is reversed. Currently, the SH-TES model has the capability to be coupled with a pressurized water reactor (PWR), where the steam from the turbine bypass valves can be directed towards the IHX during hours of low demand and be used to charge the heat the storage media in the SH-TES. A schematic of the integrated system is shown in Figure A-14.[90]

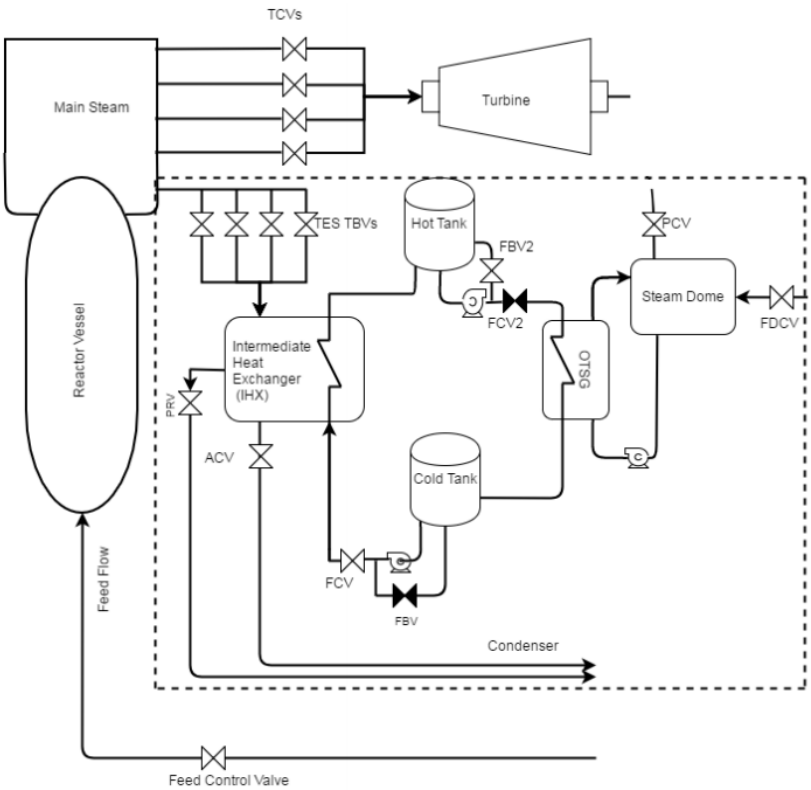

Figure A-14. Schematic of a two-tank SH-TES coupled to an light water reactor (LWR)..

Page intentionally left blank

APPENDIX B
COST BREAKDOWN FOR THE SH-TES SYSTEM FLUIDS

APPENDIX B
COST BREAKDOWN FOR THE SH-TES SYSTEM FLUIDS

B-1. HITEC XL

Table B-1. Estimated equipment costs for an SH-TES system with 500 MWe net power generation capacity with Hitec XL as storage medium.

Equipment	Capacity	Unit	Equipment Cost	Installed Cost	Cost per kWe	Notes
HX1	3150	MW	$26,718,400	$35,207,069	$70	30 units in total - 3 series X 10 parallel.
HX2	495.2	MW	$29,310,100	$35,879,873	$72	7 units in total.
HX3	962	MW	$20,822,600	$23,255,011	$47	36 units in total - 4 series x 9 parallel
HX4	862	MW	$7,977,300	$9,182,038	$18	14 units in total - 7 parallel x 2 series
Condenser	1326	MW	$38,040,000	$46,084,900	$92	90 units in total. Sizing limitations in APEA
Charging Pump	4.344	MW	$8,416,800	$9,216,254	$18	
Discharging Pump	3.519	MW	$2,478,300	$2,861,472	$6	
Power Cycle Pump	1.231	MW	$621,700	$743,330	$1	
Condenser Pump	1.758	MW	$1,740,000	$6,478,700	$13	90 units in total. To match the condenser quantities
			Total	$168,908,647	$338	

Table B-3. Estimated storage capacity dependent costs for Hitec XL at 12 hours of storage.

Component	Unit Cost ($/kWe)	Actual Cost ($)
Hot Storage Tank	22	$131,400,000
Cold Storage Tank	22	$131,400,000
Molten Salt	99	$596,206,238
Total	**143**	$859,006,238

Table B-4. Summary of LCOS analysis for SH-TES with Hitec XL as the storage medium.

System Design		**Units**
Power Rating	500	MWe
Duration	6	hr
Usable Energy	3000	MWh-e
Interval between start of discharge cycles	24	h
Depth-o- Discharge	100%	
Operating days/yr	350	
System Performance		
Round Trip Efficiency	27%	electric basis
Degradation	0.00%	per annum
Financial Parameters		
Debt Fraction	60%	
Cost of Debt	5%	
Equity Fraction	40%	
Cost of Equity	10%	
Combined Tax Rate	26%	
Contract Term/Project Life	20	yr
CAPEX		
System CAPEX	$1,027,914,885	
Total Initial Installed Cost	$171.32	$/kWh-e
OPEX		
Electricity Charging Cost	30	$/MWh-e
Charging Cost Escalation	2.50%	per annum
Operations and Maintenance (O&M),, general	1.50%	% of CAPEX
General O&M Cost Escalation	2.50%	per annum
Calculated Levelized Cost of Storage		
LCOS (6 hr discharge capacity)	$96.47	$/MWh-e

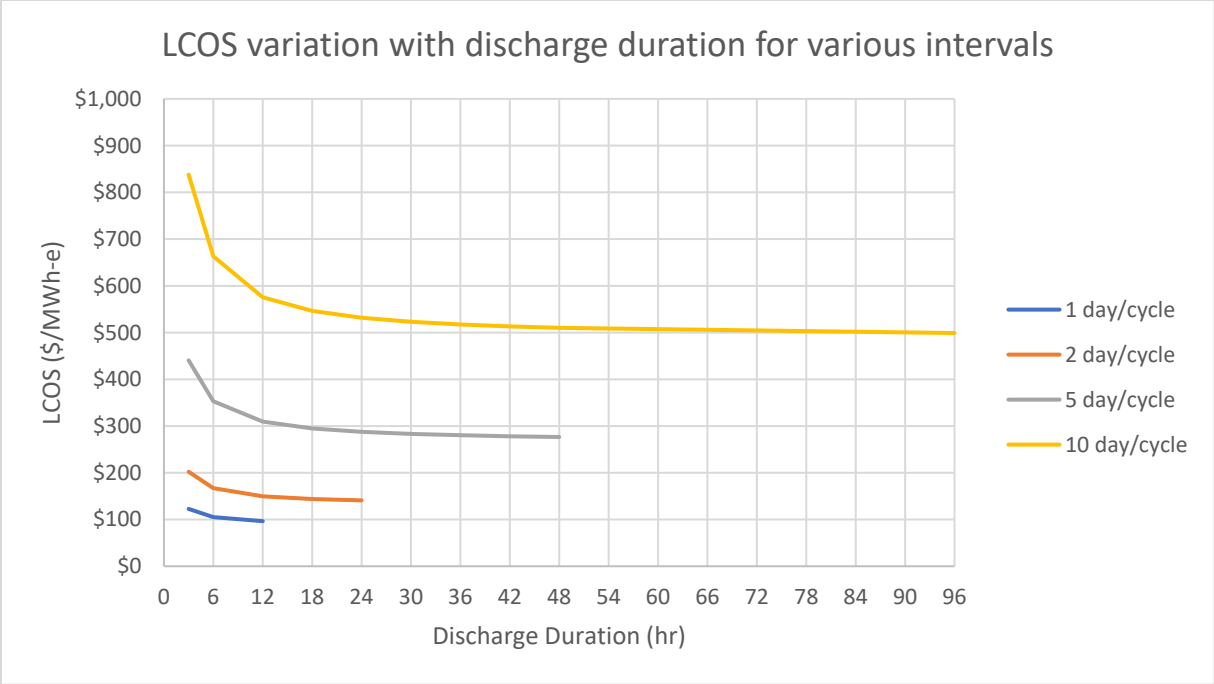

LCOS as a function of discharge cycle duration with interval between initiation of discharge cycles as a parameter for HitecXL-based SH-TES

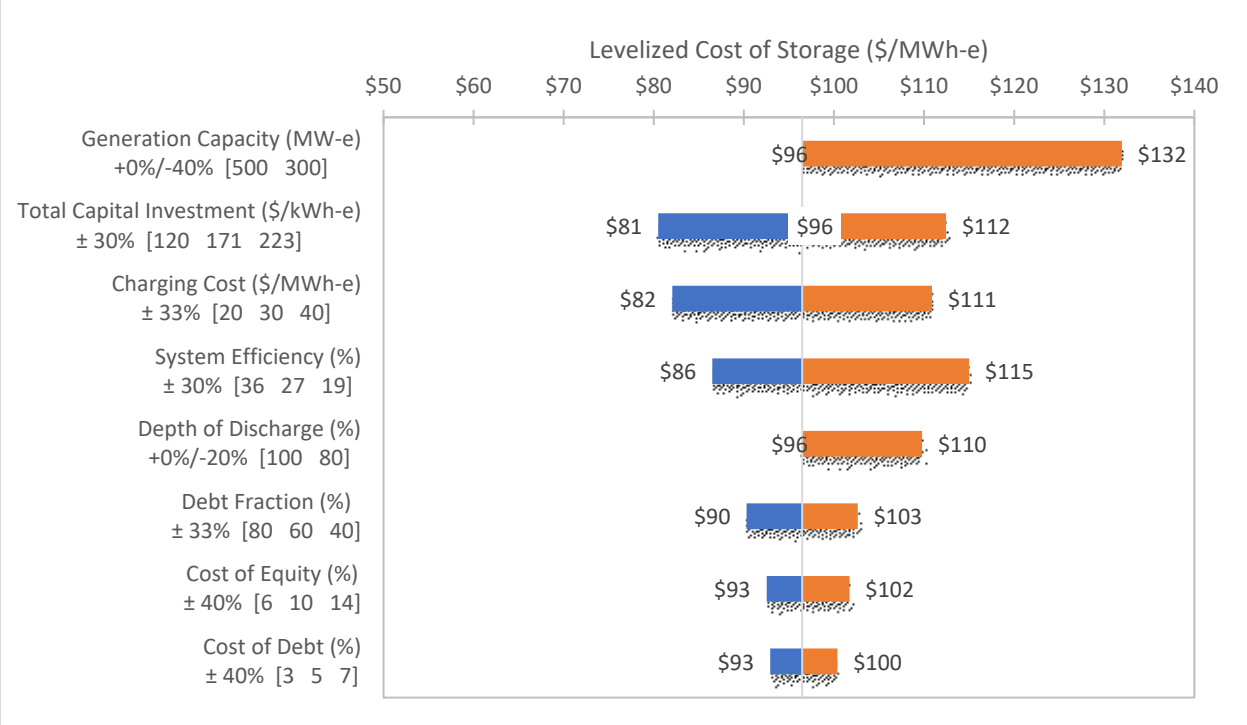

Tornado chart illustrating sensitivity of HitecXL-based SH-TES LCOS to selected parameters

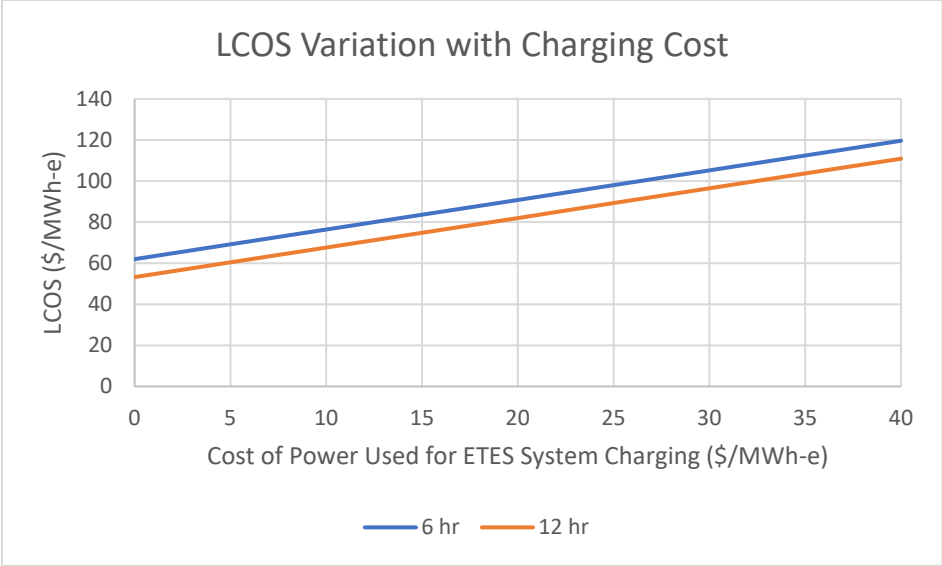

LCOS as a function of the charging electricity for an SH-TES with HitecXL

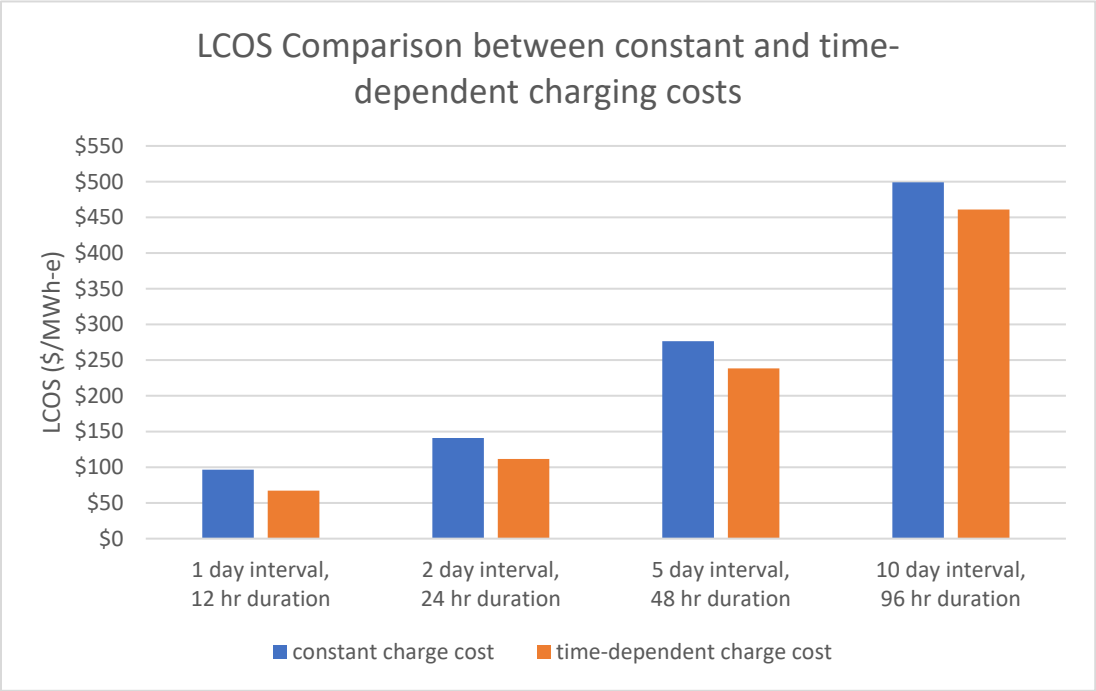

LCOS comparison for HitecXL-based SH-TES systems operating with selected discharge intervals/durations and charging costs

B-2. THERMINOL-66

Table B-5. Estimated equipment costs for an SH-TES system with 500 MWe net power generation capacity with Therminol-66 as storage medium.

Equipment	Capacity	Unit	Equipment Cost	Installed Cost	Cost per kWe	Notes
HX1	3150	MW	$30,380,100	$37,805,856	$76	36 units in total - 9 parallel x 4 series
HX2	495.2	MW	$7,961,800	$12,420,258	$25	8 units in total.
HX3	962	MW	$4,242,800	$5,499,890	$11	10 units in total - 2 series x 5 parallel
HX4	862	MW	$16,546,900	$18,370,442	$37	32 units in total - 8 parallel x 4 series
Condenser	1326	MW	$38,040,000	$46,084,900	$92	90 units in total. Sizing limitations in APEA
Charging Pump	4.344	MW	$23,103,000	$24,810,300	$50	
Discharging Pump	3.519	MW	$7,589,800	$8,365,560	$17	
Power Cycle Pump	1.231	MW	$621,700	$743,330	$1	
Condenser Pump	1.758	MW	$1,740,000	$6,478,700	$13	90 units in total. To match the condenser quantities
			Total	$160,579,236	$321	

Table B-6. Estimated storage capacity dependent costs for Therminol-66 at 12 hours of storage.

Component	Unit Cost ($/kWe)	Actual Cost ($)
Hot Storage Tank	22	$131,400,000
Cold Storage Tank	22	$131,400,000
Molten Salt	415	$2,489,401,781
Total	**437**	$2,752,201,781

Table B-7. Summary of LCOS analysis for SH-TES with Therminol-66 as the storage medium.

System Design		**Units**
Power Rating	500	MWe
Duration	6	hr
Usable Energy	3000	MWh-e
Interval between start of discharge cycles	24	h
Depth-o- Discharge	100%	
Operating days/yr	350	
System Performance		
Round Trip Efficiency	27%	electric basis
Degradation	0.00%	per annum
Financial Parameters		
Debt Fraction	60%	
Cost of Debt	5%	
Equity Fraction	40%	
Cost of Equity	10%	
Combined Tax Rate	26%	
Contract Term/Project Life	20	yr
CAPEX		
System CAPEX	$2,912,781,017	
Total Initial Installed Cost	$485.46	$/kWh-e
OPEX		
Electricity Charging Cost	30	$/MWh-e
Charging Cost Escalation	2.50%	per annum
O&M, general	1.50%	% of CAPEX
General O&M Cost Escalation	2.50%	per annum
Calculated Levelized Cost of Storage		
LCOS (6 hr discharge capacity)	$194.09	$/MWh-e

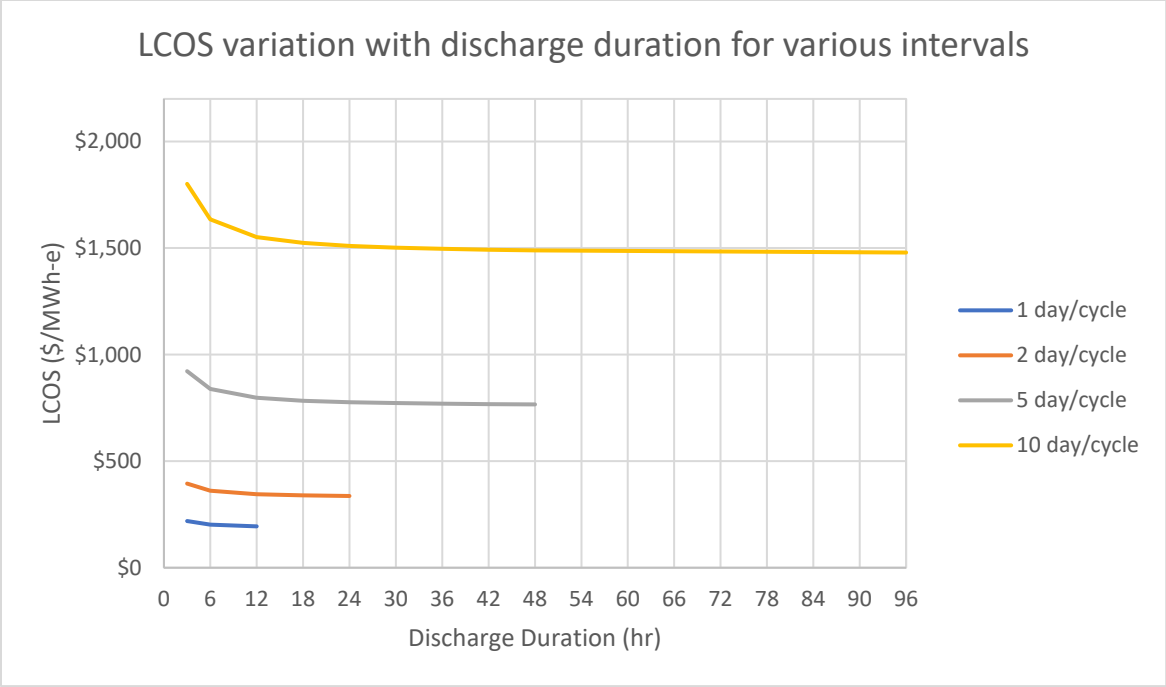

LCOS as a function of discharge cycle duration with interval between initiation of discharge cycles as a parameter for Therminol-66-based SH-TES

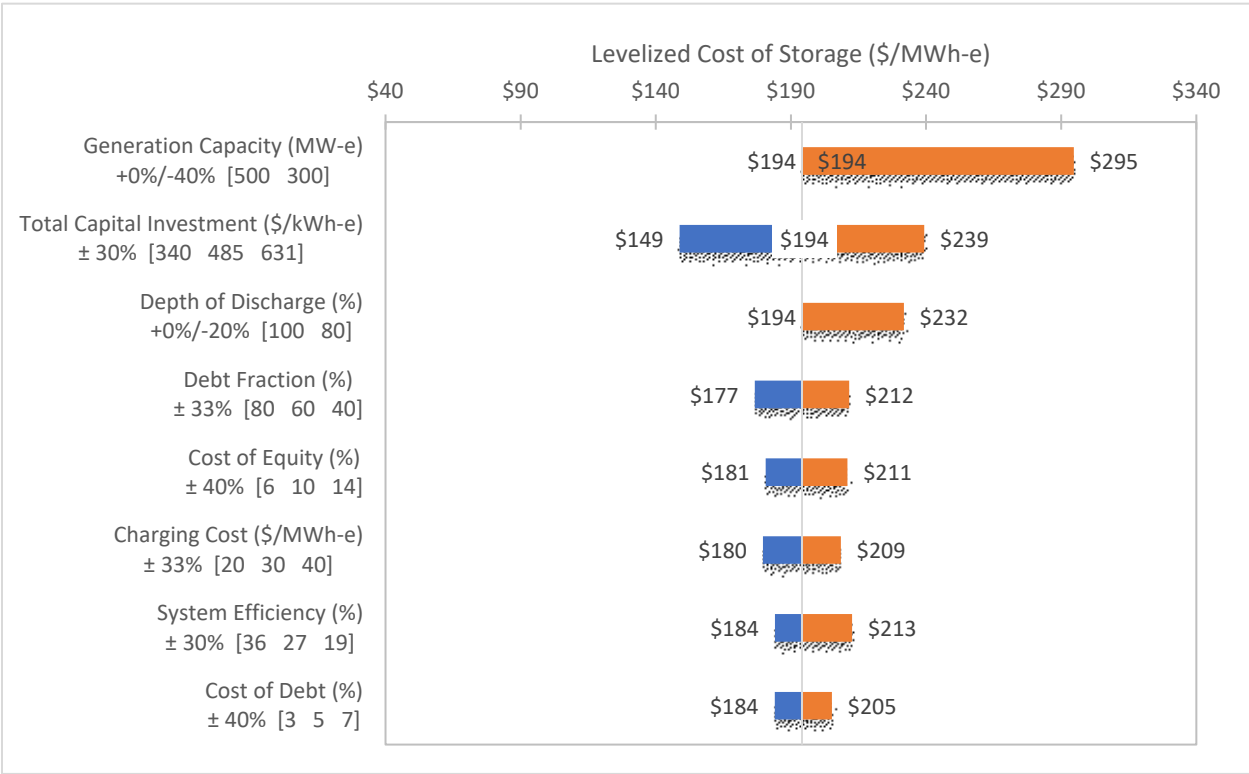

Tornado chart illustrating sensitivity of Therminol-66-based SH-TES LCOS to selected parameters

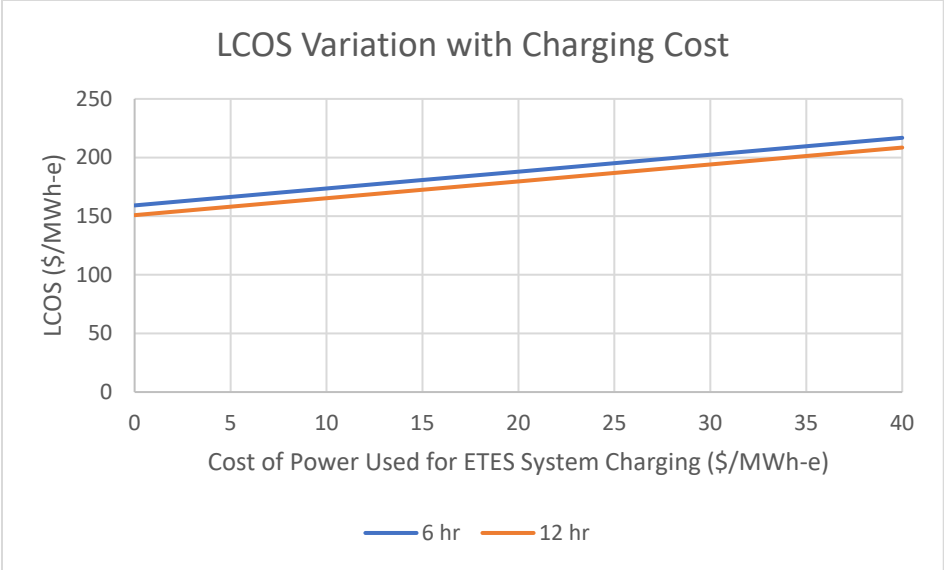

LCOS as a function of the charging electricity for an SH-TES with Therminol-66

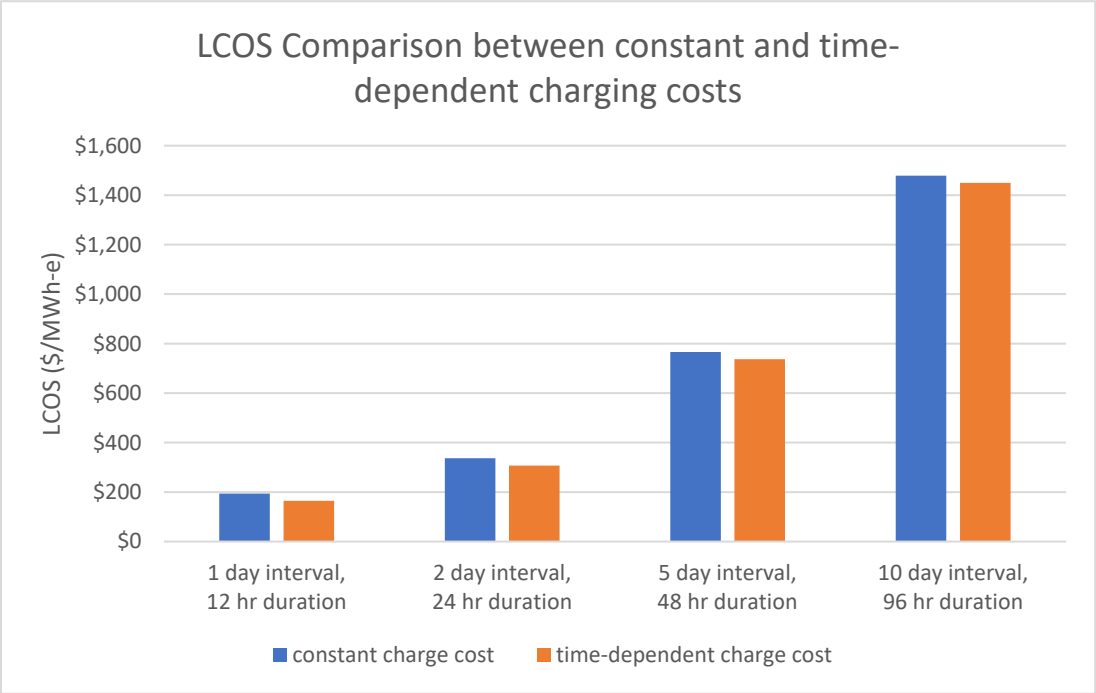

LCOS comparison for Therminol-66-based SH-TES systems operating with selected discharge intervals/durations and charging costs

B-3. DOWTHERM A

Table B-8. Estimated equipment costs for an SH-TES system with 500 MWe net power generation capacity with Dowtherm A as storage medium.

Equipment	Capacity	Unit	Equipment Cost	Installed Cost	Cost per kWe	Notes

Equipment	Capacity	Unit	Equipment Cost	Installed Cost	Cost per kWe	Notes
HX1	3150	MW	$30,925,500	$37,789,577	$76	30 units in total - 10 parallel x 3 series
HX2	495.2	MW	$5,327,900	$9,783,786	$20	6 units in total.
HX3	962	MW	$5,563,900	$6,897,738	$14	10 units in total
HX4	862	MW	$6,670,400	$7,982,791	$16	21 units in total - 7 parallel x 3 series
Condenser	1326	MW	$38,040,000	$46,084,900	$92	90 units in total. Sizing limitations in APEA
Charging Pump	4.344	MW	$27,933,800	$28,764,092	$58	
Discharging Pump	3.519	MW	$9,623,200	$10,026,379	$20	
Power Cycle Pump	1.231	MW	$621,700	$743,330	$1	
Condenser Pump	1.758	MW	$1,740,000	$6,478,700	$13	90 units in total. To match the condenser quantities
			Total	$154,551,293	$309	

Table B-9. Estimated storage capacity dependent costs for Therminol-66 at 12 hours of storage.

Component	Unit Cost ($/kWe)	Actual Cost ($)
Hot Storage Tank	22	$131,400,000
Cold Storage Tank	22	$131,400,000
Molten Salt	278	$1,669,344,706
Total	**322**	$1,932,144,706

Table B-10. Summary of LCOS analysis for SH-TES with Dowtherm-A as the storage medium.

System Design		**Units**
Power Rating	500	MWe
Duration	6	hr
Usable Energy	3000	MWh-e
Interval between start of discharge cycles	24	h
Depth-o- Discharge	100%	
Operating days/yr	350	
System Performance		
Round Trip Efficiency	27%	electric basis
Degradation	0.00%	per annum
Financial Parameters		
Debt Fraction	60%	
Cost of Debt	5%	
Equity Fraction	40%	
Cost of Equity	10%	
Combined Tax Rate	26%	
Contract Term/Project Life	20	yr
CAPEX		
System CAPEX	$1,120,623,646	
Total Initial Installed Cost	$373.54	$/kWh-e
OPEX		
Electricity Charging Cost	30	$/MWh-e
Charging Cost Escalation	2.50%	per annum
O&M, general	1.50%	% of CAPEX
General O&M Cost Escalation	2.50%	per annum
Calculated Levelized Cost of Storage		
LCOS (6 hr discharge capacity)	$159.31	$/MWh-e

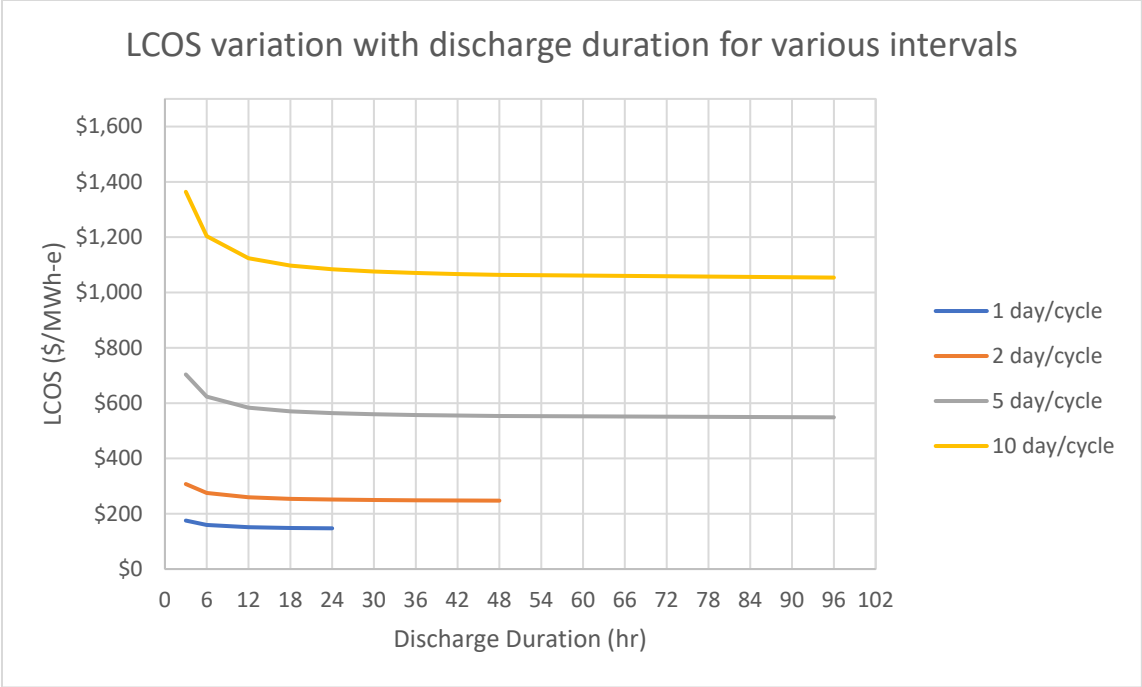

LCOS as a function of discharge cycle duration with interval between initiation of discharge cycles as a parameter for Dowtherm A-based SH-TES

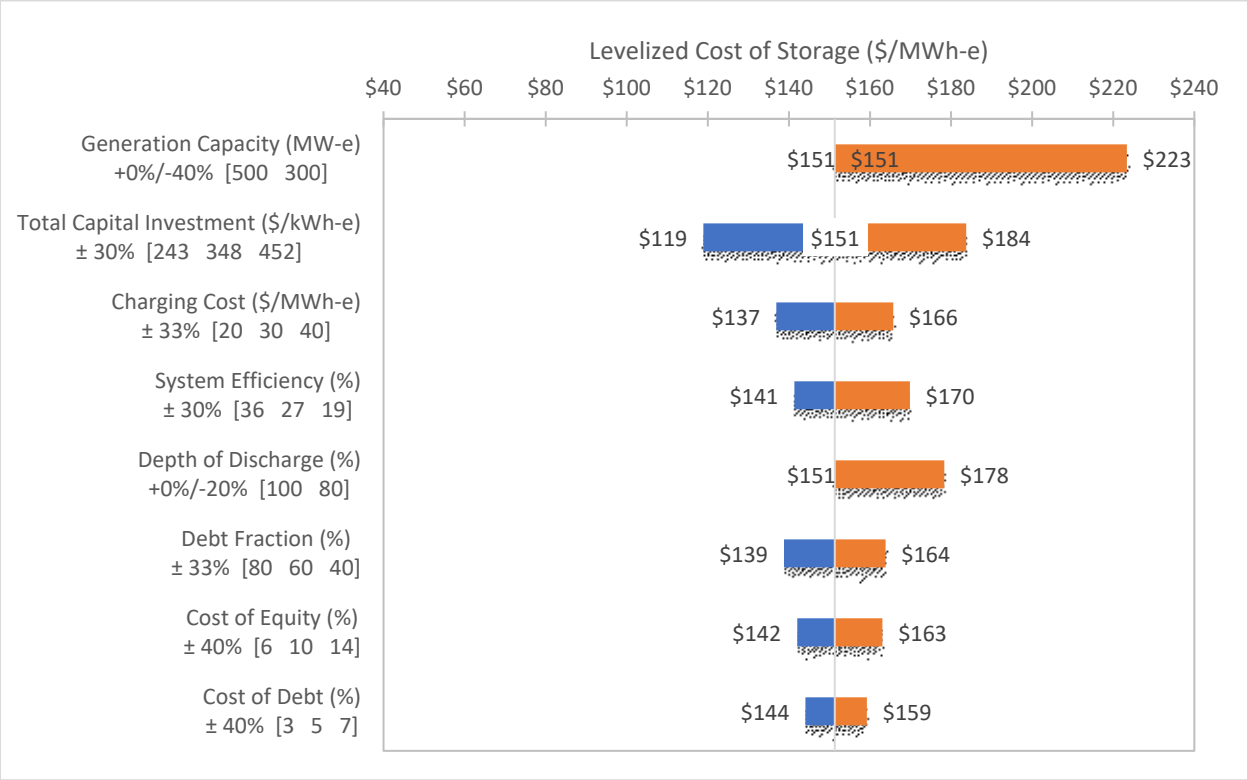

Tornado chart illustrating sensitivity of Dowtherm A-based SH-TES LCOS to selected parameters

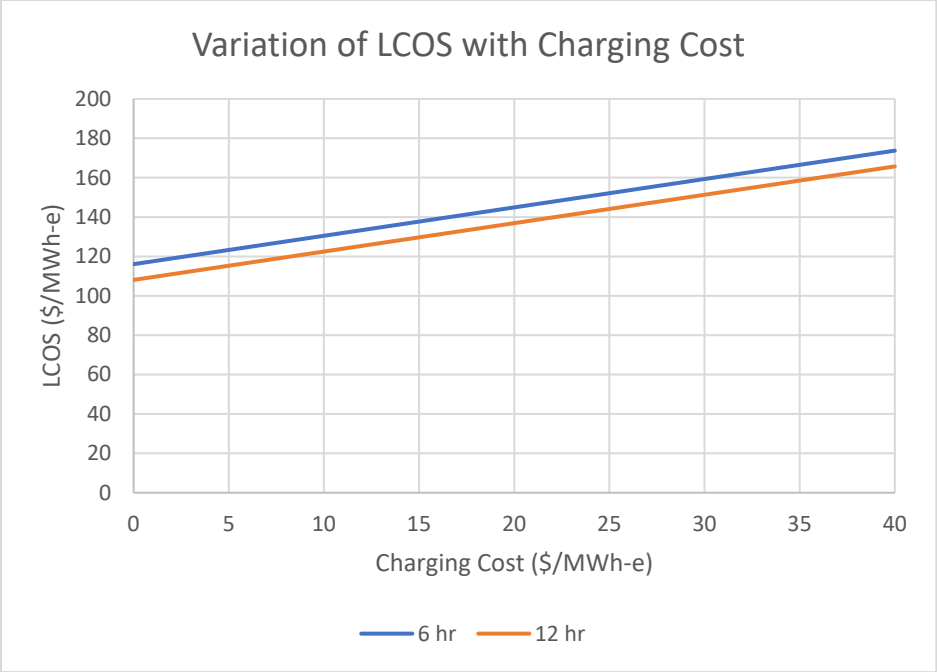

LCOS as a function of the charging electricity for an SH-TES with Dowtherm A

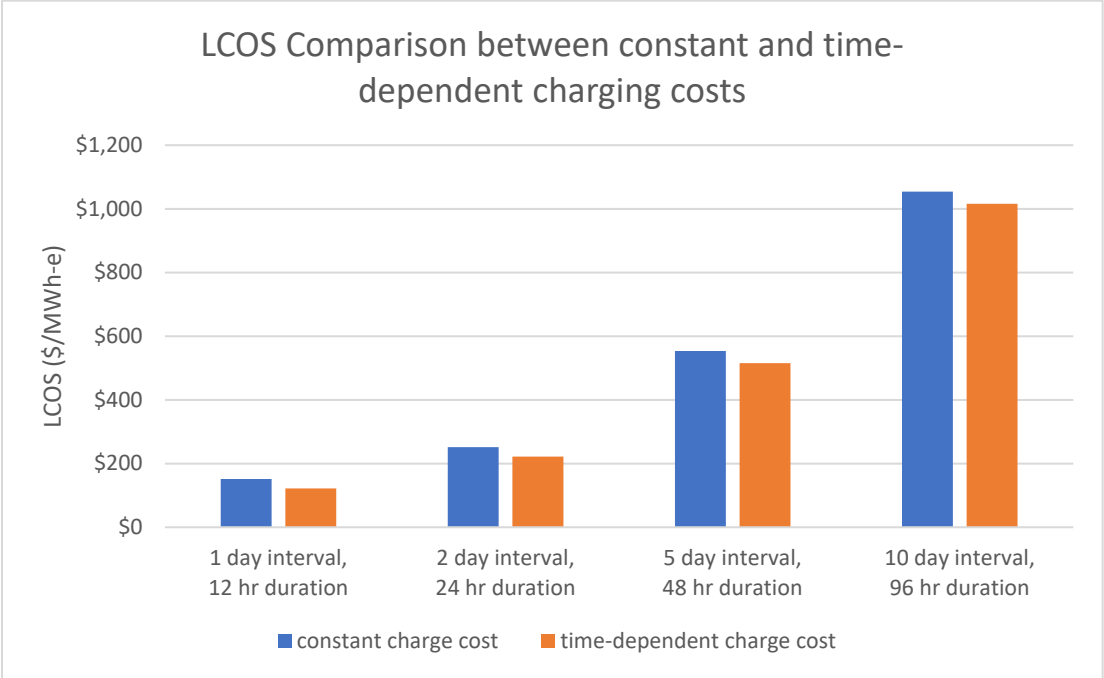

LCOS comparison for Dowtherm A-based SH-TES systems operating with selected discharge intervals/durations and charging costs

Page intentionally left blank

APPENDIX C
TES TECHNOLOGY CONSIDERATIONS

APPENDIX C

TES TECHNOLOGY CONSIDERATIONS

TES technologies are a promising solution for storing excess thermal energy during low-consumption periods, and although some of the technologies have been successfully deployed on a large scale in conjunction with CSP plants and other power generation plants, several technical challenges need to be overcome for a wider application of TES systems. The following section describes some of these requirements, concerns, and challenges.

C-1. MATERIAL-SPECIFIC REQUIREMENTS

The most generic challenge that all TES systems must overcome is storage material and heat-transfer fluid. The selection of these materials depends on the temperature range of operation, the storage type—i.e., sensible, latent, thermochemical, etc.—and the storage duration. To qualify as an optimal candidate for the storage medium as well as the heat transfer fluid, the materials must satisfy the following criteria

- High heat capacity
  This would allow for a high amount of sensible heat energy storage.
- High thermal conductivity
  Thermal conductivity along with temperature difference is the driving force for heat transfer. In solid-based SH-TES systems specifically, where the storage media cannot take advantage of the high convective heat transfer coefficient, high thermal conductivity is needed.
- Low corrosion
  Materials chosen for storage should not be corrosive to prolong the lifecycle of the TES systems.
- Low-cost, and high availability in large quantities
  To deploy storage technologies on a large scale, the storage medium and the heat transfer fluid should be cheap and readily available. If not, they add up to the capital costs of the coupled system.
- Low degradation
  Low material degradation is needed if the storage medium and heat transfer fluid is to be cycled thermally over their operational lifetimes. Material degradation adds to the capital cost of the systems.
- Non-hazardous and nonflammable
  Materials used in storage need to be non-hazardous and non-flammable, with little to no detrimental effects on the environment.
- Low vapor pressure
  Low vapor pressure allows the storage and operation of the TES systems at low pressures. Pressure vessels are expensive and add to the capital cost of the system.
- High chemical stability at elevated temperatures
  Material dissociation at elevated temperatures leads to material degradation. This would reduce the operational lifecycle of the storage medium or the heat transfer fluid and increase the capital costs.

In addition to this, phase change materials (PCMs) used in latent heat storage systems need to have

- High heat of fusion
  Latent heat systems rely primarily on the heat of fusion to store energy. The high heat of fusion would allow a larger amount of heat to be stored for the same mass.
- Low super cooling
  Supercooling is the process of cooling a fluid below its freezing point without solidifying it. This is

detrimental in latent-heat systems because of PCMs with a high degree of supercooling release more sensible heat than latent heat.

- Low volumetric expansion during phase change
  Volumetric expansion during a phase change is inevitable but should be minimal in order to avoid the need for large storage tanks.

The number of materials that are considered viable candidates in TES systems is huge. However, each TES system is unique; therefore, a detailed analysis needs to be carried out before selecting a specific working fluid and storage medium.

C-2. NUCLEAR REACTOR COUPLING CONSIDERATIONS

Some of the possible challenges and questions to keep in mind while attempting to couple a TES system to a nuclear power plants (NPP) facility are as follows.

- Where to locate the TES systems? At the nuclear facility or outside the facility?
  - If at the nuclear facility, will it need to follow nuclear-grade safety requirements?
  - If outside the facility, how will the steam transportation affect the performance and efficiency of the coupled system?
    - This needs to be understood because there will be thermal losses during the transportation of steam to and from the TES system.
- From where will the steam be drawn and how will this affect the dynamics of the nuclear reactor?
  - Changes in the steam conditions are reflected in the reactor power. How will this be managed?
    - The flow conditions at the inlet of the high-pressure turbine are correlated with the flow conditions into the reactor core. PWRs are viewed as “steam-turbine following” due to the reactivity feedback of the temperature change caused by an increase or decrease in steam flow.
- To where will the discharged steam be returned?
  - There will be pressure loss during the storage and recovery process of thermal energy. The recovered steam will be low-grade and must therefore be injected at a place different from the location from which it was withdrawn.
  - If the discharged steam is returned to a lower-stage turbine, will the turbine be able to handle the additional steam input?
- PWRs have a separate steam-generating loop whereas boiling water reactors do not. Will it be safe to draw steam from these loops?
  - How will it affect the water chemistry in the reactors?
  - How possible contamination from TES systems be limited?
- Are there special requirements during startup and shutdown?
- Are LWRs able to add additional control systems and mechanisms to their existing designs?

C-3. TECHNOLOGY GAPS

Although PCM-based TES systems are highly sought after due to their high energy density, isothermal charging and discharging cycles, and low material degradation, their low thermal conductivity leads to low charge and discharge rates. This is especially evident during the discharging cycles because a solid layer of PCM is formed between the surface of the heat exchanger and the molten PCM. Solid PCM depends purely on material conductivity and is, therefore, a limiting factor for the discharge rate.

As the discharge cycle progresses, the solid PCM thickness increases, thereby decreasing the heat transfer rate. This will eventually lead to lower efficiencies. Low-cost storage materials such as sand or silica have been proposed to be used in TES systems. However, effective heat exchangers that transfer heat from the working fluid to the solid particles are yet to be designed.

C-4. TES TECHNOLOGY CONSIDERATIONS

Thirteen categories have been identified for inclusion in the figure of merit. These include technology readiness, charging and discharging compatibility, ancillary services market application, system capacity, ramp time, cycle frequency, realignment frequency, cost, lifetime, geographical requirements, environmental concerns, and thermal support requirements. The figures of merit assigned for each category along with scaling justification are discussed.

1. Technology readiness level (TRL) is extremely important to JUMP, as the system must be fully designed in the next few years to be licensed and deployed by late 2026. To give the proper weight, the FOM value equals the TRL (0-9 scale).
2. Experienced technology integration with nuclear steam pressures and temperatures. The NuScale reactor maintains steam pressure at 2.7 MPa and 300°C. Being able to directly use this steam achieves a FOM of 2, having to somewhat downgrade this steam gives a FOM of 1, and a FOM of 0 indicates no direct use of this steam.
3. Capability to discharge high quality heat. The TES must be able to discharge its energy capacity at consistent high-quality heat. A system capable of discharging its entire store at above 175°C was given a FOM of 2. A system capable of either sliding pressure discharge with some above 175°C or a system capable of discharging between 100-175°C was given a FOM of 1. Otherwise, the FOM was 0 for this category.
4. United States electrical grid ancillary services market potential. If a TES allows for participation in the frequency regulation market, a FOM of 2 was given. If a TES allows for participation in the reserves market, a FOM of 1 was given. Otherwise, a 0 was given for this category.
5. Total energy capacity for this system is estimated at 400 MWh of heat. A system must therefore be able to manage that much energy. A system capable of this size was given a FOM of 2. One that could store 100 MWh but not 400 MWh, was given a FOM of 1, and a 0 was given otherwise.
6. Ramp time is associated with category 4, as well as energy arbitration and load following. Due to the most restrictive reserve market restrictions of 10 minutes, a ramp time to maximum power of 10 minutes or less was given a FOM of 2. A ramp time of less than one hour is assigned a 1, and any ramp longer than that is given a 0.
7. Cycle frequency, defined as the system's capability to charge and discharge. If a system can charge and discharge at will, a FOM of 2 was given. A system that could cycle only daily is given a FOM of 1, and a 0 to systems with longer cycles.
8. Realignment frequency is the need of a system to either wait on some phenomenon or correct a non-ideal process and leads to a reduction in capacity factor. If no realignment is required, a FOM of 2 is given. If realignment is required every cycle, a FOM of 0 is given. A FOM of 1 is given for values in the middle.
9. TES cost per kWh. This value is evaluated after the total FOM is calculated, to be used as a selection method later.
10. Technology lifetime refers to the time before the TES would need self-replacement. Like cost, this factor is considered after the FOM is calculated.

11. Geographical insensitivity. Because it is desired for small modular reactor (SMR)s with TES to be deployed globally with as little re-design as possible, geographical needs are considered. A FOM of 0 is given to a geography-specific technology, while a FOM of 1 is given to a TES without those requirements.
12. Environmental concerns are important and can appear in multiple stages of TES use: construction, direct use, and during deconstruction. A FOM of 1 is given to a technology that does not have any significant environmental concerns, and a FOM of 0 was given to technology with environmental concerns.
13. Minimum turndown or thermal support requirements. A system that needs heat tracing or a constant supply of heat is given a FOM of 0. A system that faces no concerns if heat is not constantly supplied is given a FOM of 1.

5. REFERENCES

1 National Renewable Energy Laboratory (NREL). n.d. "Renewable Electricity Futures Studies." NREL, Golden, CO, USA. Available at: https://www.nrel.gov/analysis/re-futures.html.

2 McMillian, C., R. Boardman, M. McKellar, P. Sabharwall, M. Ruth, and S.B.-Sitton. 2016. "Generation and Use of Thermal Energy in the U.S. Industrial Sector and Opportunities to Reduce its Carbon Emissions." INL/EXT-16-39680, NREL/TP-6A50-66763, November 2016. Idaho National Laboratory (INL), Idaho Falls, ID, USA.

3 Knighton, L.T., A. Shigrekar, D.S. Wendt, R. Boardman, B. Murphy, and B. James. 2020. "Markets and Economics for Thermal Power Extraction from Nuclear Power Plants for Industrial Processes." INL/EXT-20-58884. June 2020. Idaho National Laboratory (INL), Idaho Falls, ID, USA.

4 Boardman R.D. et al. 2019. Evaluation of Non-electric Market Options for a Light-water Reactor in the Midwest. INL/EXT-19-55090. Idaho National Laboratory. Idaho Falls, ID.

5 Frick, Konor L., et al. 2019. "Evaluation of Hydrogen Production Feasibility for a Light Water Reactor in the Midwest." INL/EXT-19-55395. Idaho National Laboratory (INL), Idaho Falls, ID, USA.

6 Knighton, L.T., et al. 2020. "Clean Energy Credits for the Production of Low Carbon Hydrogen, Steel and Ammonia using Nuclear Energy." INL/EXT-20-58508. Idaho National Laboratory (INL), Idaho Falls, ID, USA.

7 Knighton, L.T., et al. 2020. "Clean Energy Credits for the Production of Low Carbon Hydrogen, Steel and Ammonia using Nuclear Energy." INL/EXT-20-58508. Idaho National Laboratory (INL), Idaho Falls, ID, USA.

8 Knighton, L.T. et al. 2020. *Markets and Economics for Thermal Power Extraction from Nuclear Power Plants for Industrial Processes*. Report INL/EXT-20-58884. Idaho National Laboratory. Idaho Falls, ID.

9 Knighton, L.T., et al. 2020. "Markets and Economics for Thermal Power Extraction from Nuclear Power Plants for Industrial Processes." INL/EXT-20-58884. Idaho National Laboratory (INL), Idaho Falls, ID, USA.

10 Hu, H., et al., "Technoeconomic Analysis on an Electrochemical Nonoxidative Deprotonation Process for Ethylene Production from Ethane," INL/EXT-19-56936. December 2019. Idaho National Laboratory (INL), Idaho Falls, ID, USA.

11 Lazard. Levelized Cost of Storage Analysis version 6.0. 2020. Available: https://www.lazard.com/media/451418/lazards-levelized-cost-of-storage-version-60.pdf

12 Mongird, K., V. Viswanathan, J. Alam, C. Vartanian, V. Sprenkle, R. Baxter. 2020. "2020 Grid Energy Storage Technology Cost and Performance Assessment Technical Report." DOE/PA-0204. December 2020. Pacific Northwest National Laboratory (PNNL), Richland, WA, USA. Available at: https://www.pnnl.gov/ESGC-cost-performance.

13 Pacific Northwest National Laboratory (PNNL). n.d. "Lithium-ion Battery (LFP and NMC)." PNNL, Richland, WA, USA. Available at: https://www.pnnl.gov/lithium-ion-battery-lfp-and-nmc.

14 U.S. Department of Energy (DOE). 2020. "Hydrogen and Fuel Cells Program Record 20006: Hydrogen Production Cost from High Temperature Electrolysis." DOE, Washington DC, USA.

Available at: https://www.hydrogen.energy.gov/pdfs/20006-production-cost-high-temperature-electrolysis.pdf.

15 Intermountain Power Agency (IPA). 2020. "IPP Renewed." IPA, South Jordan, UT, USA. Available at: https://www.ipautah.com/ipp-renewed/.

16 Los Angeles Department of Water and Power (LADWP). 2021. "LADWP Joins HyDeal LA, Targets Green Hydrogen at $1.50/kilogram by 2030." LADWP, Los Angeles, CA, USA. Available at: https://www.ladwpnews.com/ladwp-joins-hydeal-la-targets-green-hydrogen-at-1-50-kilogram-by-2030/.

17 American Public Power Association (APPA). 2019. "LADWP embarks on hydrogen generation project." APPA, Washington DC, USA. Available at: https://www.publicpower.org/periodical/article/ladwp-embarks-hydrogen-generation-project.

18 Los Angeles Department of Water and Power (LADWP). 2020. "Intermountain Power Project & Green Hydrogen, July 2020." LADWP, Los Angeles, CA, USA. Available at: https://ww2.arb.ca.gov/sites/default/files/2020-07/ladwp_cn_fuels_infra_july2020.pdf.

19 Lord, A.S., P.H. Kobos, and D.J. Kobos. 2014. "Geologic storage of hydrogen: Scaling up to meet city transportation demands." *International Journal of Hydrogen Energy*, 39(28), 15570-15582. DOI: 10.1016/j.ijhydene.2014.07.121.

20 Reddi, K., M. Mintz, A. Elgowainy, and E. Sutherland. 2016. "Building a hydrogen infrastructure in the United States," In *Compendium of Hydrogen Energy*, Volume 4, 'Hydrogen Use, Safety and the Hydrogen Economy,' Chapter 13. DOI: 10.1016/B978-1-78242-364-5.00013-0.

21 U.S. Department of Energy–Office of Energy Efficiency & Renewable Energy (DOE-EERE). n.d. "Technical Targets for Hydrogen Delivery." DOE-EERE, Washington DC, USA. Available at: https://www.energy.gov/eere/fuelcells/doe-technical-targets-hydrogen-delivery.

22 Geology.com. n.d. "What is a Salt Dome?" Available at: https://geology.com/stories/13/salt-domes/.

23 Argonne National Laboratory (ANL). 1999. "An Introduction to Salt Caverns & Their Use for Disposal of Oil Field Wastes." September 1999. ANL, Lemont, IL, USA. Available at: https://www.evs.anl.gov/publications/doc/SaltCavbroch.pdf.

24 National Energy Technology Laboratory (NETL). 2005. "Cavern Roof Stability for Natural Gas Storage in Bedded Salt." March 2005. NETL, Pittsburgh, PA, USA. Available at: https://netl.doe.gov/node/2638.

25 Satyapal, S. 2019. "Hydrogen and Fuel Cells Enabled through the U.S. Department of Energy." U.S. Department of Energy–Office of Energy Efficiency & Renewable Energy (DOE-EERE), Washington DC, USA. Available at: https://www.energy.gov/sites/prod/files/2019/06/f63/fcto-satyapal-overview-for-ecs-meeting-2019-05-27.pdf.

26 U.S. Department of Energy–Office of Energy Efficiency & Renewable Energy (DOE-EERE). n.d. "Types of Fuel Cells." DOE-EERE, Washington DC, USA. Available at: https://www.energy.gov/eere/fuelcells/types-fuel-cells.

27 Wei, M., G. Levis, and A. Mayyas. 2020. "Reversible Fuel Cell Cost Analysis." Lawrence Berkeley National Laboratory (LBNL), Berkeley, CA, USA. Available at: https://www.hydrogen.energy.gov/pdfs/review20/fc332_wei_2020_o.pdf.

28 Foss, Andrew, Haydn Bryan, Jeremiah Pisarra, and Richard Boardman. Forthcoming. *Comparative Techno-Economic Analysis of Hydrogen and Batteries for Grid-Scale Energy Storage*. Idaho National Laboratory. Idaho Falls, ID, USA.

29 Frick, K., C.T. Misenheimer, J.M. Doster, S.D. Terry, and S. Bragg-Sitton. 2017. "Thermal energy storage configurations for small modular reactor load shedding," *Nuclear Technology*, 202(1), 53-70. DOI: 10.1080/00295450.2017.1420945.

30 Frick, K., J.M. Doster, and S. Bragg-Sitton. 2018. "Design and operation of a sensible heat peaking unit for small modular reactors," *Nuclear Technology*, 205(3), 415-441. DOI: 10.1080/00295450.2018.1491181.

31 Mikkelson, D.M. 2021. "Integrated Energy Systems with Thermal Energy Storage: Technology Selection, Preliminary Design, and Analysis." Ph.D. Dissertation, North Carolina State University, Raleigh, NC, USA. ProQuest Dissertations Publishing, 28484309. Available at: https://www.proquest.com/openview/dfee667e6eeb7d402f1d72d76bdb7dd0/1?pq-origsite=gscholar&cbl=18750&diss=y.

32 Echogen Power Systems, Inc. n.d. "ETES System Overview." Echogen Power Systems, Akron, OH, USA. Available at: https://www.echogen.com/energy-storage/etes-system-overview/.

33 Echogen Power Systems, Inc. n.d. "Supercritical CO2-Based Long-Duration Electrical Energy Storage Technical Overview," Echogen Power Systems, Akron, OH, USA. Available at: https://www.echogen.com/_CE/pagecontent/Documents/Echogen-Technical%20Overview%207.18.19-3.pdf.

34 Echogen Power Systems, Inc. 2019. "A Supercritical CO2 Power Cycle/Pressurized Fluidized Bed Combustion System Integrated with Energy Storage: Compact, Efficient and Flexible Coal Power. Contract No. 89243319CFE000022." https://netl.doe.gov/sites/default/files/2019-10/Indirect-Supercritical-Carbon-Dioxide-Power-Plant-System-Echogen.pdf.

35 Echogen Power Systems, Inc. 2019. "A Supercritical CO2 Power Cycle/Pressurized Fluidized Bed Combustion System Integrated with Energy Storage: Compact, Efficient and Flexible Coal Power. Contract No. 89243319CFE000022." https://netl.doe.gov/sites/default/files/2019-10/Indirect-Supercritical-Carbon-Dioxide-Power-Plant-System-Echogen.pdf.

36 Albrecht, K.J. and Ho, C.K. "Heat Transfer Models of Moving Packed-Bed Particle-to-sCO2 Heat Exchangers." J. Sol. Energy Eng. 141(3) Jun 2019. https://doi.org/10.1115/1.4041546.

37 Ho, C. A Review of High-Temperature Particle Receivers for Concentrating Solar Power. *Applied Thermal Engineering* Volume 109 Part B 958-969. October 2016. http://dx.doi.org/10.1016/j.applthermaleng.2016.04.103.

38 Lazard. Levelized Cost of Storage Analysis version 6.0. 2020. Available: https://www.lazard.com/media/451418/lazards-levelized-cost-of-storage-version-60.pdf.

39 Wang, K., Z. Qin, W. Tong, and C. Ji. 2020. "Thermal Energy Storage for Solar Energy Utilization: Fundamentals and Applications." In *Resources, Challenges, and Applications*, IntechOpen Limited, London, U.K. DOI: 10.5772/intechopen.91804.

40 Solutia: Eastman Chemical Company. n.d. "Therminol 66: High-Performance Highly Stable Heat Transfer Fluid." Solutia: Eastman Chemical Company, St. Louis, MO, USA. Available at: https://www.therminol.com/product/71093438.

41 Solutia: Eastman Chemical Company. n.d. "Therminol 68: Highly Stable Low Viscosity Heat Transfer Fluid." Solutia: Eastman Chemical Company, St. Louis, MO, USA. Available at: https://www.therminol.com/product/71093442.

42 Solutia: Eastman Chemical Company. 2019. "Therminol 66." Solutia: Eastman Chemical Company, St. Louis, MO, USA. Available at: https://www.therminol.com/sites/therminol/files/documents/TF-8695_Therminol-66_Technical_Bulletin.pdf.

43 Solutia: Eastman Chemical Company. 2019. "Therminol 66." Solutia: Eastman Chemical Company, St. Louis, MO, USA. Available at: https://www.therminol.com/sites/therminol/files/documents/TF-8695_Therminol-66_Technical_Bulletin.pdf.

44 Oh, S., J. Park, Y. Chae, and J. Ik Lee. 2020. "Comparison of Heat Transfer Fluids for Thermal Energy Storage System Integrated Nuclear Power Plant." *Transactions of the Korean Nuclear Society Virtual Spring Meeting July 9-10, 2020*. Available at: https://journal-home.s3.ap-northeast-2.amazonaws.com/site/kns2020spring/presentation/20S-222.pdf.

45 U.S. Nuclear Regulatory Commission (NRC). 2002. "Byron, Units 1 and 2, and Braidwood, Units 1 and 2, Updated Final Safety Analysis Report (UFSAR), Revision 15, Updated Fire Protection Report (FPR), Amendment 26, Chapter 10 - Steam and Power Conversion System." Rev. 9, December 2002. NRC, Rockville, MD, USA. Available at: https://www.nrc.gov/docs/ML1436/ML14363A457.pdf

46 Siegel, N.P., R.W. Bradshaw, J.B. Cordaro, and A.M. Kruizenga. 2012. "Thermophysical property measurement of nitrate salt heat transfer fluids." *American Society of Mechanical Engineers*, Paper No: ES2011-54058, 439-446. DOI: 10.1115/ES2011-54058.

47 Ho, C.K. 2016. "A review of high-temperature particle receivers for concentrating solar power." *Applied Thermal Engineering*, *Part B*, 109, 958-969. DOI: 10.1016/j.applthermaleng.2016.04.103.

48 Gilli, P. V., & Fritz, K. (1970). Nuclear power plants with integrated steam accumulators for load peaking (No. WB-KE--2015). Waagner-Biro.

49 González-Roubaud, E., D. Pérez-Osorio, and C. Prieto. 2017. "Review of commercial thermal energy storage in concentrated solar power plants: Steam vs. molten salts." *Renewable and Sustainable Energy Reviews*, 80, 133-148. DOI: 10.1016/j.rser.2017.05.084.

50 Holassian Mucci, J.M. 2015. "Khi solar one project overview and economic analysis." Available at: https://digibuo.uniovi.es/dspace/bitstream/handle/10651/32056/TFMJoseMariaHolassianRUO.pdf?sequence=3&isAllowed=y.

51 Lane III, R., 2016. "Modeling and integration of steam accumulators in nuclear steam supply systems." Ph.D. Dissertation. Available at: https://repositories.lib.utexas.edu/bitstream/handle/2152/45853/LANE-THESIS-2016.pdf?sequence=1&isAllowed=y).

52 Richter, M., Oeljeklaus, G., and Görner, K. 2019. "Improving the load flexibility of coal-fired power plants by the integration of a thermal energy storage." *Applied Energy*, 236, 607-621. DOI: 10.1016/j.apenergy.2018.11.099.

53 Grand View Research, Inc. 2017. "Liquid Nitrogen Market Size & Trends Report, 2018-2025." Grand View Research, Inc., San Francisco, CA, USA. Available at: https://www.grandviewresearch.com/industry-analysis/liquid-nitrogen-market.

54 Grand View Research, Inc. 2017. "Liquid Nitrogen Market Size Worth $21.3 Billion By 2025." Grand View Research, Inc., San Francisco, CA, USA. Available at: https://www.grandviewresearch.com/press-release/global-liquid-nitrogen-market.

55 Hydrogen H2 Tools. 2016. "North America Merchant Hydrogen Plants." January 2016. U.S. Department of Energy–Office of Energy Efficiency & Renewable Energy (DOE-EERE), Washington DC, USA. Available at: https://h2tools.org/hyarc/hydrogen-data/merchant-hydrogen-plant-capacities-north-america.

56 - Elgowainy, A., M. Mintz, D. Steward, O. Sozinova, D. Brown, and M. Gardiner. 2014. "Liquid Hydrogen Production and Delivery from a Dedicated Wind Power Plant." June 16, 2014. ANL-11/33, Argonne National Laboratory, Lemont, IL, USA.

57 Elgowainy, Amgad, Marianne Mintz, Darlene Steward, Olga Sozinova, Daryl Brown, and Monterey Gardiner. 2014. Liquid Hydrogen Production and Delivery from a Dedicated Wind Power Plant." June 16, 2014. ANL-11/33, Argonne National Laboratory.

58 h Satyapal, S. 2009. "DOE Hydrogen and Fuel Cells Program Record." Record #9013. U.S. Department of Energy (DOE), Washington DC, USA. Available at: https://www.hydrogen.energy.gov/pdfs/9013_energy_requirements_for_hydrogen_gas_compression.pdf.

59 Reddi, K., M. Mintz, A. Elgowainy, and E. Sutherland. 2016. "Building a hydrogen infrastructure in the United States," In Compendium of Hydrogen Energy, Volume 4, 'Hydrogen Use, Safety and the Hydrogen Economy,' Chapter 13. DOI: 10.1016/B978-1-78242-364-5.00013-0.

60 Baxter, Larry L., et al. 2019. "Sustainable Energy Solutions: Cryogenic Carbon Capture Development Final/Technical Report." DOE-SES-28697. U.S. Department of Energy (DOE), Washington DC, USA. Available at: https://www.osti.gov/servlets/purl/1572908).

61 Willson, P., et al. 2019. "Evaluation of the performance and economic viability of a novel low temperature carbon capture process." *International Journal of Greenhouse Gas Control*, 86, 1-9. DOI: 10.1016/j.ijggc.2019.04.001.

62 Song, C. F., et al. (2012). "Evaluation of Stirling cooler system for cryogenic CO2 capture." Applied energy 98: 491-501.

63 Hoeger, Christopher, Stephanie Burt, and Larry Baxter. 2021. "Cryogenic Carbon Capture™ Technoeconomic Analysis." In *Proceedings of the 15th Greenhouse Gas Control Technologies Conference 15-18 March 2021*. Available at: https://papers.ssrn.com/sol3/Delivery.cfm/SSRN_ID3820158_code4654062.pdf?abstractid=3820158&mirid=1.

64 Hoeger, Christopher, Stephanie Burt, and Larry Baxter. 2021. "Cryogenic Carbon Capture™ Technoeconomic Analysis." In *Proceedings of the 15th Greenhouse Gas Control Technologies Conference 15-18 March 2021*. Available at: https://papers.ssrn.com/sol3/Delivery.cfm/SSRN_ID3820158_code4654062.pdf?abstractid=3820158&mirid=1.

65 Sayre, A., D. Frankman, A. Baxter, K. Stitt, and L. Baxter. 2017. "Field Testing of Cryogenic Carbon Capture." CMTC-486652-MS. Carbon Management Technology Conference. DOE-SES-28697-2. Available at: https://www.osti.gov/servlets/purl/1412681.

66 Baxter, L.L., et al. 2018. "Cryogenic Carbon Capture Development." 2018 NETL CO_2 Capture Conference. National Energy Technology Laboratory (NETL), Pittsburgh, PA, USA. Available at: Available at: https://www.netl.doe.gov/projects/files/FE0028697_SES_Cryogenic_tech%20sheet.pdf.

67 Zang, G., et al. 2021. "Synthetic Methanol/Fischer–Tropsch Fuel Production Capacity, Cost, and Carbon Intensity Utilizing CO_2 from Industrial and Power Plants in the United States." *Environmental Science & Technology*, 55(11), 7595-7604. DOI: 10.1021/acs.est.0c08674.

71 Richter, M., G. Oeljeklaus, and K. Görner. 2019. "Improving the load flexibility of coal-fired power plants by the integration of a thermal energy storage." *Applied Energy*, 236, 607-621. DOI: 10.1016/j.apenergy.2018.11.099.

72 DN Tanks. n.d. "How Thermal Energy Storage Works." Available at: https://www.dntanks.com/what-we-do/thermal-energy-storage/how-tes-works/.

73 Drake Landing Solar Community. n.d. "Borehole Thermal Energy Storage (BTES)." Available at: https://www.dlsc.ca/borehole.htm.

74 Underground Energy, LLC. n.d. "ATES: Aquifer Thermal Energy Storage." Available at: https://underground-energy.com/our-technology/ates/#how-efficient-is-ates. s

75 Drake Landing Solar Community. n.d. "How It Works." Available at: https://www.dlsc.ca/how.htm.

76 Chen, X., Z. Zhang, C. Qi, X. Ling, and H. Peng. 2018. "State of the art on the high-temperature thermochemical energy storage systems." *Energy Conversion and Management*, 177, 792-815. DOI: 10.1016/j.enconman.2018.10.011.

77 National Renewable Energy Laboratory (NREL). System Advisor Model (SAM). Available online: https: //sam.nrel.gov/ (accessed on 20 May 2021).

78 Manu, K.V., P. Deshmukh, and S. Basu. 2016. "Rayleigh–Taylor instability in a thermocline based thermal storage tank." *International Journal of Thermal Sciences*, 100, 333-345. DOI: 10.1016/j.ijthermalsci.2015.10.016.

79 Hoivik, N., C. Greiner, J. Barragan, A.C. Iniesta, G. Skeie, P. Bergan, P. Blanco-Rodriguez, and N. Calvet. 2019. "Long-term performance results of concrete-based modular thermal energy storage system." *Journal of Energy Storage*, 24, 100735. DOI: 10.1016/j.est.2019.04.009.

80 Stack, D.C., D. Curtis, and C. Forsberg. 2019. "Performance of firebrick resistance-heated energy storage for industrial heat applications and round-trip electricity storage." *Applied Energy*, 242, 782-796. DOI: 10.1016/j.apenergy.2019.03.100.

81 Ho, C.K. 2017. "Advances in central receivers for concentrating solar applications." *Solar Energy*, 152, 38-56. DOI: 10.1016/j.solener.2017.03.048..

82 Shigrekar, A. 2020. "Modeling and Experimental Validation of Latent Heat Thermal Energy Storage System." November 2020. Ph.D. dissertation. University of Idaho, Moscow, ID, USA.

83 Frick, K.L, A. Alfonsi, and C. Rabiti. 2020. "Hybrid User Manual." INL/MIS-20-60624. Idaho National Laboratory (INL), Idaho Falls, ID, USA. https://www.osti.gov/biblio/1760168-hybrid-user-manual.

84 Kim, J.S., M. McKellar, S. Bragg-Sitton, and B. Richard. 2016. "Status on the Component Models Developed in the Modelica Framework: High-Temperature Steam Electrolysis Plant and Gas Turbine

Power Plant." October 2016. INL/EXT-16-40305. Idaho National Laboratory (INL), Idaho Falls, ID, USA. DOI: 10.2172/1333156.

85 Frick, K.L., and S. Bragg-Sitton. 2020. "Development of the NuScale power module in the INL Modelica ecosystem," *Nuclear Technology*, 207(4), 521-542. DOI: 10.1080/00295450.2020.1781497.

86 Greenwood, M.S. 2017. "TRANSFORM - TRANsient Simulation Framework of Reconfigurable Models." Computer Software. November 2017. Oak Ridge National Laboratory (ORNL), Oak Ridge, TN, USA. doi: 10.11578/dc.20171109.1.

87 Mikkelson, D., K.L. Frick, C. Rabiti, S. Bragg-Sitton. 2021. "Thermal Energy Storage Model Development within the Integrated Energy Systems HYBRID Repository." INL/EXT-21-61985. March 2021. Idaho National Laboratory (INL), Idaho Falls, ID, USA. Available at: https://inldigitallibrary.inl.gov/sites/sti/sti/Sort_44972.pdf.

89 Frick, K.L., S. Bragg-Sitton, and C. Rabiti, 2020. "Modeling the Idaho National Laboratory Thermal-Energy Distribution System (TEDS) in the Modelica ecosystem." *Energies*, 13(23), 6353. DOI: 10.3390/en13236353.

90 Frick, K.L. 2016. "Coupling and Design of a Thermal Energy Storage System for Small Modular Reactors." Masters of Science Thesis, Department of Nuclear Engineering, North Carolina State University, Raleigh, NC, USA.